STATISTICS AND DYNAMICS OF COHERENT STRUCTURES ON TURBULENT GRID-FLOW

by

STUART R. LOEWEN

B.Sc. Physics, University of Manitoba, 1980

M.Sc. Physics, University of British Columbia, 1984

A THESIS SUBMITTED IN PARTIAL FULFILLMENT OF

THE REQUIREMENTS FOR THE DEGREE OF

DOCTOR OF PHILOSOPHY

in

THE FACULTY OF GRADUATE STUDIES

(DEPARTMENT of PHYSICS)

We accept this thesis as conforming

to the required standard

THE UNIVERSITY OF BRITISH COLUMBIA

January 1987

©Stuart R. Loewen, 1987

In presenting this thesis in partial fulfilment of the requirements for an advanced degree at the University of British Columbia, I agree that the Library shall make it freely available for reference and study. I further agree that permission for extensive copying of this thesis for scholarly purposes may be granted by the head of my department or by his or her representatives. It is understood that copying or publication of this thesis for financial gain shall not be allowed without my written permission.

Department of PHYSICS

The University of British Columbia
1956 Main Mall
Vancouver, Canada
V6T 1Y3

Date 3 February 1987

ABSTRACT

This thesis examines the statistics and dynamics of turbulent flow structures generated by towing a grid through a tank of water. The structures were made visible by recording the paths of aluminum tracers moving with the water surface. Flow patterns recorded using a time-exposure method were manually analyzed to extract information on the structure statistics. This two-dimensional flow field was found to be composed of closed rotating 'surface eddies', open and largely translational 'river' motion and stagnant regions. Energy distributions of the eddies and rivers were obtained and characterized by Boltzmann type distributions. A newly developed computer-automated structure identification and flow field analysis system was used to study the structure dynamics. The system analyzes digital images obtained from video recordings of the tracer motion. The predominant evolution processes of initial vortex production, eddy pairing, viscous decay and the omega decay were examined. Flow Reynolds numbers, based on bar spacing, of about 10,000 were examined. The structure statistics and dynamics study was performed in order to examine the validity and viability of a new model for turbulence. The model predicts the evolution of a population of structures using rate equations where the rate coefficients are determined by the individual structure dynamics. A summary of the model is presented and contrasted with models based the the Reynolds stresses as well as computational models.

TABLE OF CONTENTS

LIST OF FIGURES

ACKNOWLEDGMENTS

Life is made more enjoyable by having cheerful and competent people to work with. There have been many summer students whose energy and diligence are much appreciated. Foremost amongst these are Alex Filuk who took an active interest in the early stages of this work and Norman Lo who built the tank that rarely leaked. Technicians Al Cheuck and Paul Burrill have built reliable apparatus and taught me the value of careful work. I benefited from the valuable work of and discussions with fellow student Alexis Lau. I was privileged to have a thesis committee of knowledgable, intelligent and interested persons. Material support for myself and the experiment was provided through the Natural Sciences and Engineering Research Council of Canada. Finally I must thank my supervisor Dr. Boye Ahlborn without whom this work would never have been started and this thesis never finished.

CHAPTER 1
INTRODUCTION

It is the basic contention of this thesis that the surface flow on grid-generated turbulence is well described by the statistics of the coherent structures of which it is composed. It is further argued that the coherent structure statistics are determined by the dynamics of individual structures' interactions and that these dynamics can be characterized by simple interaction models which may in turn be used to predict the observed statistics. This thesis supports these claims through an investigation of the statistics and dynamics of coherent structures on turbulent grid-flow. In this thesis, *turbulence* is considered to be a non-periodic and unsteady fluid flow.

Figure 1-1 shows a photo of the surface motion. Far from being a random velocity field, the flow is seen to be composed of local regions of coherently moving fluid. These "coherent structures" undergo either closed, predominantly rotational, motion (the eddies) or are open and contain mainly translational kinetic energy (the rivers). The experimental apparatus used to generate the flow was a towing tank previously designed for flow visualization studies by the author. The fluid motion was generated by a vertical bar grid that was towed through the water at speeds corresponding to a mesh Reynolds number of $\sim 10^4$. For the structure statistics study, the flow was recorded on time-exposed photographs showing the paths of aluminum flakes moving with the fluid

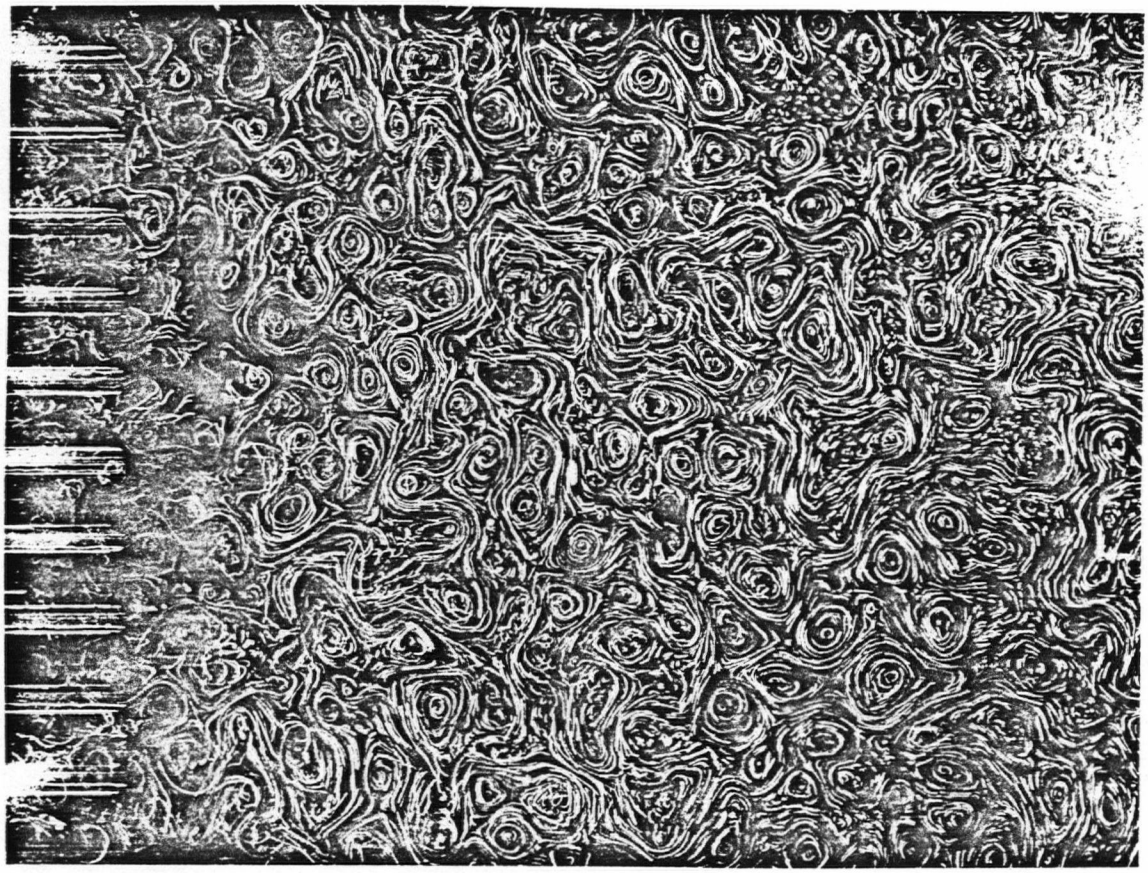

Figure 1-1 Time-Exposure of the Surface Motion.

surface. From ten photo series, each of 10 mesh width span and 40 mesh widths long, 2000 surface eddies were identified and studied. The velocities and positions of about 20,000 tracers were recorded and used to study the energy of the surface flow structures. The predominant structure evolution mechanisms were identified and examined. In addition, both the available literature and subsurface flow visualization were used to study the relationship between the surface and subsurface flow.

For the structure dynamics studies the same flow generation apparatus was used. However, in place of a still camera, a video recorder was used to record the tracer motion.

The recording was later digitized and analyzed using a computer-automated coherent structure identification and flow field analysis system. The system was developed in the course of this research by M. Sc. student Alexis Lau. It allowed for greater objectivity in the identification and description of the flow structures. It also is more suited to the dynamics studies than the time-exposure method.

It was somewhat fortuitous that in the pursuit of an M.Sc. degree this author found that coherent structures virtually covered the surface of the initial period of decaying grid turbulence. Grid-generated turbulence has several properties which make it a useful flow to study. The flow on the surface of a moderately agitated volume of heavy fluid is very nearly two dimensional. As such, it allows for a relatively straightforward analysis as compared with a fully three-dimensional flow. While a two-dimensional flow is not a completely general turbulent fluid system, much that can be learned from the surface flow of grid-generated turbulence is pertinent to more complex flows. The relative ease of flow field extraction and coherent structure identification make two dimensional flows well suited to the study of coherent structure dynamics and statistics. A desirable feature of the space-filling grid-flow is that individual structures are closely packed and thus relatively stagnant in the fluid frame of reference. Also, the grid fills the entire cross-section of the tank so that the bulk motion of the fluid is negligible. This allows for ease in structure identification and tracking. A final point in favour of studying grid-flow is the relative simplicity of the boundary conditions. The grid serves to generate the vortical structures in a well defined manner but they are then allowed to interact free from complicating boundary conditions. It is for the above reasons that the surface flow on grid-generated turbulence was the main flow studied in this thesis work. However other

flows were examined in order to isolate and characterize specific dynamical processes observed in the more complex grid-flow. The major drawback of the grid-flow system is that it is not strictly two-dimensional. This motivated the use of subsurface flow visualization to examine the near surface fluid mechanics.

Part of the motivation for this thesis was to test and develop a model for turbulence based on rate equations proposed by my supervisor Dr. Boye Ahlborn. This model describes how the statistics may be determined from the dynamics of coherent structures using rate coefficients to characterize the dynamical processes. A detailed description of this model can be found in reference [1]. The model uses a rate equation to predict the evolution of a population of energetic flow structures from knowledge of their local dynamics and their probability of interaction. In order to be successful, the model requires first that coherent structures be identified in a flow, second that they be characterized by simple and meaningful parameters and finally that their evolution dynamics be described by rate coefficients.

Structure has been known to be present in flows such as the von Kármán vortex street for over seventy years [2]. However, the presence of coherent structures in what were previously considered to be highly disorganized flows is a fairly recent discovery. Brown and Roshko's hallmark study of coherent structures in the mixing layer [3] was published in 1974. Structures have been found to be a part, not only of flows in which they are produced by the particular vorticity generation geometry, but also of highly developed turbulence. This means that coherent flow structures are an integral part of the non-linear unsteady fluid dynamics which govern the flow. As such, understanding

their properties, dynamics and reasons for occurrence is essential to the understanding of turbulent fluid flow.

The current interest in coherent structures is coincident with renewed use of flow visualization techniques. This in turn is at least partly a result of the development of high speed digital computers to the point where image processing and analysis techniques can be usefully applied to extract quantitative results from images of fluid flow. In this thesis, computer-automated flow visualization has been used both for extracting the velocity field and for the identification of regions of coherent flow.

The organization of this thesis is as follows. After this introduction, the second chapter reviews the established models for turbulent fluid flows. This survey is included to present the setting in which this thesis research has been conducted and provides a basis for a comparison with the rate equation approach which is described at the end of the chapter. The next chapter reviews experimental methods commonly used to study turbulent flow fields as well as the manual and automated flow visualization methods used for this thesis work.

Chapters 4 and 5 report the results of the work performed to examine first the coherent structure statistics on grid-generated turbulence and then the dynamics of these structures and finally how the two are related. The reader who is familiar with turbulence research will find these chapters as well as the last sections of chapters two and three of most interest as they contain the bulk of this student's original contributions. The thesis ends with the conclusion.

Much of the work presented in this thesis has been published elsewhere. Reference [1] presents the rate equation approach to predicting the statistical evolution of turbulent flow fields. Some preliminary structure dynamics observations were presented in reference [4]. The structure statistics study of the fourth chapter was first published in short form [5] with a more thorough presentation given in reference [6]. A preliminary presentation of the computer-automated coherent structure identification and flow field analysis system was published as reference [7]. A more thorough presentation of the system together with results of the structure identification study presented in the the fifth chapter of this thesis has recently been submitted for publication (see reference [8]).

CHAPTER 2
TURBULENT FLOW MODELS

> "I am a firm believer in learning to understand the forces at work instead of operating from a set of fixed rules. Obeying rules without an understanding of the reasons behind them creates an approximation of competence which leaves one vulnerable to the exceptions."
> from *Safety: The Open Coast* or *All your eggs in one Kayak*, by Matt Broze [9]

The purpose of this chapter is to review the models currently used to describe and predict the evolution of turbulent flow fields. There is no one generally accepted model for predicting properties of turbulent fluid flows. In order to produce satisfactory results for a given flow system, models invariably invoke assumptions which severely restrict their range of applicability. However, an appreciation of the various theoretical approaches will add depth to our understanding of the experimental results to be presented. This background is also presented to provide a framework from which to examine the rate equation approach. A good presentation of the 'standard' models for turbulence may also be found in reference 10.

The chapter is divided into six sections. The first section discusses the Reynolds decomposition of the Navier-Stokes equations. The next two sections describe models used to close the resultant Reynolds stress equations starting with the the eddy viscosity

model for turbulent mixing and going on to more complex models of the Reynolds stresses. The spectral energy transfer approach is discussed in the fourth section and the review aspect of this chapter concludes with the computer based approach known as large eddy simulation. The relationship between the models is shown in Fig.2-1. Our rate equation model is summarized in the last section.

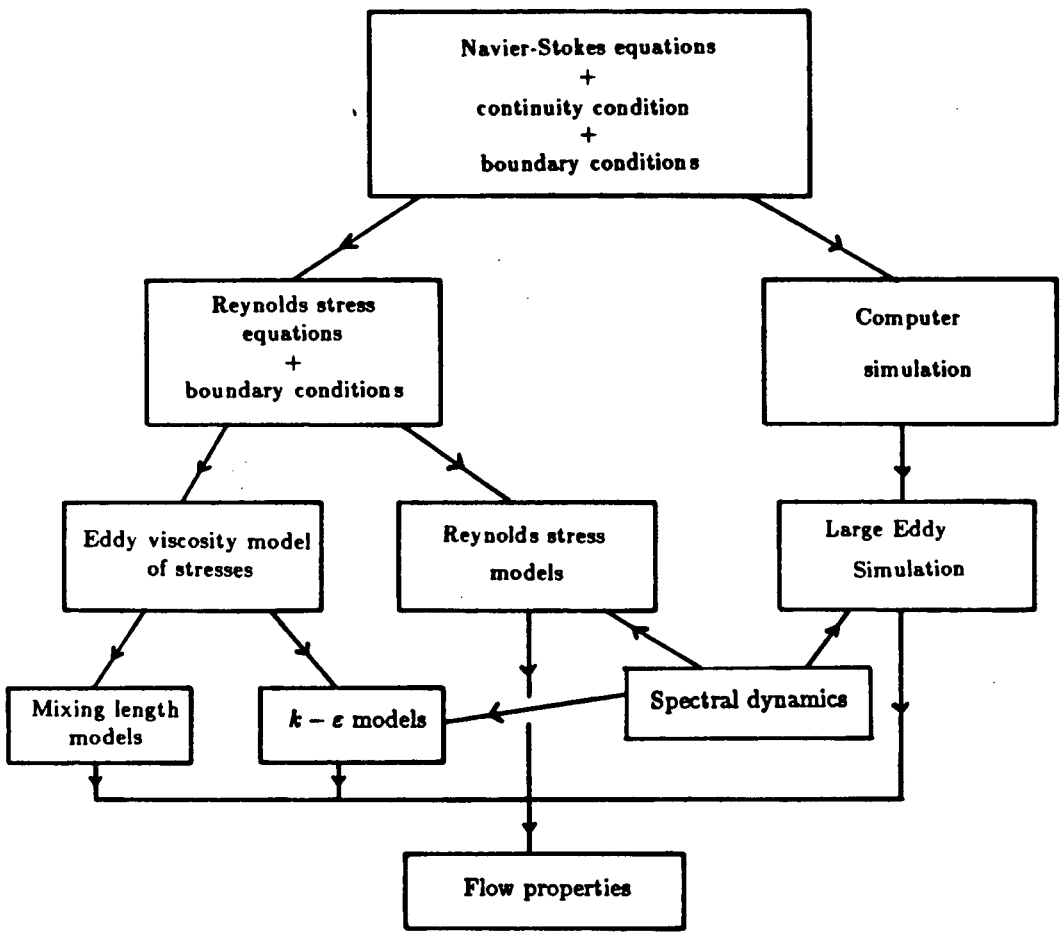

Figure 2-1 Relationship between Navier-Stokes based turbulence models.

2.1 The Reynolds Equations

The starting point with most turbulent flow models are the fluid equations of motion. We begin by writing these equations for an incompressible fluid,

$$\frac{\partial \tilde{u}_i}{\partial t} + \tilde{u}_j \frac{\partial \tilde{u}_i}{\partial x_j} = \frac{1}{\rho} \frac{\partial \tilde{\sigma}_{ij}}{\partial x_j}, \qquad (2-1a)$$

and

$$\frac{\partial \tilde{u}_i}{\partial x_i} = 0. \qquad (2-1b)$$

The standard summation convention is implied and the indices range over the three spatial dimensions. Here ρ, the fluid density, is assumed to be constant. The left side of eqn.(2-1a) is the rate of change of velocity $\tilde{u}_i$ of a fluid element following its motion. The right side contains the stress tensor $\tilde{\sigma}_{ij}$ which drives the motion. Equation (2-1b) is the continuity condition which expresses the conservation of mass for an incompressible medium.

Stokes' relation is used to determine the stress $\tilde{\sigma}_{ij}$ from the rate of strain $\tilde{s}_{ij} (\equiv \frac{1}{2}(\frac{\partial \tilde{u}_i}{\partial x_j} + \frac{\partial \tilde{u}_j}{\partial x_i}))$ and the fluid dynamic pressure $\tilde{p}$ in an isotropic Newtonian fluid,

$$\tilde{\sigma}_{ij} = -\tilde{p}\delta_{ij} + 2\mu \tilde{s}_{ij}. \qquad (2-2)$$

Here δ_{ij} is the Kronecker δ and μ is the dynamic viscosity. Using the continuity condition in the result we arrive at the equations of motion for an incompressible, isotropic and Newtonian fluid:

$$\frac{\partial \tilde{u}_i}{\partial t} + \tilde{u}_j \frac{\partial \tilde{u}_i}{\partial x_j} = -\frac{1}{\rho} \frac{\partial \tilde{p}}{\partial x_i} + \nu \frac{\partial^2 \tilde{u}_i}{\partial x_j \partial x_j} \qquad (2-3a)$$

and

$$\frac{\partial \tilde{u}_i}{\partial x_i} = 0; \qquad (2-3b)$$

the Navier-Stokes and continuity equations. $\nu(\equiv \mu/\rho)$ is called the kinematic viscosity. Together with the appropriate boundary conditions, both in space and time, these equations are the starting point for almost all studies of incompressible, isotropic, and Newtonian fluid motion.

The next step in the development of most turbulence models is to treat the dynamical variables $\tilde{u}_i$ and $\tilde{p}$ as being composed of a mean and a fluctuating component:

$$\tilde{u}_i = U_i + u_i, \qquad (2-4a)$$

$$\tilde{p} = P + p. \qquad (2-4b)$$

This procedure is called the Reynolds decomposition after Osborne Reynolds [11]. Here U_i and P are the average, either time or ensemble averaged, components of the velocity and pressure fields. For some time dependent quantity $a(t)$, the time average $\bar{a}(t)$ is defined as,

$$\bar{a}(t) = lim_{T\to\infty} \frac{1}{T} \int_{t'=t-T/2}^{t+T/2} a(t')dt' \qquad (2-5)$$

It is meaningful to speak of time-dependent time averages if,

$$d\bar{a}(t)/dt \ll \sqrt{\overline{(da(t)/dt)^2}} \qquad (2-6)$$

which states that the averages must change much more slowly than the average change. Flow fields for which the time-averaged quantities do not change with time are termed *statistically steady.*

The stress tensor $\tilde{\sigma}_{ij}$ can also be decomposed into mean and fluctuating components,

$$\tilde{\sigma}_{ij} = \Sigma_{ij} + \sigma_{ij}, \tag{2-7}$$

where the time independent mean stress tensor Σ_{ij} has the analogous Stokes' relation,

$$\Sigma_{ij} = -P\delta_{ij} + 2\mu S_{ij} \tag{2-8}$$

and the zero mean fluctuation stresses are given by,

$$\sigma_{ij} = -p\delta_{ij} + 2\mu s_{ij}. \tag{2-9}$$

The mean strain rate tensor S_{ij} and fluctuation strain rate tensor s_{ij} are given by

$$S_{ij} = \frac{1}{2}\left(\frac{\partial U_i}{\partial x_j} + \frac{\partial U_j}{\partial x_i}\right) \tag{2-10}$$

and

$$s_{ij} = \frac{1}{2}\left(\frac{\partial u_i}{\partial x_j} + \frac{\partial u_j}{\partial x_i}\right) \tag{2-11}$$

respectively.

The equations of motion for the mean flow may be obtained by substituting the Reynolds decompositions into the fluid equations of motion, eqns.(2-1), and then taking the time average of all terms in the resulting equation. Finally noting that, for physically realistic flow fields, averaging commutes with differentiation the resulting equations for the mean flow are,

$$U_j\frac{\partial U_i}{\partial x_j} + \overline{u_j\frac{\partial u_j}{\partial x_i}} = \frac{1}{\rho}\frac{\partial}{\partial x_j}\Sigma_{ij}. \tag{2-12}$$

Using the continuity equation to rewrite the second term we have

$$U_j \frac{\partial U_j}{\partial x_i} = \frac{1}{\rho} \frac{\partial}{\partial x_j} (\Sigma_{ij} - \rho \overline{u_i u_j}) \qquad (2-13)$$

or alternately using expression (2-8) for the mean stress

$$U_j \frac{\partial U_i}{\partial x_j} = \frac{1}{\rho} \frac{\partial}{\partial x_j} (-P\delta_{ij} + 2\mu S_{ij} - \rho \overline{u_i u_j}) \qquad (2-14a)$$

with the continuity of the mean flow

$$\frac{\partial U_i}{\partial x_i} = 0. \qquad (2-14b)$$

The contribution of the turbulent motion to the mean stress is called the Reynolds stress tensor,

$$\tau_{ij} \equiv -\rho \overline{u_i u_j}. \qquad (2-15)$$

We have now arrived at the starting point of the majority of the turbulence models being used and studied at the present time.

The decomposition of the flow into mean and fluctuating components in the form of either eqns.(2-4), or equivalently equations (2-7) through (2-9), allows for some tractable analysis and useful results, witness to this being that this flow decomposition was first introduced by Reynolds in 1895 and is still much used today. It should be emphasized at this point however that by introducing eqn.(2-4) the number of unknowns has been increased by four, three velocity components and one pressure variable, without increasing the number of equations. The task for the turbulence modeller is to close the system using a suitable model for the Reynolds stress tensor. In order to solve the new equations

of motion, either physically motivated or empirically obtained information in the form of additional relations must be added. That is the object of the eddy viscosity models such as the mixing length and so called $k - \epsilon$ models as well as the more general Reynolds stress models.

While the Reynolds decomposition is responsible for the considerable success in the description and calculation of turbulent boundary layer and free shear layer flows it is also responsible for the limited applicability of the approach. It can be misleading in application and results, particularly if applied to flows for which the local flow structures coherently add to the mean flow field. If the dynamics of these local fluctuations are inherently non-linear, exclusion of their coherent component will render physically motivated modelling impotent.

2.2 Eddy Viscosity Models

The task is now to provide an expression for the Reynolds stress tensor τ_{ij} so that the partial differential equations of mean motion, eqns.(2-14), can be solved. The standard approach is to write $\overline{u_i u_j}$ as proportional to the fluctuation stress tensor s_{ij} in a manner similar to how the mean strain rate S_{ij} is related to the viscous stress. There, the viscous term is μS_{ij} with μ quantifying the rate of momentum transport due to molecular motion. In an analogous manner an eddy viscosity is used to quantify the rate of momentum transport due to turbulent fluctuations by writing

$$\overline{u_i u_j} = -2\nu_T s_{ij} \qquad (2-16)$$

where ν_T is called the eddy viscosity. This relation was first developed by J. Boussinesq [12,13] starting in 1877. While the kinematic viscosity ν is an intrinsic property of the fluid the eddy viscosity ν_T is a property of the fluid flow and as such not generally a local parameter as is implied by writing eqn.(2-16). Models based on this relation are successful when applied to flows for which a local approximation for ν_T is not too grossly violated. These are flows for which a turbulent length scale ℓ is much smaller than the mean flow length scale $L\left(\equiv \frac{\partial U_i}{\partial x_j} / \frac{\partial^2 U_i}{\partial x_j^2}\right)$.

One of the oldest and most successful models for ν_T is obtained by pushing the analogy between turbulent and molecular transport a step further. The mixing length hypothesis was first put forward by Prandtl in 1925 [14] when he suggested using,

$$\nu_T = c_1 u' \ell \qquad (2-17)$$

for the eddy viscosity. Here u' and ℓ are appropriately chosen velocity and length scales while the constant c_1 must be experimentally determined for each type of flow. An example of an appropriate choice for u' and ℓ is for wall-bounded shear flow where u' is the velocity difference across the boundary layer and ℓ is the boundary layer thickness. The derivation of this relation follows the lateral motion of momentum carrying fluid lumps a distance ℓ across a shear layer where it is surrounded by fluid of average velocity difference u'. The reader interested in the rationale behind eqn.(2-17) will find presentations by either Tennekes and Lumley [15] or Schlichting [16] worth reading.

If the velocity and length scales were known everywhere in a flow and if the mixing length model was realistic the closure problem would be solved. That this is not so is partially due to the fact that in turbulent flows the largest eddies tend to have size scales

comparable to the width of the flow. The largest eddies are also the most efficient at extracting energy from the mean strain rate and thus contribute most to the Reynolds stress influence on the mean flow.

Another significant aspect of turbulent flows for which eqn.(2-17) does not account is the usual multiplicity of length scales. Many models have been proposed to describe the length scale variation within a flow. A slight elaboration of the boundary layer model described above has the velocity u' given by the local fluid speed and ℓ determined as the distance to the wall.

The more sophisticated models, the so called one-equation models, use a Navier-Stokes derived partial differential equation to determine the energy k which in turn defines the fluctuation velocity scale u'. Two-equation models use algebraic equations with experimentally determined proportionality constants to describe both the length and velocity scale in terms of k and the dissipation ε. k and ε themselves are determined from Navier-Stokes derived partial differential equations. According to W.C. Reynolds [17], as of 1976 only the zero-equation models, ones using only a partial differential equation for the mean flow, were being used in practice by the "more sophisticated engineering industries". In a more recent review Ferzinger [24] states, "Mixing length models work very well in two-dimensional shear flows. They can be modified to account for extra effects such as pressure gradients, curvature, and transpiration. . . . The major disadvantage of mixing length models is the difficulty they have with complex flows."

2.3 Reynolds Stress Models

Reynolds stress models were developed as a way of avoiding the eddy viscosity assumption and the subsequent limitations. The basic approach is to use partial differential equations to determine the Reynolds stresses. The equations used come from the fluctuation counterpart of eqn.(2-14) obtained from the original Navier-Stokes equations in the following way: The mean and fluctuating decomposition of the velocity and pressure, eqns.(2-4), are again substituted into the Navier-Stokes equations but the mean equations of (2-14) are now subtracted to obtain equations for the fluctuating quantities. The fluctuation equations are cross-multiplied by u_i and then averaged to get equations for the Reynolds stresses, the normal components of which are the fluctuation kinetic energies. These equations have the general form

$$\frac{\partial \overline{u_i u_j}}{\partial t} = Convection + Production - Dissipation + Redistribution \qquad (2-18)$$

Whereas the production term is prescribed, the convection, dissipation, and redistribution terms must be modelled. The closure problem still haunts us! Moreover the constants in the model are more difficult to obtain due to the lack of experimental techniques for the direct measurement of the quantities such as the pressure-strain correlations responsible for the redistribution of stress components. For these reasons Ferzinger [24] has suggested using full-scale computer simulations to test the models. According to Ferzinger, Reynolds stress models nearly doubled the cost of computing a given flow without yielding results significantly better than those produced by the two-equation models mentioned in the last section.

2.4 Spectral Dynamics

Development of models for the Reynolds stress tensor requires knowledge of the dynamics of turbulence. The turbulent energy equations, the normal components of eqns.(2-18) contain only mean products of fluctuating quantities at one point in space. In order to study the length scales of the turbulent fluctuations we need to consider fluctuating quantities which are measured at different points in space. The most general, statistically steady, two-point spatial correlation between fluctuating velocity components may be written

$$C_{ij}(\vec{x},\vec{r}) = \overline{u_i(\vec{x},t)u_j(\vec{x}+\vec{r},t)} \qquad (2-19)$$

where $\vec{x}$ is the position where the correlation is defined and $\vec{x}+\vec{r}$ is the position where the jth velocity component is defined.

The dimensionless correlation is called the correlation coefficient and is given by

$$R_{ij}(\vec{x},\vec{r}) = \frac{\overline{u_i(\vec{x},t)u_j(\vec{x}+\vec{r},t)}}{\sqrt{\overline{u_i^2(\vec{x},t)}}\sqrt{\overline{u_j^2(\vec{x}+\vec{r},t)}}} \qquad (2-20)$$

$\tilde{R}$ forms a second rank tensor whose individual components are such that

$$-1 < R_{ij}(\vec{x},\vec{r}) < 1 \qquad (2-21)$$

This agrees with the interpretation that R_{ij} is a measure of the degree of correlation between the two velocity components. A typical spatial correlation curve for identical velocity components appears in Fig.2-2.

At $\vec{r} = 0$ we see from eqn.(2-20) that $R_{\alpha\alpha} = 1$. It is a property of turbulent flows that fluctuating velocity components are uncorrelated for sufficiently large separations

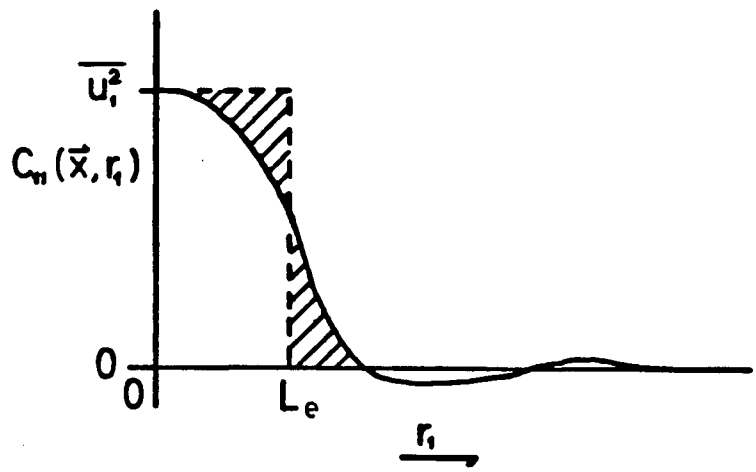

Figure 2-2 Spatial Correlation Curve.

and so we have

$$R_{ij}(\vec{x},\vec{r}) \Longrightarrow 0 \; for \; large \mid \vec{r} \mid \qquad (2-22)$$

For homogeneous flows $R_{ij}(\vec{x},\vec{r}) \Longrightarrow R_{ij}(\vec{r})$. If the mean fluid velocity is in the x_1 direction for example then $R_{11}(r_1)$ is called the 'longitudinal correlation coefficient' and $R_{22}(r_1)$ and $R_{33}(r_1)$ are 'lateral spatial correlation coefficients'. A simple measure of the length scale of the energy containing fluctuations is given by

$$L_e = \int_{r_1'=0}^{\infty} R_{11}(r_1')dr_1' \qquad (2-23)$$

called the integral length scale, see Fig.2-2.

In some flow situations a useful measure of the length scales in the fluctuations can be found from the temporal correlations. The auto-correlation curve is the average product of the same quantity measured as a function of separation time T,

$$C_{\alpha\alpha}(\vec{x},T) = \overline{u_\alpha(\vec{x},t)u_\alpha(\vec{x},t+T)} \qquad (2-24)$$

This curve is much more easily obtained from experiment than the space correlations discussed above. Only one velocity measuring probe, a correlator and a signal delay unit are needed. The auto-correlation curve is obtained by sweeping the delay time T rather than physically moving a velocity probe. The time scale of the energy containing fluctuations, the integral time scale T_e, is defined as

$$T_e = \frac{1}{\overline{u^2}} \int_{T'=0}^{\infty} C(T')dT'. \qquad (2-25)$$

The auto-correlation is of interest when one wants to examine structure dynamics as it is most closely related to the time evolution of the flow. It is also useful in the study of the spatial structure of turbulent fluctuations when it can be related to the spatial correlations. This relationship and the conditions of its applicability are discussed below.

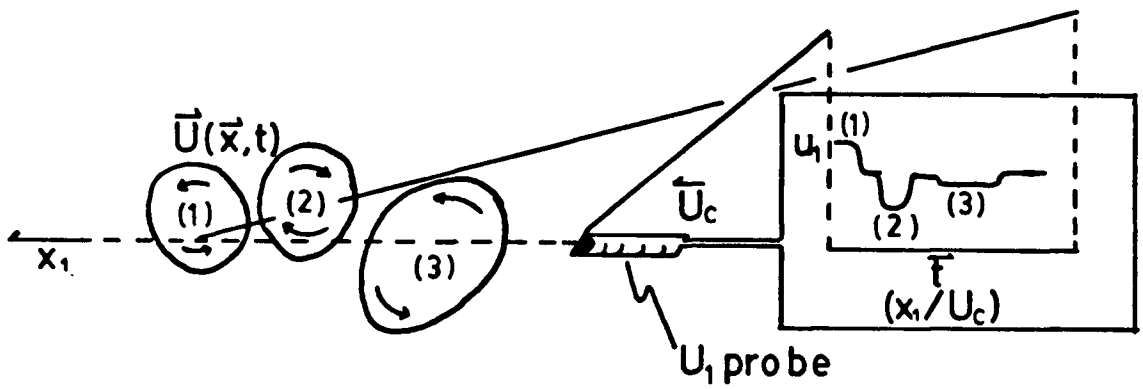

Figure 2-3 Taylor's hypothesis. Equivalence of time and space coordinates.

Consider a flow field moving past a velocity probe, see Fig.2-3. Assume the convection speed is the same for all fluid elements and the coherent structures do not evolve appreciably in the time it takes them to flow past the probe. The probe measures the velocity as a function of time. The space correlation is obtained from the time correlation of the temporally varying signal by simply multiplying the time axis of the auto-correlation by the probe speed, U_c.

$$C_{\alpha\beta}(T) = C_{\alpha\beta}(X/U_c) \qquad (2-26)$$

the integral time scale can thus be related to the integral length scale by the relation,

$$T_e = L_e/U_c \qquad (2-27)$$

This coordinate transformation and the conditions when it can be applied are called "Taylor's hypothesis" after G.I. Taylor who first formalized it or alternately the "frozen" turbulent field hypothesis. The important point to note is that Taylor's hypothesis can only be applied when the flow field does not change appreciably during the time it takes the sampling probe to traverse a distance greater than the length scale of interest. In addition the fluid elements must have a constant convection velocity, U_c. For the purpose of studying coherent structures Taylor's hypothesis may be applied when the eddies have a lifetime that is long compared with the probe transit time. Additionally the structure drift velocity must be negligible compared with the probe speed.

Just as a fluctuating flow field can be described by the spatial correlations we can describe it by the Fourier transforms of the correlations without loss of information. The

Fourier transform of the spatial correlation tensor is called the three dimensional wave vector spectrum,

$$\Phi_{ij}(\vec{k},\vec{x}) = \left[\frac{1}{(2\pi)^3}\right]\int_V \overline{u_i(\vec{x},t)u_j(\vec{x}+\vec{r},t)}exp(i\vec{k}\cdot\vec{r})d\vec{r} \qquad (2-28)$$

with $\mid \vec{k} \mid = 2\pi/\lambda$ being the wave number. It is impractical to measure or work with all velocity components needed to define this spectrum.

Another spectrum which is simple enough to be useful is the *three-dimensional spectrum.* This spectrum is obtained by removing the directional information from the wave vector spectrum by integrating $\Phi_{ij}(\vec{k},\vec{x})$ over spherical shells centered at $\vec{k} = 0$;

$$E(k) = \frac{1}{2}\oint_S \Phi_{ii}(\vec{k})d\sigma. \qquad (2-29)$$

It is most useful when applied to isotropic flows as information about flow orientation has been removed. The factor of $\frac{1}{2}$ is included to make the integral of the three-dimensional spectrum $E(k)$ equal to the kinetic energy per unit mass

$$\int_0^\infty E(k)dk = \frac{1}{2}\overline{u_i u_i}. \qquad (2-30)$$

Discussions of spectral dynamics in isotropic flows are presented in a number of texts [15, 18]. A more rigorous presentation is given by Hinze [19]. Figure 2-4 shows the qualitative variation of the three-dimensional spectrum $E(k)$ for fully developed flows. The energy is supplied to the turbulent spectrum at wavenumber $k_o = 1/L_o$ where L_o corresponds to a characteristic length scale of the flow generation mechanism. For three-dimensional flows the energy continually cascades to higher wavenumber due to the action

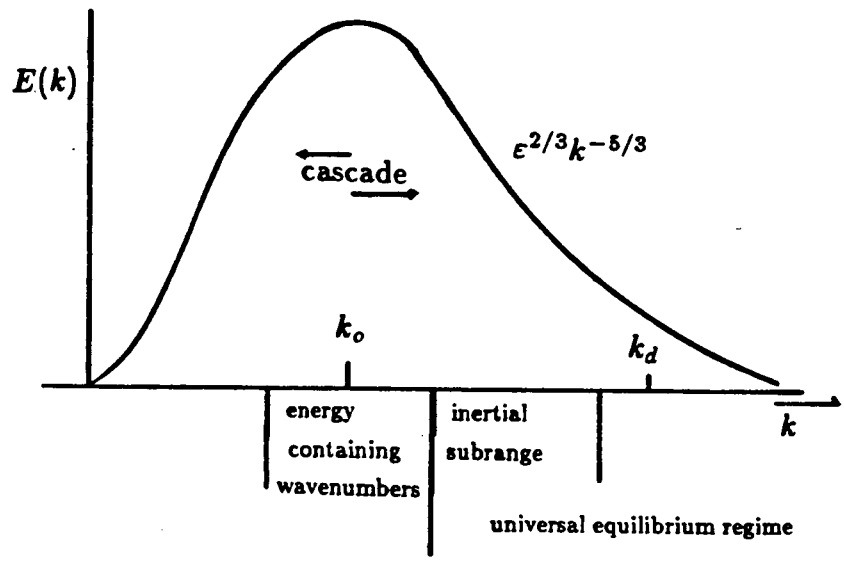

Figure 2-4 The three-dimensional spectrum $E(k)$ for fully developed turbulence.

of vortex stretching. The integral length scale of eqn.(2-23) is shown near the center of the distribution of energy containing wavenumbers. The shape of the spectrum in this region is dependent on the flow generation mechanism and the boundary conditions. In 1941 Kolmogorov hypothesized the existence of a universal equilibrium regime where the flow is independent of the shape of the spectrum at lower wavenumbers [20]. The idea is that in the energy cascade to smaller size motion the flow loses all information about the large scale geometry. The shape of the spectrum is solely determined by the dissipation ε and the kinematic viscosity ν. For extremely high Reynolds numbers, Kolmogorov further hypothesized the existence of an *inertial subrange* where the shape of the spectrum can only depend on the rate of energy transfer through the spectrum. This transfer rate is equal to the dissipation as the inertial subrange carries all the energy that is dissipated in the viscous dominated small scales near k_d. A simple dimensional analysis leads to the now famous $\varepsilon^{2/3}k^{-5/3}$ functional form of $E(k)$. $k^{-5/3}$ inertial subranges have been found

in many high Reynolds number flows including a tidal channel flow [21]. Stewart and Townsend [53] have shown that the conditions necessary for the existence of the inertial subrange are not met in laboratory conditions. This does not, however, prevent $k^{-5/3}$ spectra from being found in the lab as often happens*.

While inertial ranges are expected in two-dimensional turbulence, see ref. [23], the spectral dynamics are quite different from what is found in three dimensions. Vortex stretching , the predominant mechanism of energy transfer in three-dimensional flows, is not possible for two-dimensional motion. Also, in the two-dimensional inertial range the mean-square vorticity as well as the kinetic energy per unit mass are constants of the motion. This has the effect that transfer upward in wavenumber must be accompanied by comparable or greater downward transfer through the action of eddy pairing. In two-dimensional turbulence the energy cascade is to lower wavenumber with inertial ranges found at larger size-scales than the scale at which the energy is fed into the fluid system.

Turbulent flows are modelled using the three-dimensional spectrum by Fourier decomposition of the Navier-Stokes equations. The equations are then closed in a manner similar to that in which the Reynolds stresses are estimated. A spectral energy transfer function is introduced which describes how processes at one wavenumber affect the amplitudes at another. The problem is, however, that eddys are not stationary waves and so the spatial Fourier decomposition is not a natural description of them. Eddys are localized in space and so are associated with many wave numbers and the phase relation amongst them in a non-trivial way. Spectral energy transfer functions are thus either quite complex or very restricted in applicability. However insight into spectral dynamics

* I. S. Gartshore private communication

of the tractable case of isotropic and homogeneous turbulence provides conceptual tools by which other flows can be appreciated. Also, the spectral dynamics of isotropic and homogeneous flows are thought applicable to the small scale motion of a broad range of fluid flow systems.

2.5 Computational Models

The Navier-Stokes equations allow for a complete computer simulation only at very low Reynolds numbers. As the Reynolds number increases the range of length scales in the flow increases. The Large Eddy Simulation (LES) technique suggested by Leonard in 1973 [25] handles this problem by solving filtered Navier-Stokes equations for the large "eddies" while modelling the action of the small "eddies" using subgrid scale terms. The term *eddy* is now being used as in the language of Fourier analysis where it is treated as synonymous with a disturbance over a narrow range of wavenumber.

What follows is a representative outline of the filtering and subgrid scale analysis as presented by Aupoix [26]. It is common to deal with the Fourier transform of the Navier-Stokes equations. The transformed equations read:

$$\frac{\partial}{\partial t}\hat{u}_i(\vec{k}) + \nu k^2 \hat{u}_i(\vec{k}) = -ik_j(\delta_{ij} - \frac{k_i k_l}{k^2}) \int\int \delta(\vec{k} - \vec{p} - \vec{q}) u_j(\vec{p}) u_l(\vec{q}) d^3\vec{p}\, d^3\vec{q} \quad (2-31a)$$

for the momentum equation and

$$k_i \hat{u}_i(\vec{k}) = 0 \quad (2-31b)$$

for the continuity equation. Here $\tilde{u}(\vec{k})$ is the Fourier transform of the velocity field and $\delta(\vec{k})$ is the Dirac function. The right hand side stands for both the advection and pressure term. Each wave vector $\vec{k}$ interacts with all wave vectors $\vec{p}$ and $\vec{q}$ such that $\vec{k} = \vec{p} + \vec{q}$.

The velocities and pressure are next decomposed into two terms, a large-scale component, $\bar{u}$, and a small scale component, $u' = u - \bar{u}$, using a convolution filter G. The filtered value of a velocity component reads

$$\bar{u}_i(\vec{x}) = \int u_i(\vec{x}')G(\vec{x} - \vec{x}')d^3\vec{x} \qquad (2-32)$$

or more simply in Fourier space

$$\bar{\hat{u}}(\vec{k}) = \hat{u}(\vec{k})\hat{G}(\vec{k}) \qquad (2-33)$$

For convenience a step-function low pass filter is employed artificially to separate the large $|\vec{k}| < k_c$ and small $|\vec{k}| > k_c$ scales in the flow. What results is a governing equation for the large scale eddies with a subgrid scale term which must be modelled. The subgrid scale term represents the interactions between wavenumbers above the filter cut k_c and those below it. This decomposition is similar to, but more sophisticated than, the Reynolds decomposition of section 2.1. The closure problem remains however.

The Fourier transformed energy equation for an isotropic flow is

$$(\frac{\partial}{\partial t} + 2\nu k^2)E(k) = T(k) = \int\int S(k,p,q)d^3p d^3q. \qquad (2-34)$$

Here $E(k)$ is the energy spectrum of eqn.(2-29) and $T(k)$ is the total energy transfer into wavenumber k. Several models give expressions for the detailed energy transfer $S(k,p,q)$

at wavenumbers p and q. The more recent two-point closures impose the equality of ensemble-averaged energy transfer between wavenumber k and the small scales. Older models simply imposed energy conservation across the cut, k_c.

An implementation of the modelling is presented by Aupoix as follows: "At each time step the energy spectrum of the large scales is calculated. With the knowledge of the energy spectrum of both the large and the small scales, the EDQNM* routine can then compute on one hand the subgrid scale transfer and the eddy viscosity $\nu_T(k)$ in the large scales and, on the other hand, the energy transfer $T(k)$ in the small scales. So the evolution of all scales can be computed."

It should be mentioned that the LES models are more successful when applied to flows for which a physical scale separation occurrs [28]. An example being the flow behind a bluff body where the relatively homogeneous small scales produced by the separated boundary layer interact with the shed vortices which are of the body dimension in size.

2.6 The Rate Equation Approach

In sharp contrast to the above models is our rate equation approach. As mentioned in the introduction, much of the motivation behind this study of coherent structures on grid-generated turbulence was to test and develop a model for turbulence based on rate equations. This model was proposed by my thesis advisor Dr. Boye Ahlborn. The model and some simple applications of it were described in a recent publication [1]. Its essential feature is that the statistical evolution of energy-containing coherent structures is described using a rate equation. The different types of evolution processes that a

* a statistical description of the small scale motion, see [27]

structure can undergo are characterized by rate coefficients in a manner similar to that by which the evolution of energy states in an interacting system of excited or ionized atoms (a plasma) is modelled. In a sense, our model takes the analogy of flow structures with atoms a step further than was done first by Boussinesq in the eddy viscosity model and then by Prandtl in his mixing length approach.

The interactions of an energetic flow structure with its environment are classified into three main types. A structure can interact with its fluid surroundings through viscous dissipation, with its flow environment through the mean shear stress and with other structures by eddy-eddy collisions. The rates of these dynamical processes are quantified by the coefficients A, B and C respectively. The time rate of change of the number of structures of a given type is then determined by the rate equation

$$\frac{dn_\alpha}{dt} = \sum_{k \geq \alpha}^{m} A_{\alpha k} n_k + \sum_{k} B_{\alpha k} n_k + \sum_{k,\ell} C_{\alpha k l} n_k n_\ell - C_{k \alpha \ell}. \qquad (2-35)$$

There being one rate equation for each of the m distinct structure types. At present we need not specify what physical parameters determine the structure type. For a given flow system a structure may be uniquely characterized by its size and energy. In the statistics analysis of section 4.4 we characterize the structures by either size or energy. The rate coefficients must be derived from the local interaction dynamics and the probability that a particular encounter will occur. The A coefficient quantifies the rate at which structure type α is produced by viscous decay of structures having greater energy (thus α forms the lower bound in the summation). The B coefficient describes the probability that an α type structure will be produced when a k type structure interacts with a shear stress in the fluid. The C coefficient quantifies the probability that structure

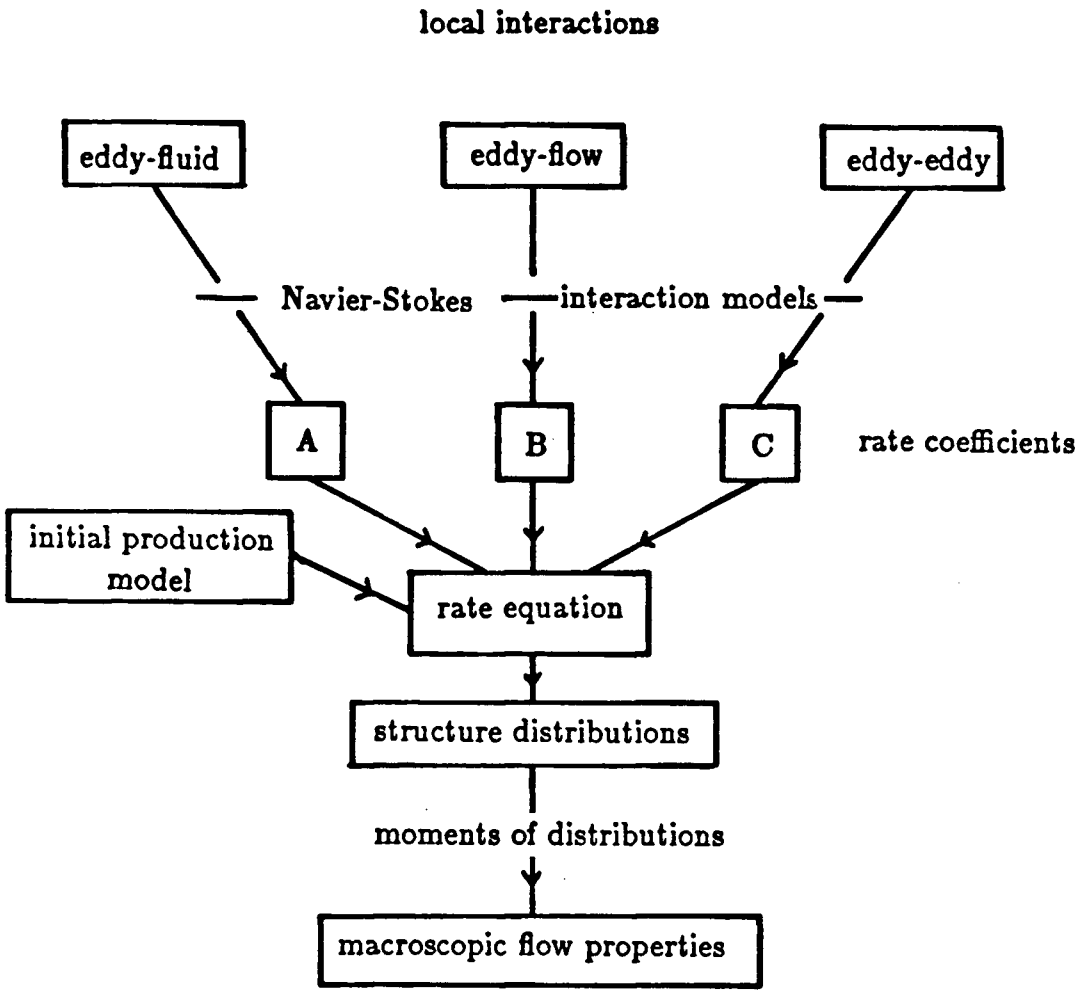

Figure 2-5 Structure diagram of the rate equation model.

types k and ℓ will collide and produce a structure of type α. If the rate coefficients truly capture the essence of the structure evolution then equation (2-35) provides a general framework for describing the evolution of a population of structures. If the structures are characterized by their size and energy then the rate equation describes the evolution of the number of structures of a particular size and energy. This model has the inherent quality of addressing one of the more vexacious problems in turbulence modelling; namely locally deterministic evolution and long term unpredictability. The approach allows one naturally to account for structure dynamics. The rate coefficients may in principle be determined either through experimental observation or calculated using the fluid equations of motion. Figure 2-5 shows a structure diagram of the rate equation model.

In order to establish the validity and viability of the rate equation approach a number of fundamental and practical questions need to be answered. Some of the fundamental questions are:

1) Can the flow structures be identified and characterized by simple physical parameters?

2) Can the evolution of these structures be adequately characterized by rate coefficients?

3) Can the rate coefficients be determined by local considerations?

4) Do the coherent structures account for most of the unsteady flow in a turbulent fluid?

5) Can the initial production of structures be predicted?

6) Can the identification of a structure be made objective?

7) Can a coherent structure be identified unambiguously?

Some of the practical questions are:

1) Are there general unique 'relaxed' states to the structures?

2) Can analysis of a fluid flow provide sufficient statistical data to evaluate the rate equation model.

3) Are there flow structures which are common to many turbulent flow systems?

4) Can the recognition of a structure be automated?

5) Can the predicted structure populations be used to predict flow properties of practical interest such as drag, mixing, heat transfer or gust levels?

This thesis advances the rate equation model by addressing many of these questions in relation to grid-generated turbulence. Before going on to discuss the experimental observations a description of the apparatus and visualization techniques used in this research is presented along with a review of other methods used in the experimental study of fluid flow.

CHAPTER 3
FLOW FIELD ANALYSIS

" Many turbulent flows can be observed easily; watching cumulus clouds or the plume of a smokestack is not time wasted for a student of turbulence." from *A First Course in Turbulence*: by Tennekes and Lumley [15]

The purpose of this chapter is to describe methods used to produce, observe and analyse flow fields in the study of turbulent fluid dynamics. There are basically two experimental techniques available for the study of the fluid motion. Flow visualization acquires two- or three-dimensional flow fields at discrete points in time while anemometry provides continuous velocity time records at discrete points in space. Both methods were used in this study of grid-generated turbulence although the emphasis in this thesis is on the flow visualization work. The first section of this chapter describes the towing tank which was built to produce and study the turbulent grid-flow. A review of flow visualization techniques and the coherent structures decomposition of turbulent velocity fields is presented in the second section. The third section describes the acquisition of spectra and conditional sampling, methods which are rooted in the use of single and multi-point velocity probes such as laser and hot-wire anemometers. Finally, the manual and automated coherent structures analysis techniques used in this thesis are described.

3.1 The Towing Tank

A turbulent flow field was generated in a water-filled towing tank using a vertical bar grid of M=5.08cm spacing and d=1.26cm bar diameter. The surface flow field was recorded using a 35mm camera fixed in the lab frame of reference, see Fig.3-1. The camera had a motor drive so that a series of photos could be taken as the flow evolved. For the structure dynamics studies an underwater cart was fitted to the tank. This permitted clearer visualization of the formation region near the towed models. The underwater cart consisted of a plastic sheet which slide between tracks of aluminum U-channel mounted near the tank bottom. The same drive system was used for both carts. The camera's shutter was triggered by an optical pick-up which detected reflective bands placed on the drive cable. The cart speed, Ug, was controlled to better than 1% using a $\frac{1}{2}$ horse power constant speed motor. The speed controller setting and step pulley combination allowed for a grid speed range of from 2 to 200 cm/sec. Kill switches were placed at either end of the cartway to guard against operator inattention. A more detailed description of the experimental apparatus may be found in reference [30].

For the surface flow investigations aluminum filing tracers of $\approx$ 0.5mm size were applied by scraping an aluminum block with a file. The tracers were illuminated with four flood lamps placed at a low angle of incidence with respect to the fluid surface in order to avoid reflection into the camera. Particular attention was paid to the water surface. Periodic skimmimg was needed to remove contaminants which could significantly alter the properties of the surface motion.

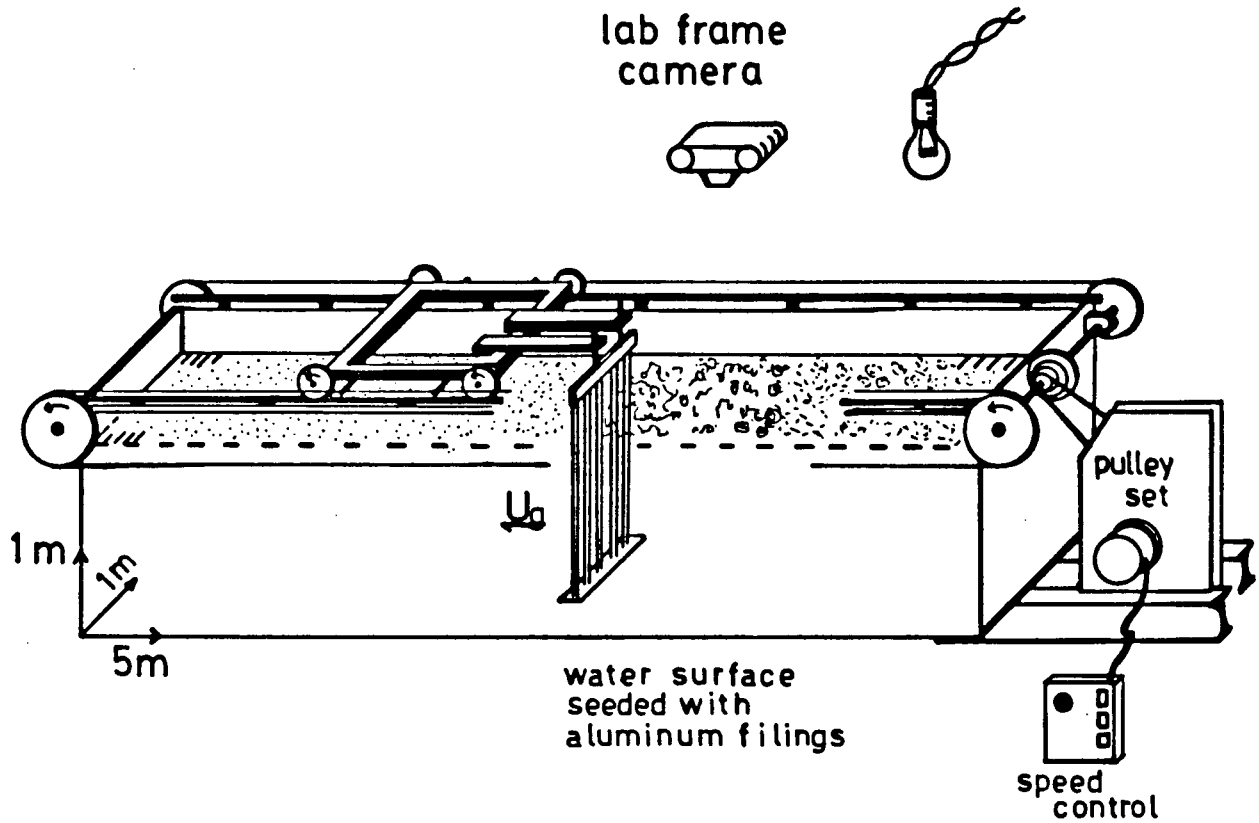

Figure 3-1 The towing tank.

The tank was built with clear plastic side walls to facilitate subsurface flow visualization. A slide projector was used to produce a sheet of light parallel to either the water surface or the tank side wall. Either wood chips or biological entities were used for the subsurface tracers. The latter were allowed to form in the tank over the course of a few months. They were found to be very nearly neutrally bouyant and reflected light almost as effectively as the wood chips. In both the surface and subsurface studies the tracers produced clearly visible streaks on time-exposed photographs. These streaks

indicated the local flow velocity. For the structure dynamics study the video-camera simply replaced the still camera.

3.2 Visualization and Coherent Structures

Before the development of the hot-wire anemometer, flow visualization was the major method used to study the motion of fluids. Flow visualization provides flow field information over entire areas or volumes of a fluid but usually for discrete points in time. Moreover, quantitative analysis is much more involved than for anemometry.

The advent of hot-wire anemometry saw the decreased use of flow visualization in the study of fluid dynamics. For many decades of research, flows of engineering and scientific interest have been extensively investigated through its clear but narrow view. The renewed use of flow visualization is thus not only due to the newly acquired capabilities in image processing, but also to the diminishing returns in the use of point velocity probes. With this new look at some well studied flows the setting was then ripe for a more coherent view vis-à-vis the fragmented statistical concept of turbulence.

The interested reader will find a wealth of visualization techniques and novel variations in references [31,32,33] among others. An excellent collection of flow visualization photos has been assembled by Van Dyke [34]. Figure 3-2 shows a general classification scheme of flow visualization techniques used in the study of fluid flow. They are crudely divided into methods which exploit light scattering from particles and those which make use of variation in refractive index of a fluid depending on the flow conditions.

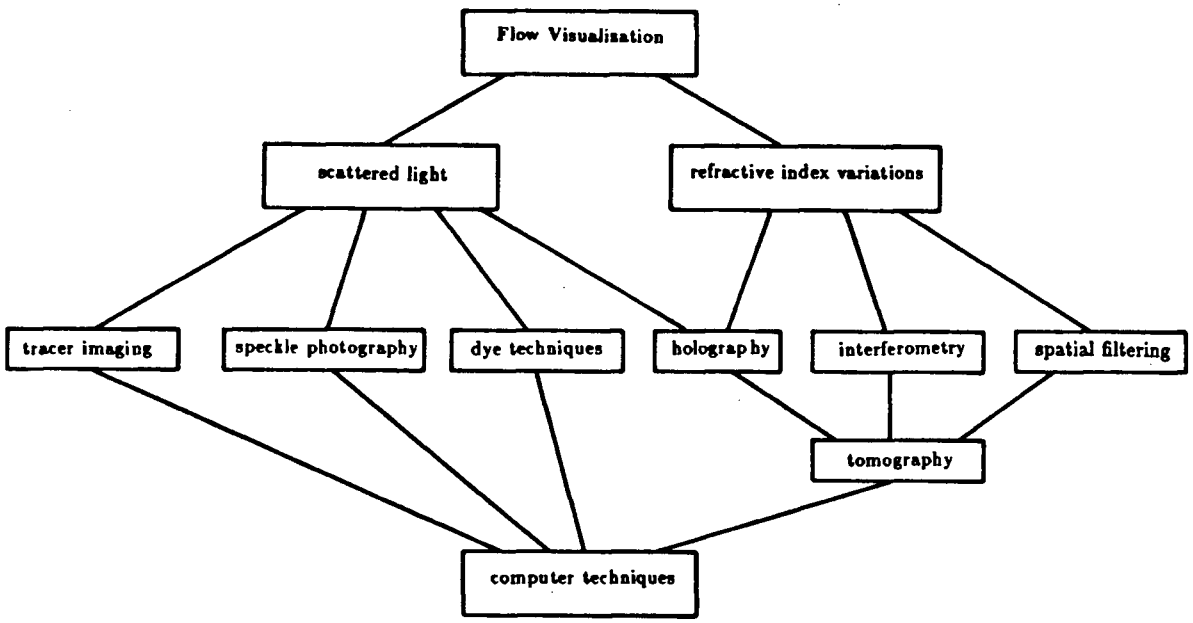

Figure 3-2 Classification scheme of flow visualization techniques.

Interferometers yield a picture of the refractive index through a volume of compressible fluid or mixture of fluids of differing optical properties. Spatial filtering is used in the schlieren technique to produce an image of the average first derivative of the index of refraction while the shadowgraph technique yields the mean second derivative.

Another visualization technique is to follow the motion of a convected fluid which has been dyed with a material that is visually distinct from the background medium. A common combination is ink in water. This technique is quite effective in showing the outlines of structures responsible for mixing. It has been used most effectively in the

study of coherent structures in turbulent boundary layers. An ingeneous extension of this method is the use of a fluorescing dye in a flow illuminated by a sheet of laser light. This method allows for visualization in planes throughout a flow and allows one to 'look inside' three dimensional flows. The dye technique does not lend itself to quantitative extraction of velocity fields and its use has largely been confined to qualitative studies.

The newer (~1977) technique of speckle photography allows for acquisition of the motion in a cross section of a fluid. The fluid is illuminated by a monochromatic sheet of pulsed coherent light. A random pattern of speckle pairs with variable distance and orientation is imaged at the photographic plane. The resulting *specklegram* can be reconstructed to produce a speckle pattern in which the spacing and orientation of successive speckles are directly related to the motion of the fluid. Additionally the speckles are modulated by Young's fringes which give the magnitude and orientation of the in-plane components of the fluid velocity without the need for particle tracking. As Lauterborn points out [35], the speckle method can be considered as an extension of the usual multiple-exposure technique but makes use of Fourier space for direct orientation determination (the motion sense must still be determined by other methods). An extra bonus with this technique is the easy extension to smaller displacements through the inverse resolution properties of space and the Fourier domain.

Holographic techniques allow the phase information from phase objects such as density variations or particle distributions to be stored and reconstructed later. The reconstruction can be done with a new state of the flow system to produce an interference pattern highlighting the differences between say a quiescent or steady flow state and a more vigorous flow. This reconstruction can be performed for a single instant in time

in what is known as double-exposure holographic interferometry. It can be done continuously in the case of real-time interferometry. In order to overcome accuracy and processing speed limitations of holographic interferometry, heterodyne reconstruction can be used to increase the resolution by orders of magnitude.

Tomography is a method of image reconstruction from multiple projections. According to Lauterborn it shows promise but as of 1984 was just starting to be applied to the study of fluid flow.

The use of flow visualization has elucidated the presence and role of structure in turbulent flows, however most of the reports have been confined to qualitative descriptions of the structure properties. A notable exception is the work of Hernan and Jimenez [36] who quantified the spatial extent of mixing structures in the developing mixing layer. They used a computer-automated geometric identification on ciné film recordings of regions of active mixing highlighted with reactive gases. The identification involved fitting ellipses to the visually distinct mixing regions. They examined the growth and pairing history of the elliptical structures. and growth evolution. Because of the visualization method employed little could be said about the reasons for the observed evolution as the velocity field cannot be extracted from such data.

The contouring of the hydrogen bubble wire visualization (an interesting variation of the tracer method) and picture processing data of Utami and Ueno [39] are suggestive of coherent structures. Mory and Hopfinger [40] used particle tracking to extract structure functions in a rotationally dominated turbulent flow and Sheu et al [41] used a three-dimensional measurement technique to extract bulk flow data from the motion of tracers

in a mixing chamber.

Tracer particle techniques in general are well suited to quantitative analysis. The time-exposure method has been used in the laboratory since the early days of fluid dynamics research. Indeed, part of the inspiration for the present work came from study of a large private collection of photographs of fluid motion made by F. Ahlborn in the early decades of this century [37]. In this technique, optically reflective particles are placed either in a fluid for volume studies or on a fluid for surface studies. It has been used for quantitative studies of two-dimensional laminar flows for nearly a century by measuring streak properties from tracer images recorded on time exposed photographs. A number of variations on the time-exposed particle tracking technique have been used in this thesis work.

Before going on to present the analysis methods used in this thesis to identify and analyze coherent structures some observations of other authors is presented. The term 'coherent structure' is used to describe a region of flow which has a more predictable structure and evolution internally than it does with its surroundings. Lumley [42] has suggested that coherent structures are significant in "young" flows which are still influenced by production geometry. He suggests that the current discoveries of coherent structures are partially a result of researchers looking in early flow regimes with flow generation apparatus having more quiescent preconditions. This however, does not explain the emergence of large scale coherent structures from an initially random vorticity computer modelled flow [43]. It is this author's belief that coherent structures are in some cases a property of the initial flow conditions and in others an intrinsic property

of the subsequent fluid mechanics. It is quite possible that the mechanics governing the motion of fluids allows for an infinite variety of behaviour.

At present there appear to be as many or more coherent structure identification algorithms as there are researchers. This is due in part to the newness of the research and in part to the variety of flows studied and tools used in these studies. Researchers using anemometers have been quick to supply prescriptions for coherent structure identification. Hussain [44] has tried to come up with the canonical definition of a coherent structure. He calls a coherent structure,

> "A large scale connected region of fluid mass having a phase correlated vorticity over its spatial extent."

Hussain's method requires a previous bias as to where or when the structures may be found and will only work for structures repetitively generated. His use of anemometry is evident in the expression, "phase correlated vorticity".

Lumley [42] has proposed a recognition method which avoids the use of conditional sampling which he feels allows for too much of the experimenter's bias to enter into the data collection. Lumley's "eigenfunction" approach is an orthogonal decomposition of a velocity record using gaussian vorticity distributions as the basis functions. The method is rooted in the statistical description of turbulence and the use of point velocity probes. It predefines the basis functions and so cannot be said to be a completely "non-prejudicial" approach.

The definition used for the automated structure recognition in this thesis is;

> A connected, large-scale fluid mass outlined by the closed contour of minimum angular velocity, within which there exists one, and only one, local maximum in angular velocity.

Implicit in our definition is that it be applied to analysis of two dimensional flow fields. The identification of structures based on this definition is described in section 3.3.2. While not strictly needed, the condition that the structure be "large-scale" is used to remove angular velocity peaks of size too close to the resolution limits of the analysis system.

It has been the advent of the high speed digital computer and image acquisition, processing and analysis techniques which has opened the door for a truly quantitative analysis of image derived velocity fields in unsteady and turbulent fluid flows. The application of this technique is furthermore not limited to two-dimensional flows. The flow analysis system used for the structure dynamics section of this thesis constitutes a fully automated flow field acquisition, processing and analysis package. The work at UBC appears to be the first to use particle tracking to obtain flow fields for coherent structure analysis. The system has been described in detail in the M. Sc. thesis by Lau [38]. A summary of its principles and methods appears in the next section.

3.3 Our Methods

3.3.1 Manual Analysis

For the structure statistics studies of chapter four a manual method was used to identify the eddies. The raw data for those experiments were a number of time exposed photographs of tracer particle paths such as Figs.4-1. The analysis of these photographs consisted of identifying the visually observed regions of closed coherent motion by tracing

the largest closed contour following the tracer paths. An eddy radius was then defined as the radius of a circle having an enclosed area equal to that of the structure. The manual recognition of the structure geometry was completed by assigning an eddy center as the position about which the motion appeared to rotate. The internal velocity structure of the eddy was then recorded in a mechanical though tedious procedure using a digitizing table. While this method suffered from personnel subjectivity and fatigue* it was useful in obtaining a description of the structure statistics.

3.3.2 Automated Analysis

The structure recognition was subsequently formalized and automated in the M.Sc. work of Alexis Lau [38] and used for the structure dynamics part of the present thesis. What follows is a summary of the method as presented in a paper recently submitted by Lau, Loewen and Ahlborn [8].

Figure 3-3 shows the computer-automated flow field analysis system developed at UBC. The flow was visualized by recording successive aluminum tracer positions on a video tape. Each video frame was then digitized as a binary 256×192 pixel array by a Micro-Works DS-65 digitizer residing on an Apple II microcomputer. Figure 3-4 shows one of the less noisy digitized frames. The digitized data were transferred to the UBC mainframe computer where all subsequent analysis was performed.

The procedure for the noise reduction was to fill in holes and remove isolated pixels while preserving meaningful connectivity. A dynamic tree search following adjacent points ("on" pixels) was used to create a list of the position and size of each tracer for

* About 800 person-hours were needed to analyze the statistical data used below.

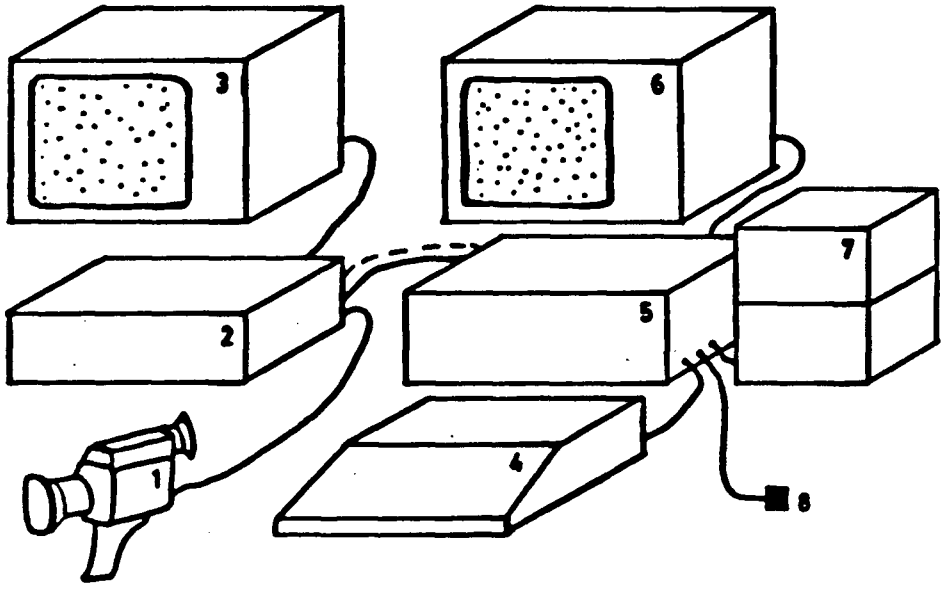

1 video camera
2 video recorder
3 TV for video system
4 microcomputer keyboard
5 microcomputer with VCR controller and digitizer
6 microcomputer display monitor
7 mini disk storage drives
8 telecommunication link to mainframe computer

Figure 3-3 Flow field analysis system.

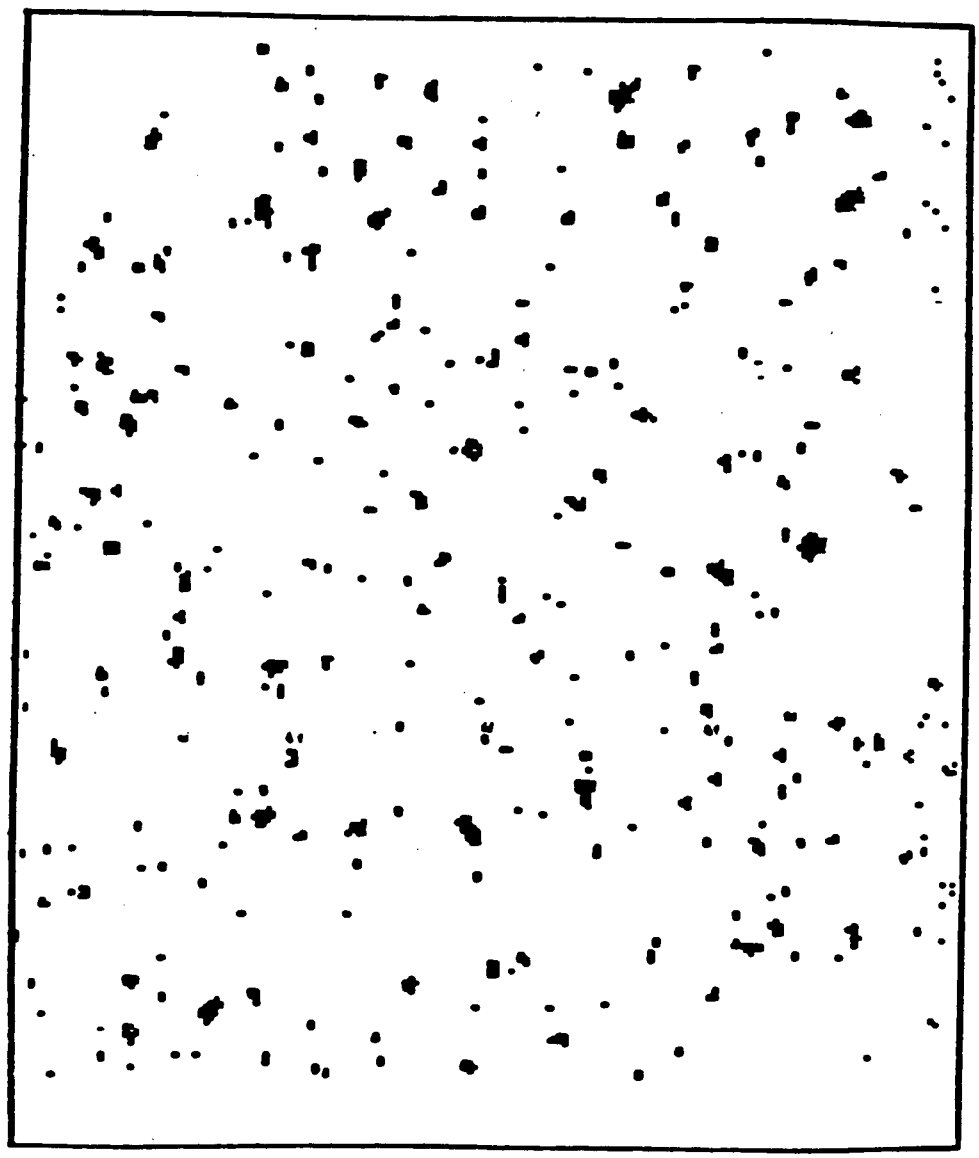

Figure 3-4 Raw digitized image. Binary 256 × 192.

all of the digitized frames. The flow history was then reconstructed by tracking and connecting the successive tracer positions shown in Fig.3-5.

The tracking procedure was a bootstrap search using a polynomial fit to project the most likely next particle position. For each new frame of data, the position and size of candidate tracers determined the best match with the previously tracked paths. The final result is a time connected list of tracer particle positions over the exposure time of the run - *a streak.* Figure 3-6 shows a sample connection. Streak trajectories were then fitted by polynomials to give various flow parameters of interest over desired flow times. In particular, the linear and angular velocities were determined from the successfully tracked data. The scattered set of values were then interpolated onto an equally spaced grid to provide angular and linear velocity fields for the subsequent analysis. In the automated analysis the angular velocity is determined with respect to the point determined by the local radius of curvature. This is different from the method used in the manual analysis where the angular velocity was determined with respect to the visually assigned structure center.

Coherent structures were identified by applying our definition to the field of angular velocity. From the interpolated mesh fields of linear velocities, each structure was parameterized with properties like size, average linear and angular velocity and internal kinetic energy. The flow kinematics, dynamics and interactions could then be studied using these structure parameters.

The definition of a coherent structure must be understood before deciding which parameters are to be extracted from the trajectories. Definitions based on vorticity are

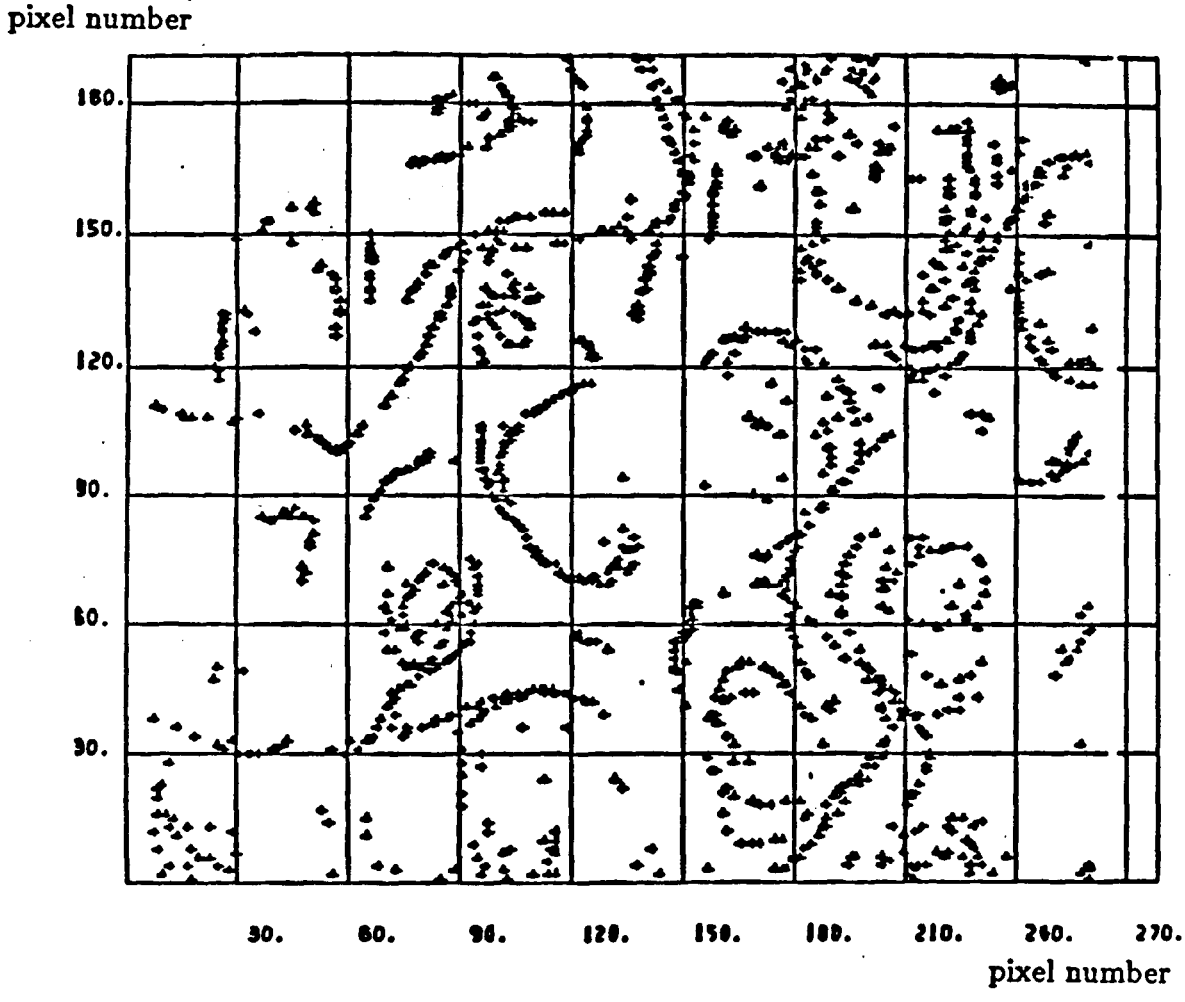

Figure 3-5 Successive tracer centers. Superposition of 15 frames.

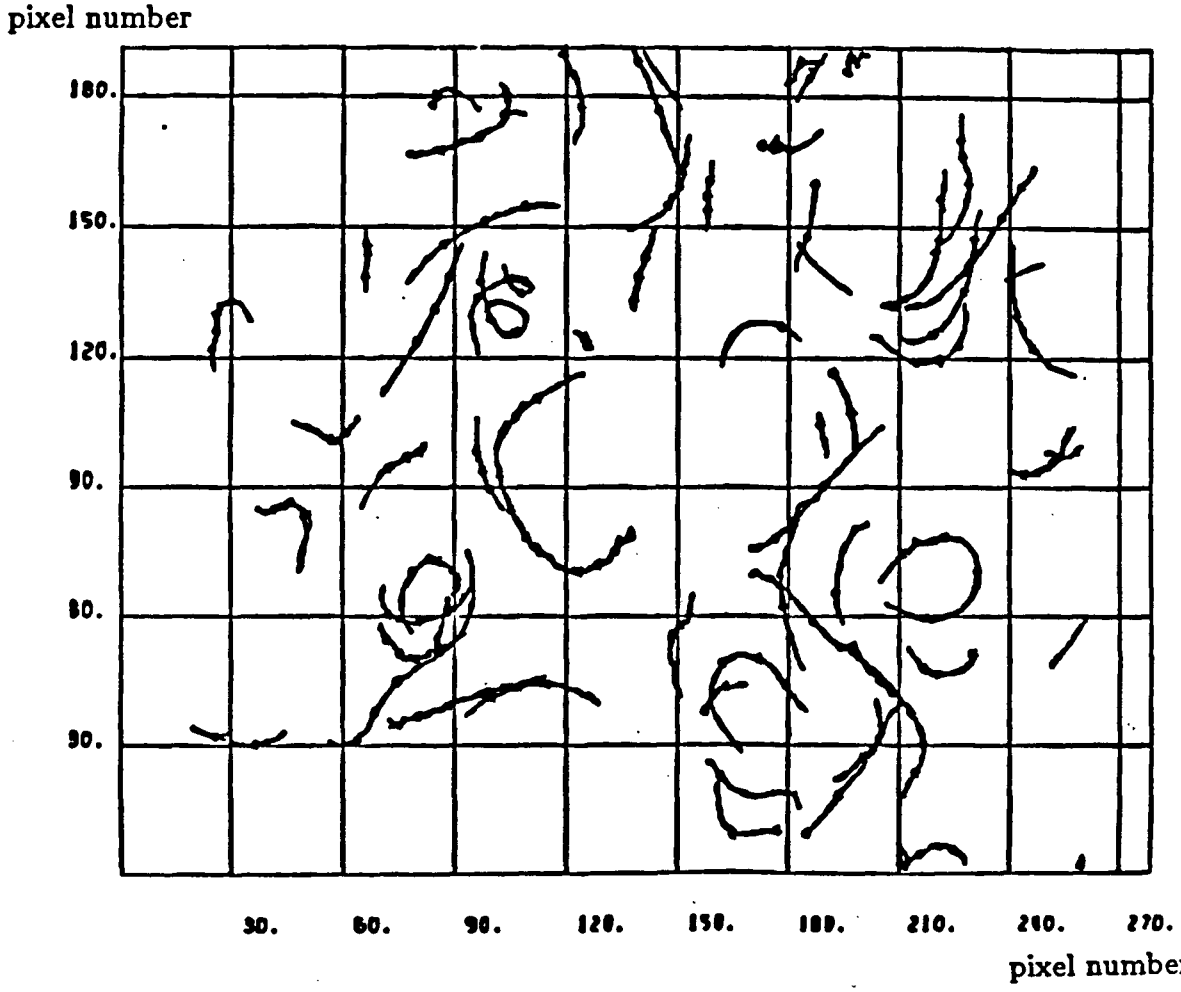

Figure 3-6 Tracked tracer paths.

commonly used in the literature. However our diagnostic technique together with the close relationship between vorticity and angular velocity for our two-dimensional flow motivate our use of a definition based on angular velocity. For the structure dynamics studies a coherent structure -*an eddy*- is defined here as:

> A connected, large-scale fluid mass outlined by the closed contour of minimum angular velocity, within which there exists one, and only one, local maximum in angular velocity.

To extract information about these coherent structures the streak data is first processed to produce the interpolated mesh field of angular velocity. From this grid, local maxima are located and then the bounding contour for each peak is found. As two or more adjacent positions may have the same extremum value, the peaks cannot be located just by local consideration (a computationally efficient way to proceed). As Lau puts it in his thesis, 'The task is similar to the problem of finding a mountain top in a forest when one is lost and cannot see too far. The motto is "keep on climbing up your steepest track, do not descend or turn back on a level track." If a non-decreasing track can no longer be found, one must be at a local maximum.'

Figure 3-7a shows the results of applying our definition to a sample one dimensional scalar field. The recognition process is implemented by first "climbing" from each point on the grid until either a peak or a previously marked path is found. In the latter case the climb is terminated and the path number is reassigned to equal the one encountered, see Fig.3-7b. Corresponding to the actual angular velocity grid, an identification grid is used to record the path numbers. Once expeditions have started from every grid point

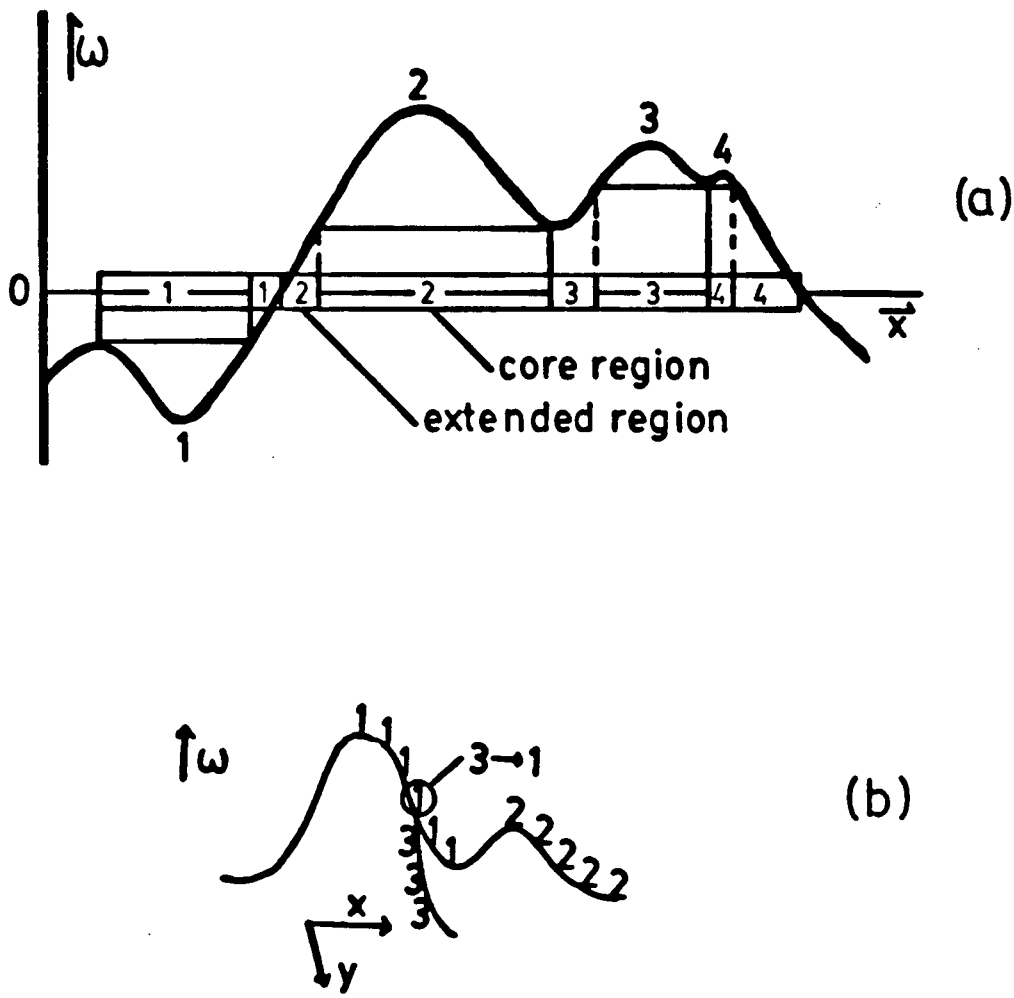

Figure 3-7 Coherent structure identification. (a) Sample one dimensional scalar field. (b) Path number assignment.

we have effectively determined distinct, internally connected regions within which a non-decreasing path exists between any grid point and its peak. Each of these regions define an *extended region.*

The second problem of finding a minimum closed contour around the peak is now straightforward. We simply find the maximum angular speed among all the values of the boundary points. Any contour value higher than this will definitely enclose the peak without entering into another region. Once this value is found, the core of the coherent structure is defined as the area within the extended region for which the grid-points have values higher than this one. This completes the operational procedure to find the boundary of the coherent structure. It should be noted that in our procedure all points in the flow field are associated with either the core or extended region of a coherent structure. After the initial identification the data set is further refined to remove small scale structures. This is consistent with our interest in large scale structures and is done by removing possibly mistracked streaks which are inconsistent with the rest of the data. The entire analysis procedure is then repeated on the refined data.

Figure 3-8 shows the coherent structures identified by applying the analysis to a two-dimensional velocity field obtained from the grid-flow experiments. The identified regions correspond closely to our intuitive notion of a coherent structure. Figure 3-9 shows the same plot but with angular velocity contours overlayed. The analysis system just described was used for the structure dynamics studies of chapter 5. Before going on to present the results of this work, a section on how anemometry based flow field analysis is used in the study of structure in flows.

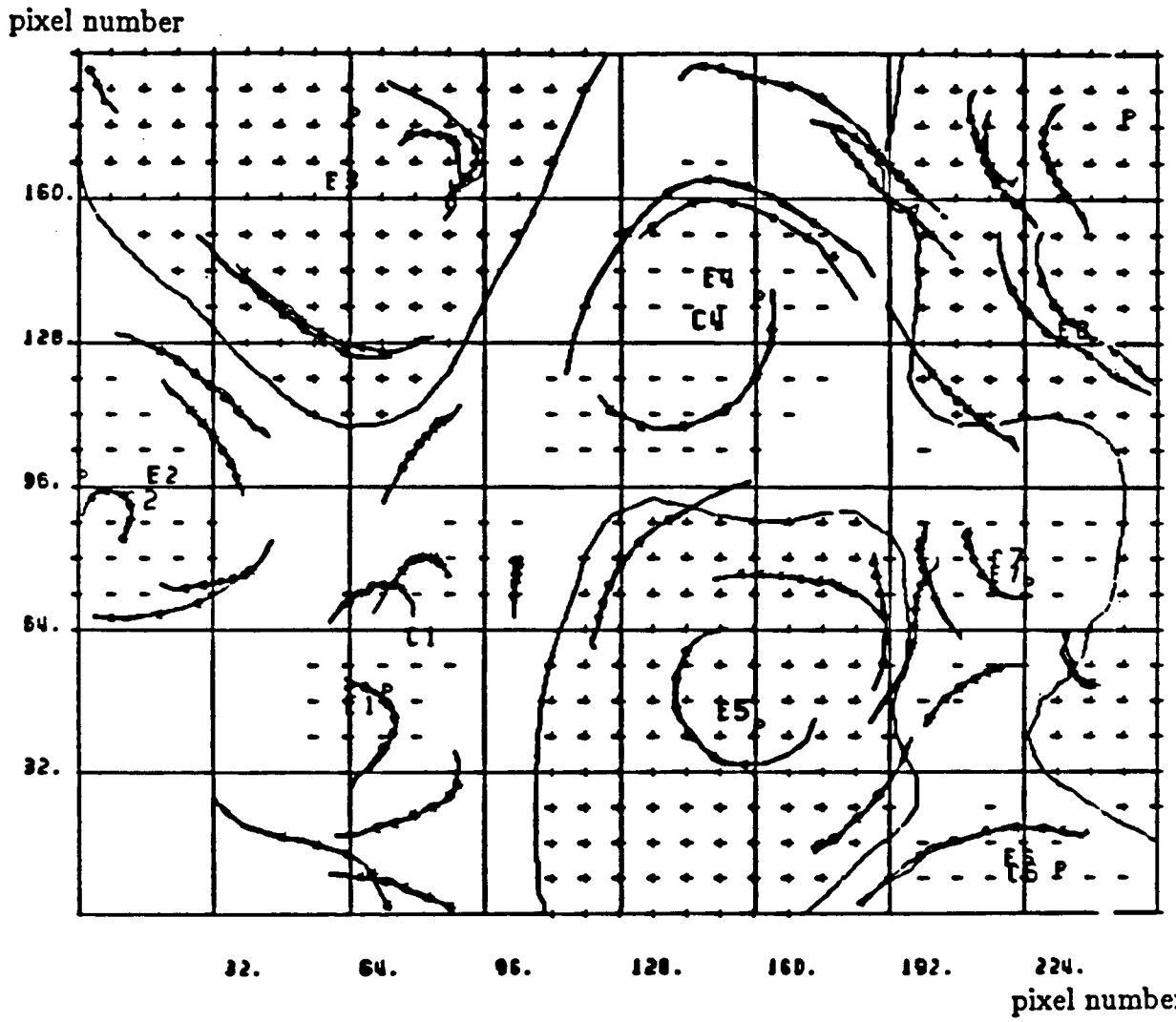

Figure 3-8 Identified structures. 1 second (30 frame) streaks. + indicates counter-clockwise rotation - indicates clockwise rotation

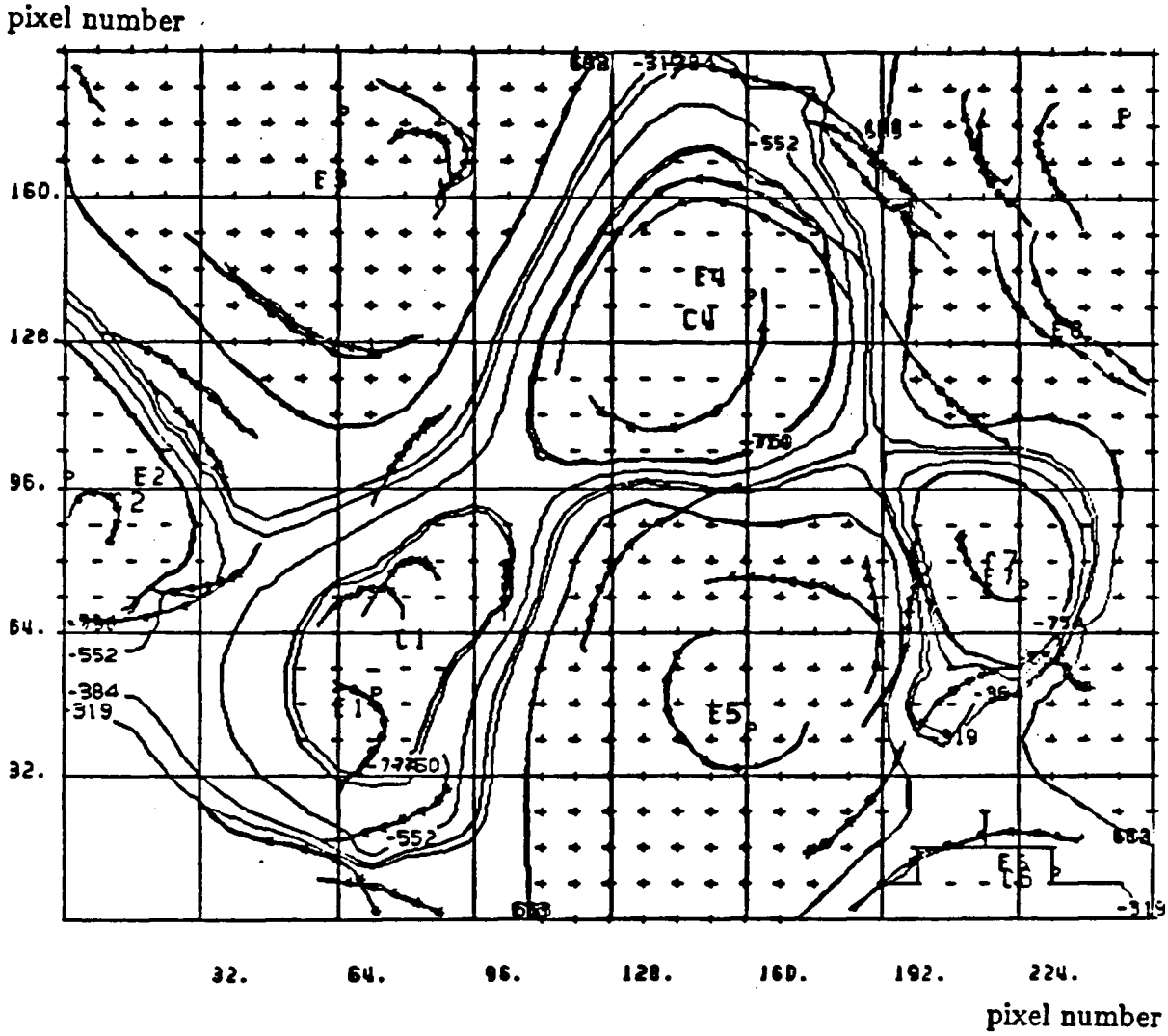

Figure 3-9 Contour plot of identified structures. + indicates counter-clockwise rotation - indicates clockwise rotation

3.4 Anemometry Based Flow Analysis

It was the development of hot-wire anemometry in 1935, coincident with Taylor's statistical theory of turbulence [45] which allowed researchers to measure fluid velocities at points in a flow continuously and accurately. The very high frequency response and reasonable spatial resolution of these devices makes them well suited for studying time varying velocities. The impact of hot-wire anemometry to the study of turbulent fluid flow has been enormous. The laser doppler anemometer is a less intrusive point probe which produces data similar to the hot-wire. Pitot tubes are useful for measurement of steady or slowly varying velocity fields.

Together with a suitably adjusted linearizer a hot-wire anemometer, in its most basic configuration, produces a voltage signal proportional to the longitudinal speed of the flow. This signal can be electronically averaged or high-pass filtered to obtain the mean and fluctuating velocity components respectively.

The principles of the statistical approach to studying and modelling turbulence have already been presented in the last chapter. In this study of grid-generated turbulence, Fourier analysis of hot-film anemometry derived velocity records was used to examine the near-surface fluid dynamics. The most convenient quantity to measure was the spectral density of the u_1 fluctuating component, $E_{11}(f)$ at a given position $\vec{x}$. $E_{11}(f)$ is twice the component of the kinetic energy per unit mass due to longitudinal velocity fluctuations, u_1, at temporal frequency f. The power spectral density can be obtained by Fourier analyzing the fluctuating velocity component $u_1(\vec{x},t)$ measured with a directionally sensitive

probe at a fixed position $\vec{x}$. To see this, we first write the time dependent longitudinal fluctuating velocity $U_1(t)$ in its Fourier representation,

$$u_1(t) = 2\pi \int_{-\infty}^{\infty} df[a(f)cos(2\pi ft) + b(f)sin(2\pi ft)]. \qquad (3-1)$$

$a(f)$ and $b(f)$ are the Fourier coefficients for the periodic basis functions of frequency f,

$$a(f) = \frac{1}{\pi} \int_{-\infty}^{\infty} dt u_1(t) cos(2\pi ft) \qquad (3-2a)$$

$$b(f) = \frac{1}{\pi} \int_{-\infty}^{\infty} dt u_1(t) sin(2\pi ft). \qquad (3-2b)$$

The power spectrum, $E_{11}(f)$, is obtained from the Fourier coefficients as

$$E_{11}(f) = \frac{1}{\tau}\pi^2[a^2(f) + b^2(f)] \qquad (3-3)$$

for sampling time τ.

The power spectrum may alternately be defined in terms of the autocorrelation $C_{11}(T)$ of eqn.(2-24). These two functions form a cosine transform pair,

$$E_{11}(f) = \int_0^{\infty} C_{11}(T) cos(2\pi fT) dT \qquad (3-4a)$$

$$C_{11}(T) = 4 \int_0^{\infty} E_{11}(f) cos(2\pi fT) df \qquad (3-4b)$$

The limits of integration are from 0 to ∞ as $E_{11}(f) = E_{11}(-f)$ and $C_{11}(T) = C_{11}(-T)$ for statistically steady flows.

The two definitions of $E_{11}(f)$, eqns.(3-4a) and (3-3), are equivalent. To see this we insert the Fourier representation for $u_1(t)$, eqns.(3-1), into the definition of the autocorrelation, eqn.(2-24). Multiplying the velocity representations and integrating out the

cross terms in $a(f)$ and $b(f)$ we have

$$C_{11}(T) \equiv \overline{u_1(t)u_1(t+T)} = lim_{\tau\to\infty}\frac{1}{\tau}\int_0^{\tau} df[a^2(f)+b^2(f)]cos(2\pi ft). \qquad (3-5)$$

The cosine transformed quantity in this expression is equivalent to the definition for $E_{11}(f)$ in eqn.(3-3). From eqn.(3-4b) we see that

$$C_{11}(0) = \int_0^{\infty} E_{11}(f)df \qquad (3-6)$$

Using eqn.(2-24) for the autocorrelation we have

$$\overline{u_1^2} = \int_o^{\infty} E_{11}(f)df \qquad (3-7)$$

This equation identifies the total fluctuating kinetic energy $\overline{u_1^2}$ with the area under the power spectral density curve.

The temporal spectra at position $\vec{x}$, $E_{11}(f,\vec{x})$, may be related to the spatial structure of the flow. Applying Taylor's hypothesis to the power spectral density measurement we arrive at the relation

$$\Phi_{11}(k,\vec{x}) = \frac{1}{2\pi}U_c E_{11}(f,\vec{x}). \qquad (3-8)$$

The power spectral density is related to the k_{11}-wave number spectrum $\Phi_{11}(k,\vec{x})$ through the longitudinal convection velocity U_c at which the probe samples the flow field. This is the Fourier transform equivalent of the relationship between the spatial and temporal correlations. This includes the same restrictive assumptions, namely that the convection velocity U_c is constant and that the flow does not change appreciably while the probe

samples a distance greater than the length scales of interest. Using the definition of the integral time scale T_e, eqn.(2-25), in eqn.(3-4a) for $f = 0$ we see

$$E_{11}(0) = 4\overline{u_1^2}T_e. \qquad (3-9)$$

And applying Taylor's hypothesis in the form of eqn.(2-27) we see that the integral length scale can be obtained from the power spectral density $E_{11}(f)$ as

$$L_e = U_c E_{11}(0)/(4\overline{u_1^2}). \qquad (3-10)$$

L_e is interpreted as being the average size of the energy containing structures. It is one of the most basic parameters used to describe the spatial structure of a turbulent flow field. This length scale determination is used in the comparison of anemometry and flow visualization presented in the near surface fluid dynamics study of section 5.1.

Over the last two decades, the technique of conditional sampling has been developed for the study of structure in anemometry signals. According to a review by Antonia [46] it has been applied to the study of the turbulent-nonturbulent interface of shear flows, shear layers perturbed by interaction with another field of turbulence, periodic flows and to the study of coherent structures in different shear flows. Conditional sampling is a process used to highlight specific features of a flow by only sampling the flow field when certain previously selected conditions are met. It has been used by the anemometry community to provide quantitative information to complement qualitative observations of coherent structures obtained from flow visualization studies.

This chapter has presented some of the major experimental techniques available for the study of turbulent fluid flow as well as the methods used in this thesis work. The next chapter describes the statistical study of turbulent grid-flow performed by the author.

CHAPTER 4
STRUCTURE STATISTICS

"One must learn by doing the thing; though you think you know it, you have no certainty until you try."
Sophocles 495-406 BC

The experimental methods have been presented in the last chapter. This chapter describes an investigation of the statistics of coherent structures on the surface of a turbulent body of fluid. After finding the structures it was necessary to see if they could be identified and characterized in a simple but useful manner. Next, it was of interest to see if the structure statistics could be simply described. Answers to both these questions should contribute to our understanding of the role that coherent structures play in a turbulent flow. The experimental observations are given first, followed by a statistical analysis of the size and energy distributions of the open (river-flow) and closed (eddy-flow) coherent motions. In the last section of this chapter, the measured eddy energy statistics are used to infer values for the rate coefficients.

4.1 Experimental Observations

The experimental apparatus has already been described in chapter 3. Figures 4-1(a),(b),(c) show a series of photos taken in the lab frame of reference with the cart moving from right to left at the speed U_g = 20cm/sec. The interframe separation is 3 seconds. The left side of Fig.4-1(a) shows the receding grid while the right side of Fig.4-1(c) is at an average distance of X=200cm from the grid, corresponding to about 40 mesh widths. A non-dimensionalized distance scale in units of mesh widths ($X' = X/M$) is shown in Fig.4-1(a).

The exposure time of each frame is 1 sec. Hence a typical streak of 1cm path length indicates a local speed of u_o = 1cm/sec. For distances greater than a few mesh widths from the grid the flow patterns did not evolve significantly during the 1 sec exposure time. The average speed thus corresponds closely to the instantaneous value. It should also be noted that for photos taken in the fluid reference frame u_o is small compared to the cart speed of $U_g = 20cm/sec$. Photos taken in the cart frame of reference show practically straight streaks without clear indication of coherent structures and are not suitable for this analysis.

The time evolution of the flow can be studied on subsequent frames by comparing the same region of flow, for instance, the lower right corner of each photo in the sequence of Figs.4-1. If one is interested in statistical averages, sections of the flow in some interval ΔX centered about the average value X can be examined. Figure 4-1(b) shows such a sample bin. The X scale given below each photo shows some overlap, so that

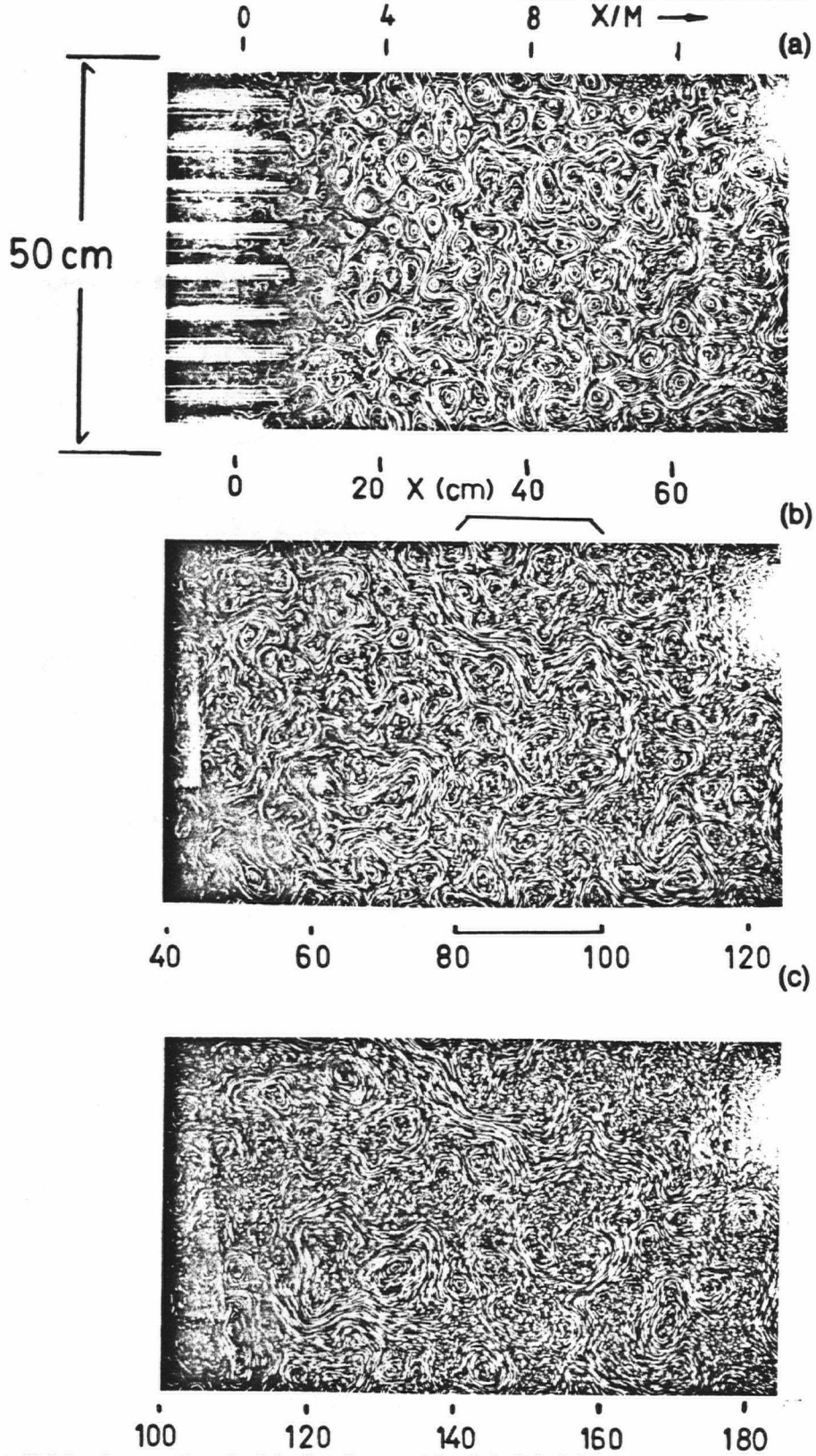

Figure 4-1 Eddy formation behind a bar grid. (a),(b),(c), viewed in fluid frame $\tau_{exp} = 1sec$ taken at time intervals of $\Delta t = 3$ sec.

the distribution obtained from an interval at the right edge of Fig.4-1(b) should be statistically equal to the distribution obtained from the left edge of Fig.4-1(c).

For the structure statistics analysis ten photographic series containing about 20,000 individual streaks were traced by hand and their endpoint positions were digitized and transferred to computer memory. Streaks contained within a manually identified structure boundary were grouped while other streaks were considered to be part of the inter-eddy (river) flow. The flow field was analyzed only in the center section of the towing tank where it is not affected by the side walls. This thesis reports analysis results for U_g = 20cm/sec (a mesh Reynolds number of 10,000) although qualitatively similar results were found for 30 and 40cm/sec grid speeds [30].

The flow photos show clear evidence of organized fluid motion. One can distinguish relatively stagnant areas, where the filings produce points instead of traces, and moving sections, where the streak length is proportional to the local fluid speed. The moving fluid appears to undergo either locally rotating motion with closed streamlines (surface eddies), where a local angular speed ω can be defined, or it shows predominantly translational motion that may be characterized by an average river speed u_o. A small number of rapidly decaying eddies were observed, but for the statistical analysis the surface flow is considered to be composed of either eddies with angular speed ω, rivers with translational speed u_o, or stagnant fluid where u_o and ω are negligible. Both eddies and rivers can store kinetic energy that contributes to the internal energy of the unsteady surface flow.

For the purpose of obtaining a statistical description of the eddies, their boundary is determined by enclosing the largest area while drawing a closed line following the

visible tracers. This definition is similar to that of "the minimum closed angular velocity contour" for the automated recognition of structure cores described in the last chapter. Typical eddy identifications using the manual method are shown in Fig.4-2. After the structure is outlined, an eddy radius is assigned as the radius of a circle enclosing an area equal to that covered by the structure. It was found that three observers independently assigned radii that differed by less than 5%. Structure centers were assigned as the position about which the surface eddies appeared to rotate.

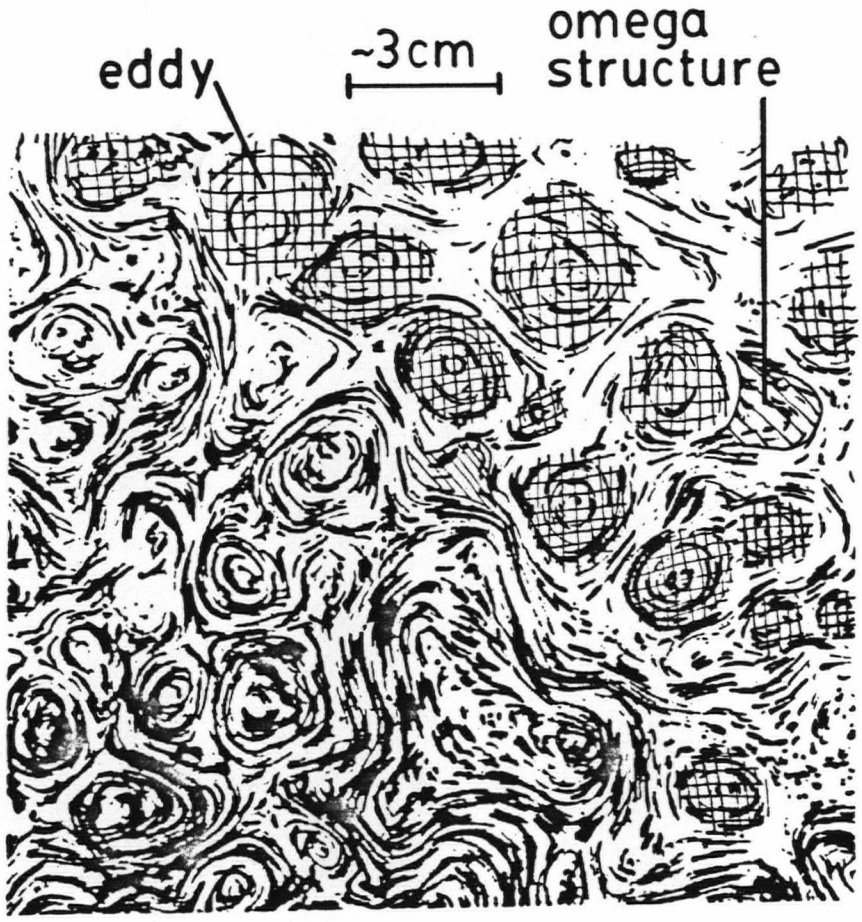

Figure 4-2 Typical structure identification.

For the 20cm/sec grid speeds vertical displacement of the fluid surface was observed to be less than a few millimeters. Significant near-surface vertical motion must therefore be accompanied by converging or diverging flow at the surface. This would appear as relatively stagnant regions of the material surface. If the accompanying stress was strong enough to overcome the surface incompressibility, one would record either convergent or divergent tracer motion. For cart speeds less than 50cm/sec (grid Re $\approx$ 25,000) no signs of subsurface vertical motion were found on the flow photos. One can therefore consider the surface motion for $U_g = 20cm/sec$ as being two-dimensional.

The relative abundance of open and closed structures is easily determined. One has to measure the surface area fraction or concentration $c_e = S_e/S_b$, $c_r = S_r/S_b$, and $c_{st} = S_{st}/S_b$ of eddies, rivers and stagnant areas. For this purpose the total surface areas of all eddies S_e, of all the rivers S_r, and of all the stagnant areas S_{st} were measured and divided by the total area analyzed, the bin area S_b.

Figure 4-3(a) shows the concentration of these flow components as a function of position X. The statistical analysis was performed in $\Delta X = 20cm$ wide bins. The distance X is the center of the bin. The downstream distance can alternately be quoted in terms of the number of mesh widths (X'). Between X=0 and X=20cm ($X' = 4$) the motion and evolution is too rapid to be analyzed from photos such as Figs.4-1. The near grid eddy concentration, c_o, is obtained from a simple initial vortex production model described in the next chapter. After the initial production the eddy area fraction c_e decays while the fractions of river area c_r and the stagnant area c_s increase. About 20 mesh widths downstream, the river area fraction starts to decrease as well. This follows the ultimate dissipation of the grid induced motion to a quiescent state. When the eddy area fraction

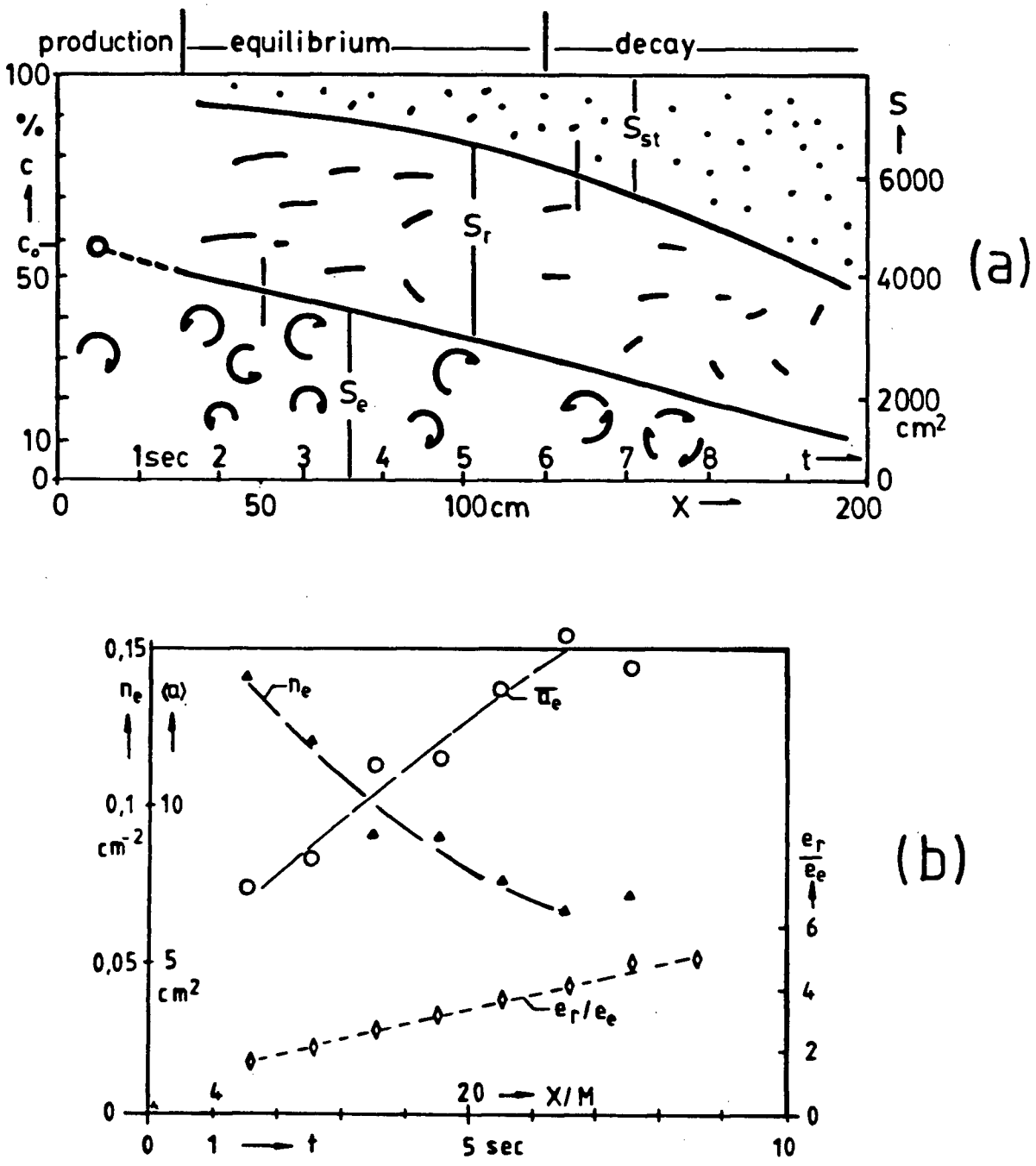

Figure 4-3 Evolution of surface flow pattern. (a) Fraction of surface are S covered by eddies S_e, rivers S_r, and stagnant fluid S_t. (b) Eddy number density n_e, average eddy area $\overline{a_e}$, and energy density ratio e_r/e_e.

c_e is high one expects significant interaction between eddies, so that the eddy distribution should be governed by eddy "collision" processes. When the eddy fraction becomes low, their distribution will mainly change through (viscous) eddy-fluid and eddy-flow interactions, hence Fig.4-3(a) is divided into the production range $0 \leq X' \leq 6$, a collisional or equilibrium regime with $6 \leq X' \leq 23$ and a (collisionless) decay range with $23 \leq X'$. The production region is defined as the range in which the initial vortex generation is observed to occur. The collisional or equilibrium region is where frequent structure interaction results in an equilibrium energy distribution. In the decay region, the dynamics of the widely spaced flow structures appear to be viscosity dominated. Shown in Fig.4-3(b) is the eddy number density $n_e = N_e/S_B$ (where N_e is the total number of surface eddies) and the average eddy area $\bar{a}_e = 1/n_e$. The latter curve shows a steady increase of the average structure size with downstream distance. The energy density ratio of the two flow types, e_r/e_e, is also shown as a function of distance. Here, e_r and e_e are the average kinetic energies per unit mass of the river and eddy flow structures. The determination of these energy densities is discussed in the following two sections.

4.2 River Flow

The open structures (rivers) appear to have their origin in the momentum defect "shadow" behind the grid bars. The resulting anisotropy in the river orientation decays during the observation period and becomes negligible about X=200cm downstream of the grid. This is in agreement with studies of the bulk flow in which grid-generated turbulence

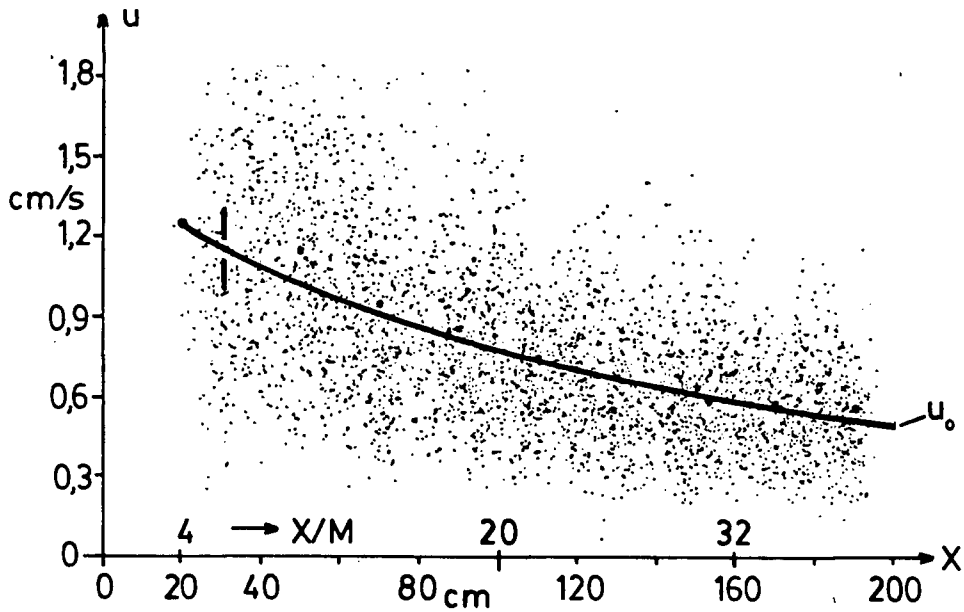

Figure 4-4 River-speed scatter plot. Bin averaged river speed u_o as solid line.

is found to be approximately isotropic within 40 or 50 mesh widths downstream (about 200cm for our experiment) [47].

The speed and positions of a large number of tracers in the rivers were determined from the digitized data. Figure 4-4 shows a scatter plot of these speeds for the grid speed U_g = 20cm/sec. The average speed, $\bar{u}$, is drawn as a heavy line through the point constellation. These raw data have again been divided into 20cm wide bins. The number of points in these bins N(u,X) can then be used to generate energy and speed distribution

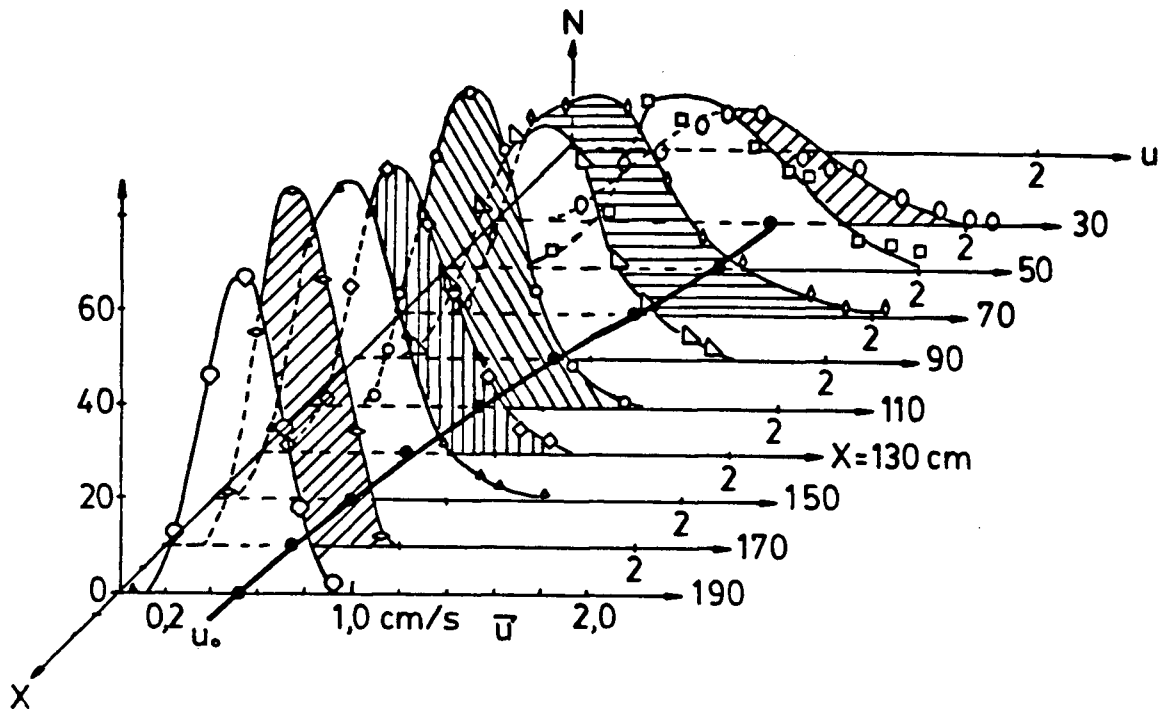

Figure 4-5 Evolution of river-flow speed distribution.

functions. The net translational motion is negligible for this flow as the fluid is confined to the tank and the grid fills the tank's cross-section.

Figure 4-5 shows the speed distribution N(u,X). Figure 4-6 shows the distribution of local kinetic energy

$$E_r = \frac{1}{2} m_r u_o^2, \qquad (4-1a)$$

which can be extracted from the measured data as follows: Each bin in Fig.4-4 can be characterized by an average value for the speed, u_o. In addition, one must assign a value for the average mass $m_r = \rho l a_r$ associated with each streak, because each streak

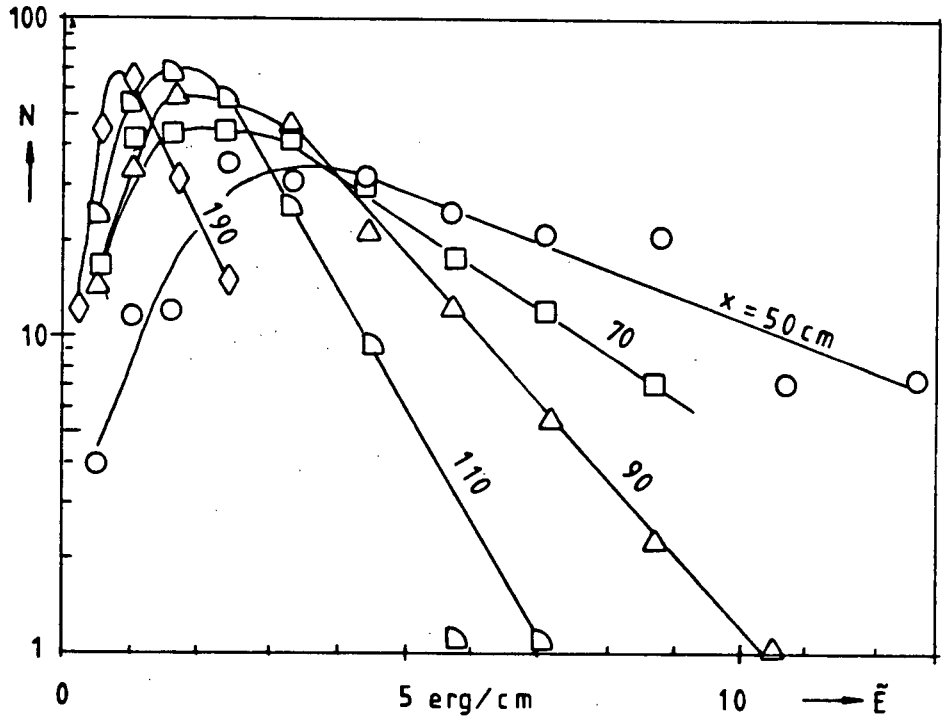

Figure 4-6 River-flow energy distribution.

represents a local patch, of area a_r, of coherently moving fluid. Here l is the depth of the observed surface pattern. The value of the depth which is represented by the surface flow will differ depending on distance from the grid. In particular, the depth will grow with distance downstream, see section 5.1. In the analysis that follows ℓ should be considered to be the very shallow depth of the fluid surface. Assuming that the streaks are evenly distributed one can estimate the average area per streak, a_r, by dividing the total river area $S_r = c_r S_b$ by the total number of streaks, N_r, in the ΔX range. Then $m = \rho l a_r$ was determined at nine X positions and it was found that the average surface area represented

by each streak varied by not more than 10%. The average value is $a_r = 7.1cm^2$ so that the kinetic energy represented by each streak becomes approximately (in cgs units)

$$E = 1/2\rho l a_r u_o^2 = (7.1/2)\rho l u_o^2. \qquad (4-1b)$$

It should be mentioned that the seeding density was much higher than the value of a_r indicates as only a representative sampling of the river speed was performed. Not knowing how far the motion extends into the fluid the energy per unit depth, $\tilde{E} = E/l$, is defined. Another useful quantity associated with the river motion is the energy density

$$e_r = E_r/m_r = u_o^2/2 \qquad (4-1c)$$

Here e_r contributes to the total energy density of the flow with the fraction $e_r c_r$.

As mentioned in the introduction to this chapter it was of interest to see if the energy distributions of the structure populations could be characterized in a simple way. Figure 4-6 shows the energy distributions in semilog plots. The high-energy tail of the distribution can be represented by an exponential characterized by a parameter θ_r. The curve has a half-width $\Delta\theta_r$. In addition, the low-energy part of the distributions were plotted in log fashion and it was found that $logN$ grows approximately proportional to $logE_r$. The data are therefore approximated by

$$N(E_r) = const\ E_r^{\alpha} exp(-E_r/\theta) \qquad (4-2a)$$

where $N(E_r)$ is the number of structures per unit energy interval having energy E_r. The experimental curves all have a well defined maximum N_m at the abscissa $E_m = E(N_m)$. The function (4-2a) has its maximum at $E_m = \alpha\theta_r$, so that $\alpha = E_m/\theta_r$ can be extracted

from the measured position of the maximum. The experimental result from the river energy curves is

$$\alpha = 0.8 \pm 0.1. \qquad (4-2b)$$

Equation (4-2a) is similar to the Maxwell-Boltzmann function used to describe the energy distributions of many interacting systems. Examples are the excitation, radiation, and kinetic energy in plasmas, as well as the kinetic energy of gases. Boltzmann functions are equilibrium distributions and so are only found if the interaction time scale of the system's constituents is small compared to the system's evolution time. In such cases a temperature can be defined for each energy mode by θ, the slope of the graph of $N(E)$ at large E, or $\Delta\theta$, the width of the distribution at half the peak energy. In a plasma, the temperatures of electrons, heavy particles, and electronic excitation or vibration, often differ. We may expect a similar difference between the eddy and river distributions.

In the equilibrium region of the river energy distribution we can interpret the parameter θ_r as a river "temperature" that describes the spread in the river energy distribution. Knowing the constant α, θ_r determines the most probable energy state $E_m(= \alpha\theta_r)$. The distribution functions, Fig.4-6(a), remain Boltzmann type from X=30 to X=130cm. The river energy mode must therefore be in a form of equilibrium that is maintained by a high interaction rate between the structures in the flow. Figure 4-7(a) shows the river temperature θ_r, the energy half-widths $\Delta\theta_r$ and the energy E_m at the maximum of the distribution N_m as a function of distance from the grid. The statistical uncertainty of any θ value is less than 10%. It is surprising how much order exists in the distribution

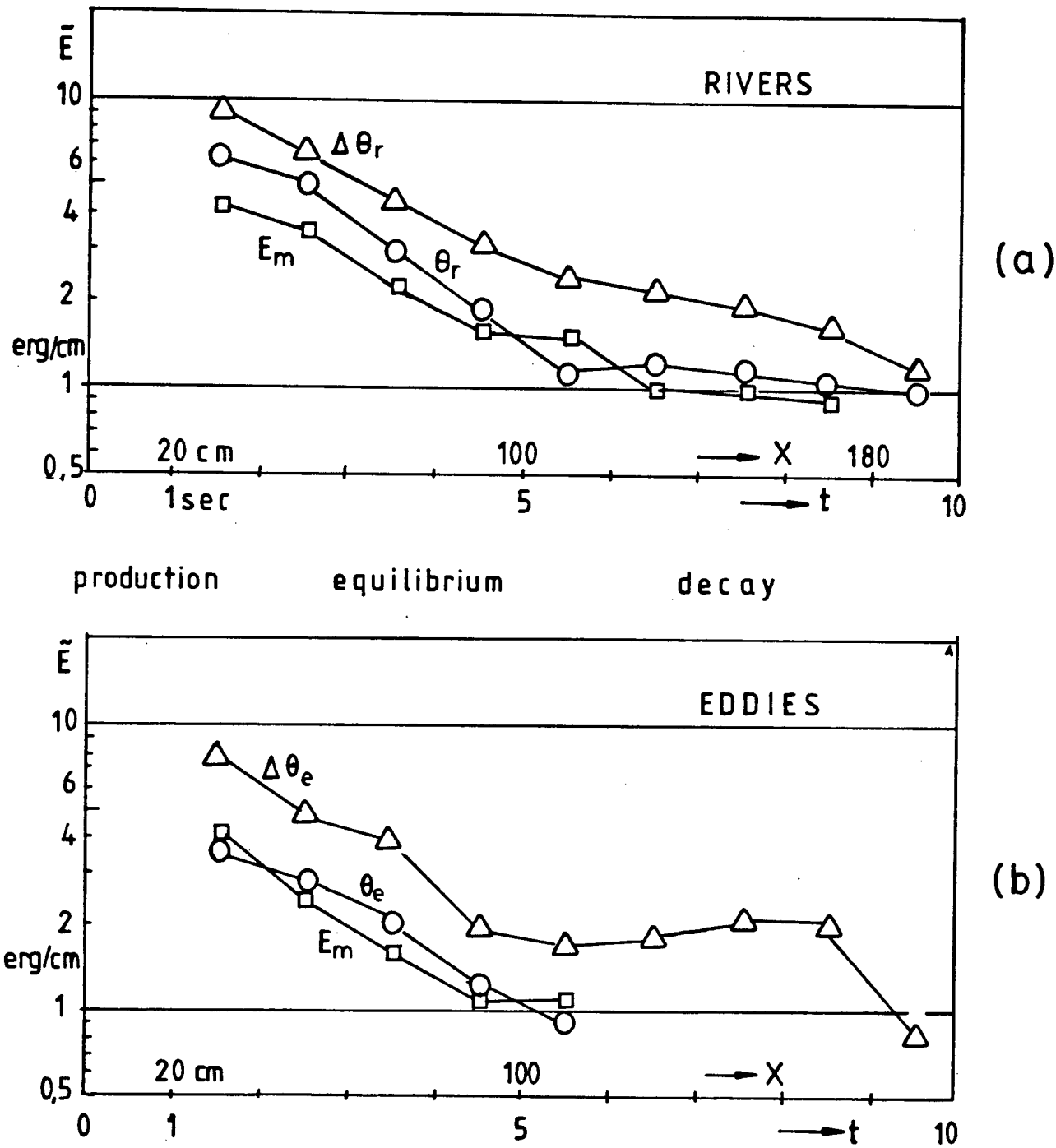

Figure 4-7 "Temperature" decay. (a) River temperature θ_r. (b) Eddy temperature θ_e.

of these open flow structures. It will be interesting to see whether there is a similar equilibrium for the energies of the closed surface structures.

4.3 Eddy Distributions

The closed surface flow structures (surface eddies) are connected regions in which the fluid elements appear to rotate about a common axis. An important feature of our flow visualization analysis is the characterization of the internal flow of the eddies. Typically, eight streaks per eddy were recorded. The average angular speed for each structure was then calculated and averaged for all eddies in a particular size and distance range as follows. We simplify the tracer path information and define the angular displacement σ of a tracer as the angle which the two endpoints of the streak subtend with respect to the estimated eddy center. The angular speed ω is then found by dividing σ by the exposure time. This angular speed at radius R from the eddy center defines a tangential speed $U_R = \omega R$. A typical eddy velocity profile is shown in Fig.4-8(a).

We further simplify each eddy's velocity structure by least squares fitting a rigid body profile (the heavy line) to the internal speeds. An angular speed is thus assigned to each structure. This crude simplification of the internal velocity structure is performed in order to have a simple characterization for used in the structure statistics analysis. More realistic profiles would have a smooth variation in velocity at the structure boundary such as shown in Fig.5-9. Figure 4-8(b) shows how these values are distributed for all eddies in the radius range $1.4 \leq R \leq 1.5$cm which are located in a bin ($\Delta X = 20$cm) centered at X=70cm. An average angular speed was assigned to this sample range as

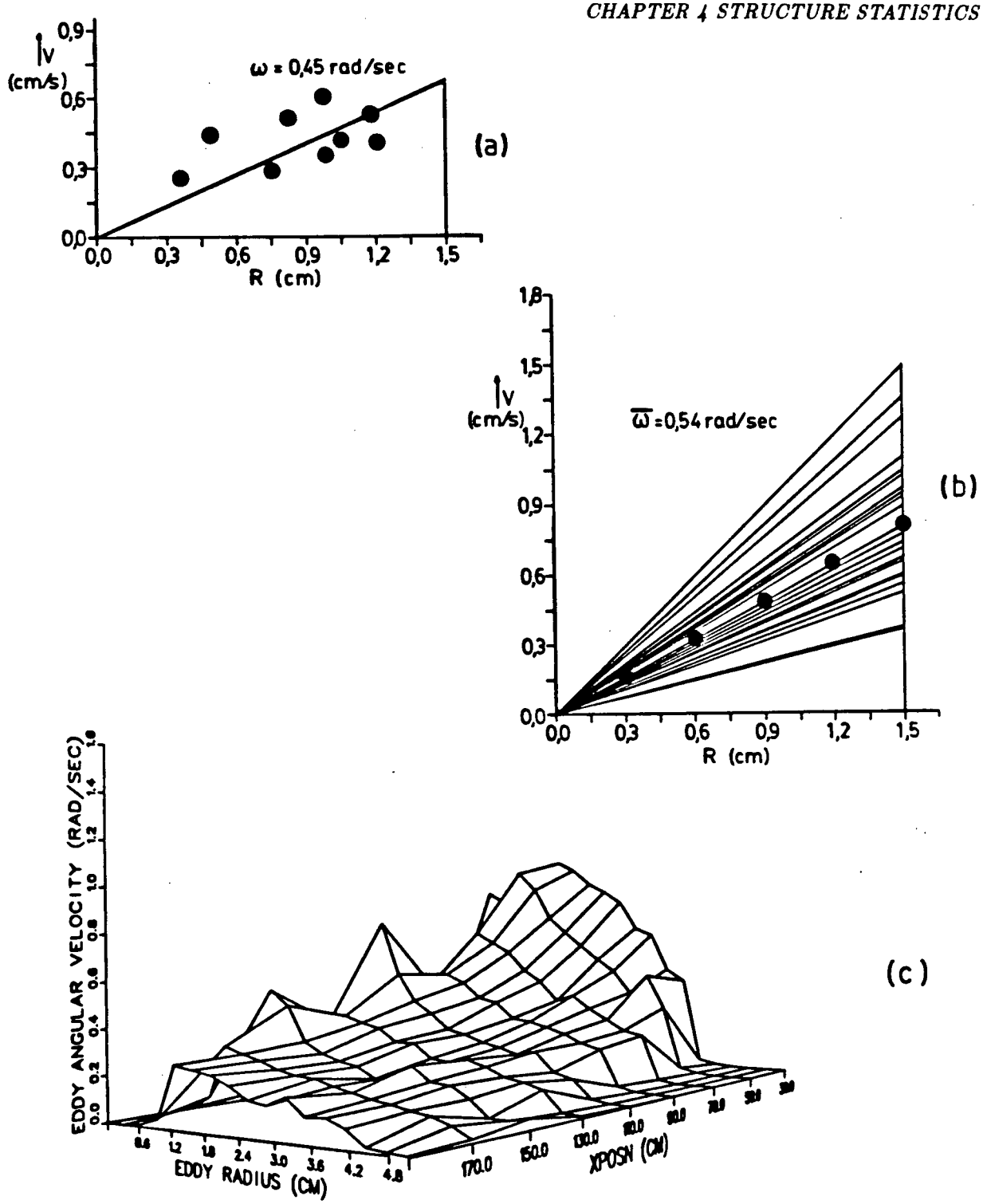

Figure 4-8 Surface eddy flow structure. (a) Velocity profile for an eddy at $X = 71$ cm. (b) Velocity profiles for all 25 eddies at $X = 70 \pm 10$ cm. (c) Angular speed distribution of surface eddies.

indicated by the circled line. Figure 4-8(c) shows the angular speeds of all surface eddies as a function of structure size R and downstream distance X. The general trend is of linearly decreasing $\bar{\omega}$ with increasing R and generally decreasing $\bar{\omega}$ with downstream distance X. The variation in $\bar{\omega}$ for the extreme values of R is due to low sample number.

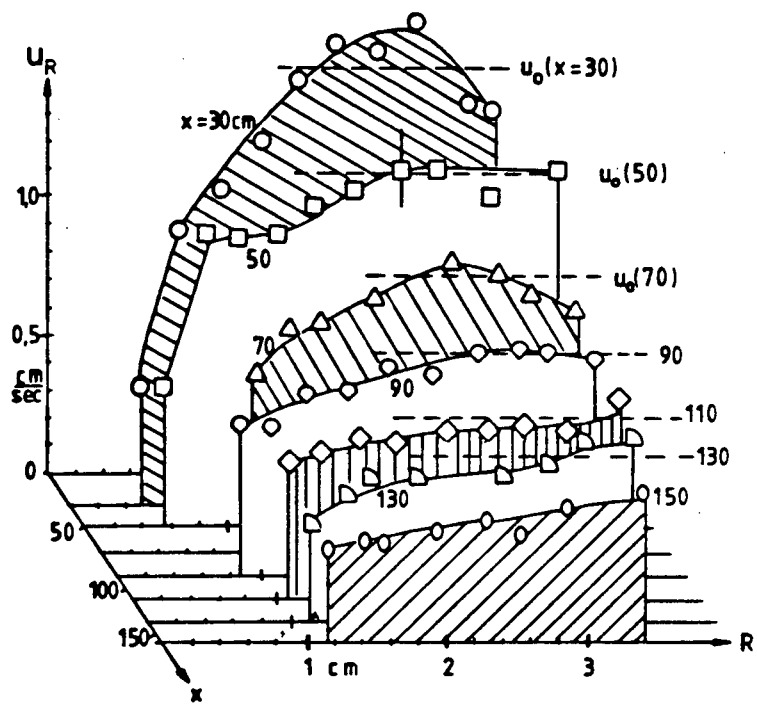

Figure 4-9 Averaged peripheral speed of eddies.

Plotted in Fig.4-9 are the averaged velocities $U_R = R\bar{\omega}$ at the edge of eddies of radius R for the distances analyzed. For comparison the average river velocities are also indicated. It is seen that the small eddies move slower at their edge than the rivers and

some large eddies move faster. However, on average the edge speed U_R is close to the river speed u_o

$$U_R = R_j \bar{\omega}_j \approx u_o. \qquad (4-3)$$

This result can be interpreted as showing that on average the angular speed is inversely proportional to structure size. This experimental observation indicates an effective coupling exists between the eddies and the rivers.

The energy content of eddies can be described by three quantities: the total eddy energy (extracted from our model of rigid body rotation and cylindrical eddies of small depth ℓ)

$$E_j = (1/2) I \bar{\omega}_j^2 = (1/4) m R_j^2 \bar{\omega}_j^2 = (\pi/4) \rho l \; R_j^4 \; \bar{\omega}_j^2 \; (erg) \qquad (4-4)$$

(where I is the moment of inertia and ρ is the density of the fluid), the surface eddy energy per unit eddy depth

$$\tilde{E}_j = (\pi/4) \rho R_j^4 \; \bar{\omega}_j^2 \; (erg/cm), \qquad (4-5)$$

and the eddy energy density, or specific energy

$$e_j = E_j / m_j = (1/4) \; R_j^2 \; \bar{\omega}_j^2 \; (erg/g). \qquad (4-6)$$

All three are functions of the average angular speed $\bar{\omega}$ that is known from the statistical analysis. It would be preferable to consider the mean square angular speed $\overline{\omega^2}$ for this energy analysis as opposed to the square mean $\bar{\omega}^2$ used here. In further study of the structure's speed profile, section 5.4, it is found that these two quantities are proportional to each other. Our use of $\bar{\omega}^2$ will thus affect the magnitude of our inferred energy

quantities by a constant factor and not undermine the analysis to follow. With the experimental observation of eqn.(4-3) one can give these energies as a function of the river speed $u_o \approx R_j\bar{\omega}_j$

$$e_j \cong \frac{u_o^2}{4}, \quad \tilde{E}_j \cong (\pi/4)\rho R_j^2 u_o^2. \qquad (4-7)$$

The total energy density of the turbulent motion is the sum of the river and the eddy energies,

$$e = \bar{e}_r + \bar{e}_e = c_r e_r + \sum_j c_j e_j \approx (1/2)u_o^2[c_r + (1/2)c_e], \qquad (4-8a)$$

where c_j is the concentration of eddies of radius R_j, namely

$$c_j = N(R_j)\pi R_j^2/S_b, c_e = \sum_j c_j \qquad (4-8b)$$

Equation 4-8(a) indicates that the rivers may contain a significant fraction of the total kinetic energy of the surface motion.

The eddy size spectrum N(X,R) can be used to characterize the spatial structure of the rotating coherent motion. The measured data for the 20cm/sec flow are shown in Fig.4-10. Comparing the distributions at various distances from the grid it is seen that the center of the eddy distribution shifts to larger size as the turbulence decays. The increase of the number of large structures stops after about six seconds ($X = 110cm$ downstream), when the eddy concentration has fallen below $c_e \approx 30\%$, and the population becomes dominated by viscous (spontaneous) decay processes.

The eddy flow represents a reservoir of rotational kinetic energy, which may be described by an energy density e_e that is averaged over the total surface area. More inter-

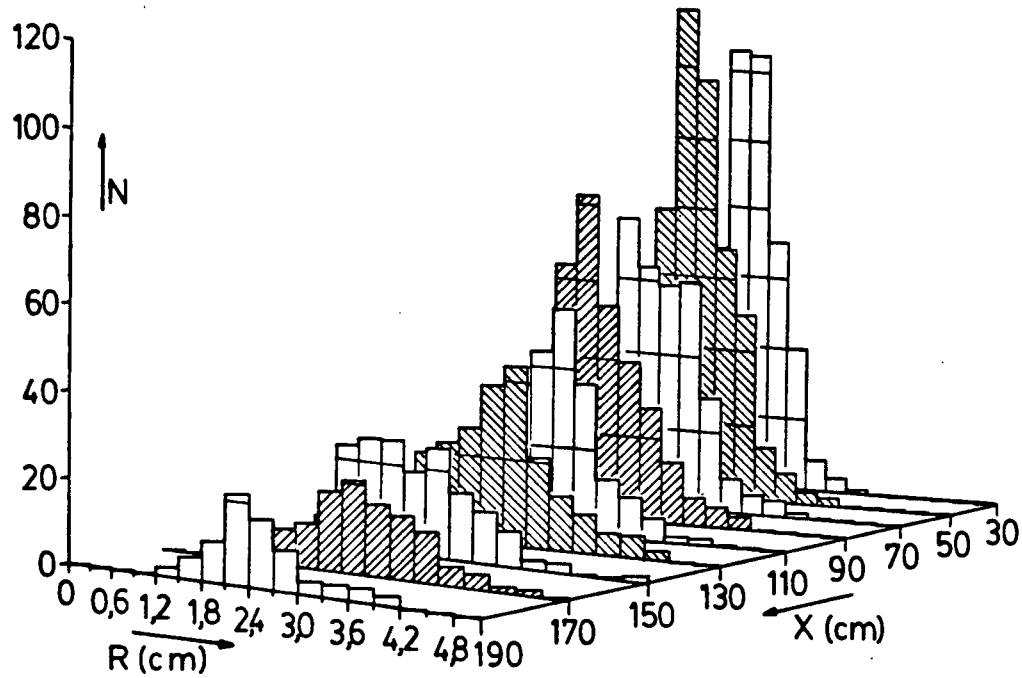

Figure 4-10 Eddy size distribution $N(X, R)$.

esting at this time is to consider the eddies as individual entities that have the energy $\tilde{E}$ per unit length stored within the observed surface layer of the flow.

For any eddy of given radius and known angular speed $\bar{\omega}$ one can calculate an energy $\tilde{E}$. Since the eddy size distribution N(X,R) is also known one can determine the eddy energy distribution $N[\tilde{E}(R)]$. Again, we are interested in the form of the curve $N[\tilde{E}]$ versus $\tilde{E}$ as characterized by the *energy width* and the slope of the high energy tail. For that purpose the distribution is plotted in semilog fashion in Fig.4-11(a). In the range $50cm \leq X \leq 110cm$, the high energy tail is well approximated by a straight line. When

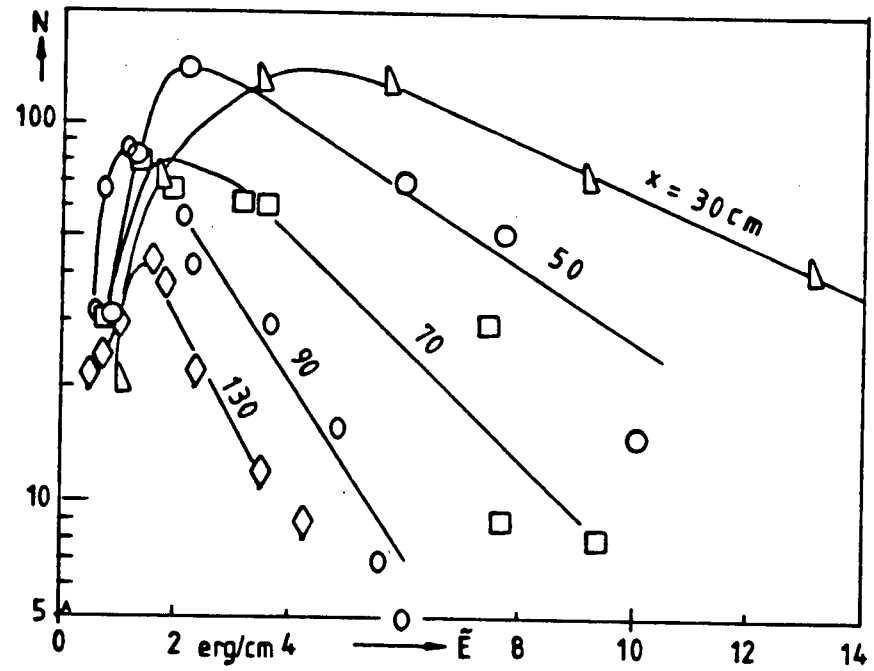

(a)

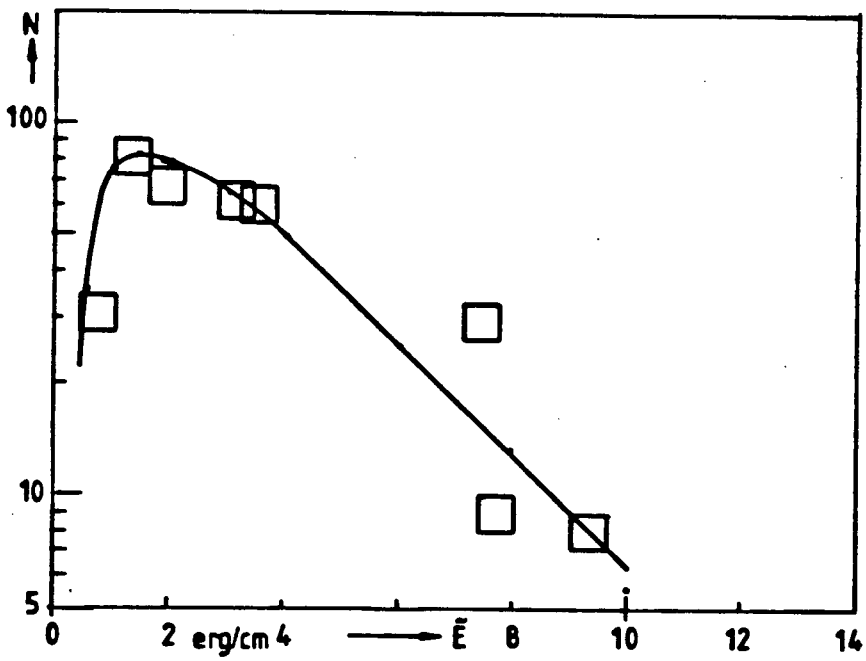

(b)

Figure 4-11 Eddy energy distribution $N(X,E)$. (a) Evolution with distance. (b) Curve-fit for X=70cm using eqn.(4-9a). $\theta_e = 2.8 erg/cm \quad \alpha = 0.86$

plotting the lower energy part of the distribution in log-log fashion it was observed that $N(\tilde{E})$ rises approximately proportional to $\tilde{E}^{\alpha}$. The experimental data can therefore be represented by

$$N(\tilde{E}) = const\tilde{E}^{\alpha}exp(-\tilde{E}/\theta_e) \qquad (4-9a)$$

where $N(\tilde{E})$ is the number of structures per unit energy interval having the energy $\tilde{E}$. This energy distribution is again similar to a Boltzmann function. It is an indication that frequent interactions are coupling the eddy energies. Figure 4-11(b) shows the curve fit plotted over the single distance of $X = 70cm$.

Just as for the rivers, the position of the distribution's maximum has been measured in order to determine the exponent $\alpha(= \tilde{E}_m/\theta_e)$ with the result

$$\alpha = 0.9 \pm .1. \qquad (4-9b)$$

The river and eddy energy distribution's values for α, eqns.(4-2) and (4-9) are seen to be similar in value.

The slope of the tail of the distribution is characterized by the parameter θ_e, which may be called the "eddy temperature". The energy half-width $\Delta\theta_e$ and the eddy temperature θ_e have been measured in the equilibrium range for various distances X. They are shown together with E_m in Fig.4-6(b). The number of eddies in the decay range $X \geq 120cm$ is too small to assign meaningful values to these statistical parameters. It is interesting to see that the eddy and river temperatures initially have the same magnitude and decay at about the same rate.

We investigated whether the eddy energy density could be obtained as the product of eddy number and eddy temperature multiplied by some suitable constant and found that the data in the equilibrium range could be approximated by the relation

$$e_e = K\theta_n N_e/S_e = Kn_e\theta_e, \qquad (4-10)$$

where the numerical constant has the value $K \simeq 0.65$. The empirical relation (4-10) is analogous to the standard relation for the internal energy ($e = const \times NKT$, where K is the Boltzmann constant) of a system of particles in thermal equilibrium.

We have shown that the surface flow structures on grid-generated turbulence can be identified and described by simple parameters. Furthermore, we have found that the distributions of these structure properties follow meaningful trends as the flow evolves. Also, to good approximation the distributions themselves may be characterized by simple parameters.

Before going on to discuss the structure dynamics it will be of interest to analyze the evolution of the structure statistics in terms of the rate equation model presented in the second chapter.

4.4 Energy Decay of the Surface Flow

The velocity fields of eddies and rivers were recorded as a function of distance X from the grid, and from these data we derived the size, angular speed and energy distributions. The distance from the grid may alternately be considered as a measure of the age of the turbulent motion, namely the time since the grid has passed the lab frame position

$t = X/U_g$. Thus, study of the structure statistics as a function of distance allows one to investigate some aspects of structure dynamics. The total energy density and the partial values for the eddy and the river modes are given in Fig.4-12. The observation period has been divided into the production, the equilibrium, and the decay range. In the equilibrium range there is strong coupling between and within the two modes. Eddies and rivers have about the same temperature as shown in Figs.4-7, and the eddy edge speed U_R is about equal to the average river speed u_o. It is noted, however, that the energy density of the two structure types decay at different rates. The energy losses occur more readily in the rotational (eddy) motion than in the translational (river) motion.

The eddy-eddy interaction should contribute most significantly to the evolution of the initial distribution, as frequent occurrence of such events requires a high number density. The time variation of the distributions allow one to estimate whether eddy-eddy interactions are important. For this purpose we write a rate equation for the change of numbers of eddies N of some radius R where the A, B, and C coefficients are in general dependent on the particular eddy radius and flow environment.

$$\frac{dN}{dt} = (A + B)N + CN^2 \qquad (4-11)$$

The rate coefficients A, B, and C quantify the evolution of the population of structures due to interactions with the fluid (frictional decay), with the fluid flow surrounding the eddies (pumping and tearing) and with other eddies (collisions) respectively. Equation (4-11) is a simplification of the more detailed rate equation (2-35) where each of the terms on the right-hand side is replaced by a summation of contributions to a particular eddy size's population change from all other eddies in the distribution. Equation (4-11)

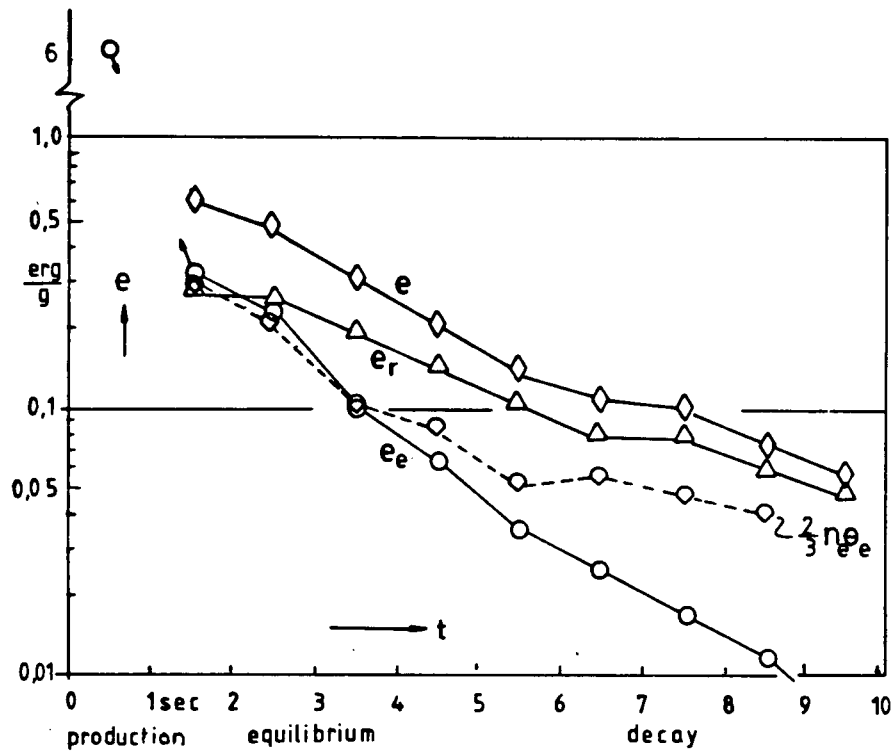

Figure 4-12 Energy densities as function of time. For eddies e_e, rivers e_r, and the total flow e.

contains only the dominant terms that are of interest here. The A and B coefficients are local to the distribution so eqn.(4-11) is a first order model for the sum of these rates. For our smoothly varying distribution adjacent structure numbers are nearly equal. The coefficient C as written here is a gross simplification of the pairing process which would involve interaction between structures of smaller size. The value found here should only be taken as an indicator of the influence of collisional processes (i.e. non-local within the distribution). At this point, it is not necessary to have any detailed knowledge of the rate coefficients. However, a quadratic term (coefficient $C \neq 0$) must be present if the

eddy concentration has any influence on the interaction dynamics. Here C is obtained from a numerical evaluation of the size spectrum decay. For that purpose eqn.(4-11) and the differentials are replaced by differences

$$Y = \frac{1}{N}\frac{\Delta N}{\Delta t} = (A + B) + CN. \qquad (4-12)$$

The left-hand side of eqn.(4-12) contains numbers that can be obtained from the data by slicing through the N(R,t) distributions in the time direction, see Fig.4-13. When Y is plotted as a function of N a straight line should result. The slope of this line is C and the intercept gives the sum of A and B.

To demonstrate this approach an analysis was carried out for eddies of radius R=1.4cm, and the results are shown in Fig.4-14. For R=1.4cm the linear least squares fit has the intercept $A + B = -0.70sec^{-1}, \sigma = 0.55sec^{-1}$, and the slope $C = +4.6 \times 10^{-3}sec^{-1}, \sigma = 6.3 \times 10^{-3}sec^{-1}$. A model estimate of the rate coefficient A will be presented in chapter five. The line intersects the N axis at N=152. Here C is positive, implying the collisional processes of two or more structures combining will increase the number of eddies of radius R=1.4cm. For large N the production of this size eddy by merging of smaller ones would tend to compensate for the two loss mechanisms. For small N one would expect a rapid decay of eddies of this radius. This agrees with observation. Similar results were obtained for data taken at other structure sizes.

The statistical properties of the eddies and rivers arise from the interaction of the structures with their surroundings. The next step is to see if the dynamics of these structures can be identified and quantified and then used in the rate equation model to predict the observed statistics.

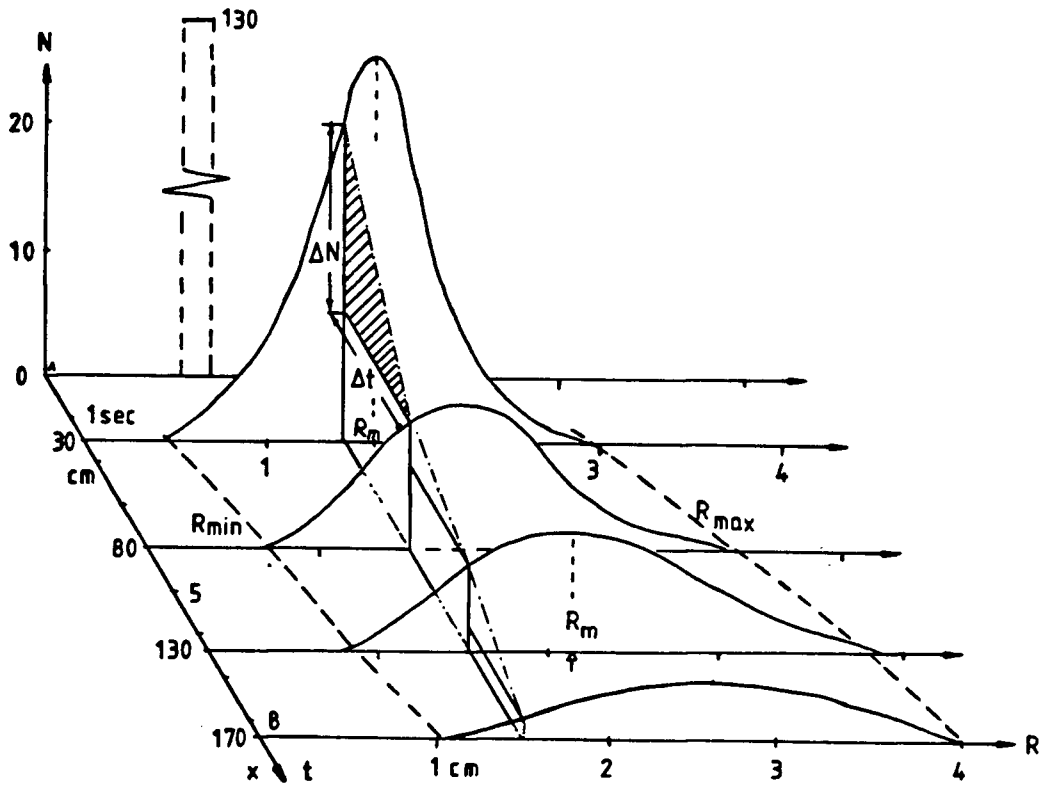

Figure 4-13 Eddy size-spectra time slice.

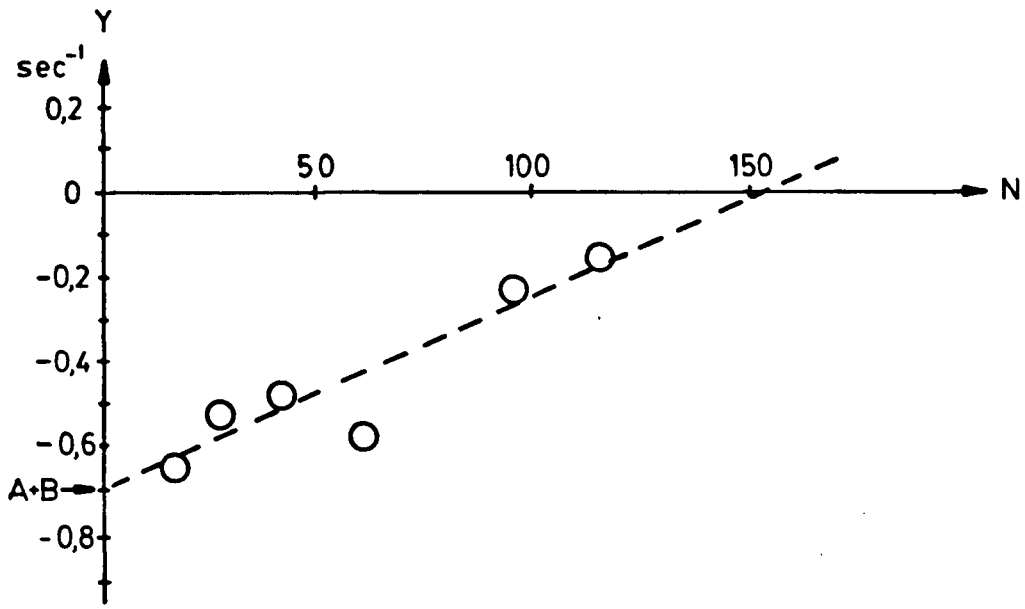

Figure 4-14 Graphical determination of rate coefficients. $Y = (1/N)(\Delta N/\Delta t)$. Experimental N values for $R = 1.4cm$ are taken for time intervals in the range $1.5 \leq t \leq 9.5$ sec and averaged with adjacent values.

CHAPTER 5
STRUCTURE DYNAMICS

A crucial question for the rate equation approach is whether the dynamics of individual structures can be characterized and categorized. The present chapter reports an experimental examination of the dynamics of the rotating flow-structures found on grid-generated turbulence. In this chapter the river-flow is treated as belonging to the background fluid flow in which the eddies evolve. The river-flow will predominantly evolve through viscous decay although it is possible that eddies could be produced by an inverse omega decay process. The analysis tools developed for this study have already been presented in chapter 3. The first section examines the near surface fluid dynamics in order to provide a more in-depth understanding of the observed surface motion. This is followed by a survey of the way the structures are observed to interact. Section three describes the initial vortex production and presents a simple kinematic model which predicts the initial structure population. A model for the viscous decay rate is given next and is compared with experimental results from the grid-flow. Observations of the omega decay and eddy pairing and tearing are then presented. The chapter ends by discussing the prediction of statistics from the observed dynamics.

5.1 Near Surface Fluid Dynamics

The surface structures studied in this thesis are considered to be the "footprints"* of more exotic creatures residing in the body of the fluid. It is therefore instructive to investigate the dynamics of the bulk and near-surface motion. Contaminated surfaces are known to have viscosities orders of magnitude higher than clean ones which in turn have a viscosity much higher than the same fluid in bulk [48]. While not completely clean, the surface flows studied in this thesis showed little effects of contamination. The elasticity of the film of surface contamination will suppress vertical displacement and make the surface act something like a rigid wall in relation to the subsurface flow.

The theory of homogeneous turbulence impinging upon a rigid wall has been examined by Hunt and Graham [49]. They found a growing viscous boundary layer adjacent to the wall and a larger inviscid "source layer", see Fig.5-1. In the source layer the isotropic bulk flow reorients to eliminate vertical motions. The viscous boundary layer has a thickness $\delta_\nu \simeq 4(\nu X/U_g)^{1/2}$ ($\approx 0.5cm$ for U_g = 20cm/sec at X=30cm). The larger inviscid source layer has a thickness $\delta_s \sim L_{x\infty}$, where $L_{x\infty}$ is the streamwise integral length scale in the bulk of the flow, see section 3.4. In reference [30], $L_{x\infty}$ was found to steadily increase from a value of 1.3cm at X=30cm for U_g = 20cm/sec. At the edge of the viscous surface layer ($z = 0$) the kinetic energy of the turbulent motion ($\overline{v_{x0}^2} + \overline{v_{y0}^2}$) is the same as in the bulk of the fluid where it is equal to ($\overline{v_{x\infty}^2} + \overline{v_{y\infty}^2} + \overline{v_{z\infty}^2}$), but the velocity component normal to the surface has vanished ($v_{z0} = 0$). The energy in this component has been partitioned (equally for an isotropic bulk flow) to the streamwise v_{x0} and lateral v_{y0} motions. A similar phenomenon is observed in stratified flow in the laboratory [50,

* As aptly described by A. K. M. F. Hussain (private communication).

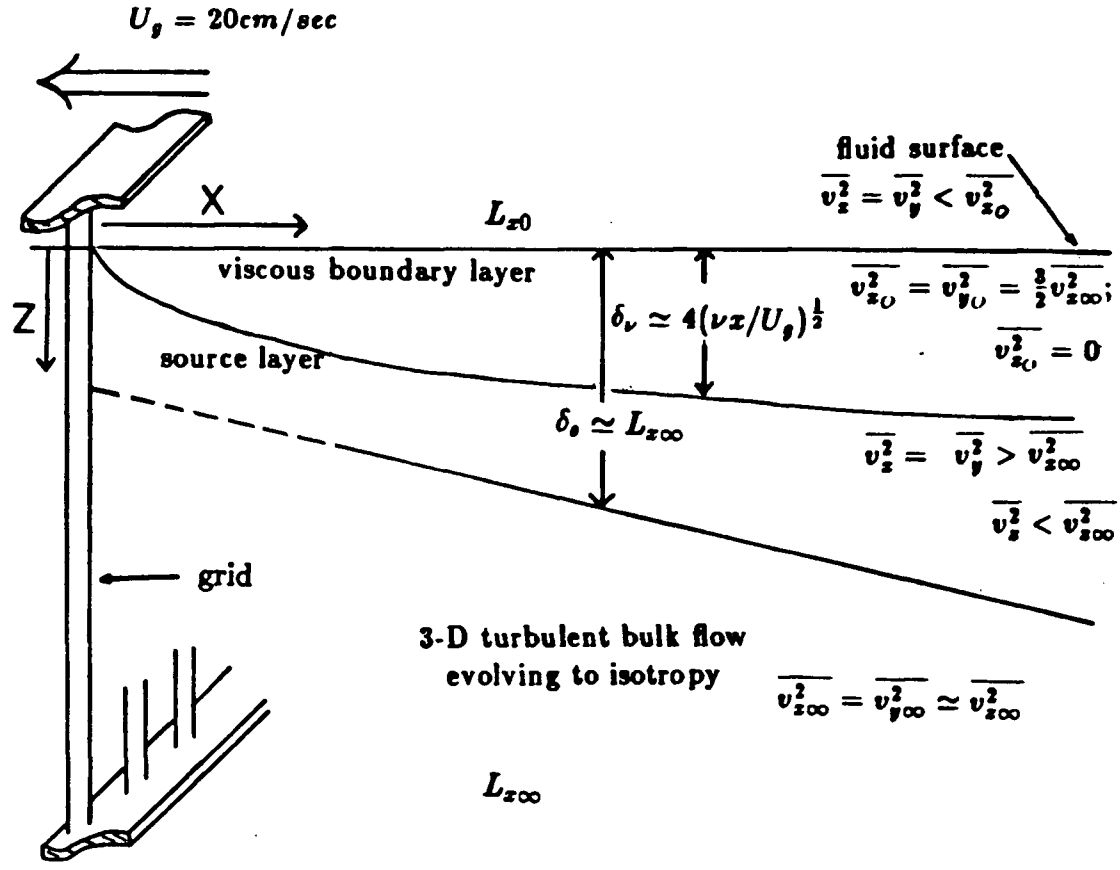

Figure 5-1 Near surface boundary layers.

51], the ocean, in magnetohydrodynamics [52] and the atmosphere [53] where layers of constant density lock the turbulent flow into quasi-two-dimensional motion. One may think of a surface flow as a highly stratified fluid layer. It is also interesting to note that a strong analogy exists between rotating and stratified unsteady flows [54] so that the results reported here should be pertinent to geostrophic turbulence. Indeed a striking similarity is seen between the flow fields on grid-generated turbulence and that observed within a rapidly rotating volume of fluid, see the photos of Mory and Hopfinger [40].

That we may expect results similar to those predicted by Hunt and Graham is supported by the experimental observation by Brumley [55] of the reorienting "source" region for vertically oscillating grid-generated turbulence impinging upon a shear free surface of water. Brumley also found evidence of the viscous boundary layer indicating (to him) that his fluid surface may not have been perfectly cleaned.

A comparison of experimentally determined surface and bulk integral length scales, L_{xo} and $L_{x\infty}$ respectively, is reported in [30] for the present apparatus and a 40cm/sec grid speed. The power spectral density, $E_{11}(f)$ of eqn.(3-3), was obtained through Fourier analysis of velocity records measured with a hot-film anemometer. The integral length scale of the bulk flow, $L_{x\infty}$, was then calculated from an extrapolated value for $E_{11}(0)$ using eqn.(3-9). The surface length scale L_{xo} was calculated in a similar manner from velocity records of surface flow generated by computer using the observed structure statistics N(X,R) and $\bar{\omega}(X,R)$. An alternate method of directly averaging the mean eddy chord over the $N(R)$ distribution was found to give a nearly identical length scale value. Near the grid the magnitudes of these length scale measures were equal within the experimental uncertainties. As the flow evolved, the bulk motion length scale $L_{x\infty}$ increased more rapidly than L_{xo}.

In the same report, the relationship between the longitudinal component of the turbulent kinetic energy for the surface and bulk motions were compared for a 40cm/sec grid speed. The energy decay curves were surprisingly similar in shape with the bulk motion being consistently 20 times more energetic than the corresponding surface eddy energy density. This factor will depend on the isotropy of the actual structure orientation, the

eddy-river energy ratio and the degree of contamination of the fluid surface. The influence of surface contaminant induced viscosity on the surface motion was examined. It was found that motion on a contaminated surface was initially less vigorous, decayed more quickly and grew in size scale more rapidly than the flow of a freshly skimmed surface.

A direct comparison between the surface and subsurface coherent structure properties is not possible as subsurface structures have yet to be studied for this flow. However, some qualitative subsurface flow visualization was accomplished using a sheet lighting technique. The results showed two-dimensional flow immediately behind the grid and just beneath the surface, see Figs.5-2. Figure 5-2a is a flow photo of the motion in a 2cm wide sheet parallel to and 3cm beneath the fluid surface. The image of the moving grid can be seen at the top. The predominantly two-dimensional structures immediately behind the grid soon appear disorganized. This indicates that a large fraction of the motion is occurring normal to the sheet of light. The flow is becoming isotropic. Fig.5-2b shows the motion in a few centimeter wide sheet of light parallel to the side walls of the tank. In most of the photo as much motion appears to be occurring in the vertical as in the horizontal direction. Predominantly horizontal motion can be seen very near the surface and perhaps at the very left side of the light sheet were the grid has just disappeared. The bulk of the flow is chaotic and three-dimensional and not amenable to our present two-dimensional visualization and coherent structure analysis methods. Similarity between power spectra of longitudinal velocity fluctuations generated from the surface structure statistics and those measured with a hot-film anemometer [30] suggest a similar velocity structure over large scales may exist. Also, the close agreement in

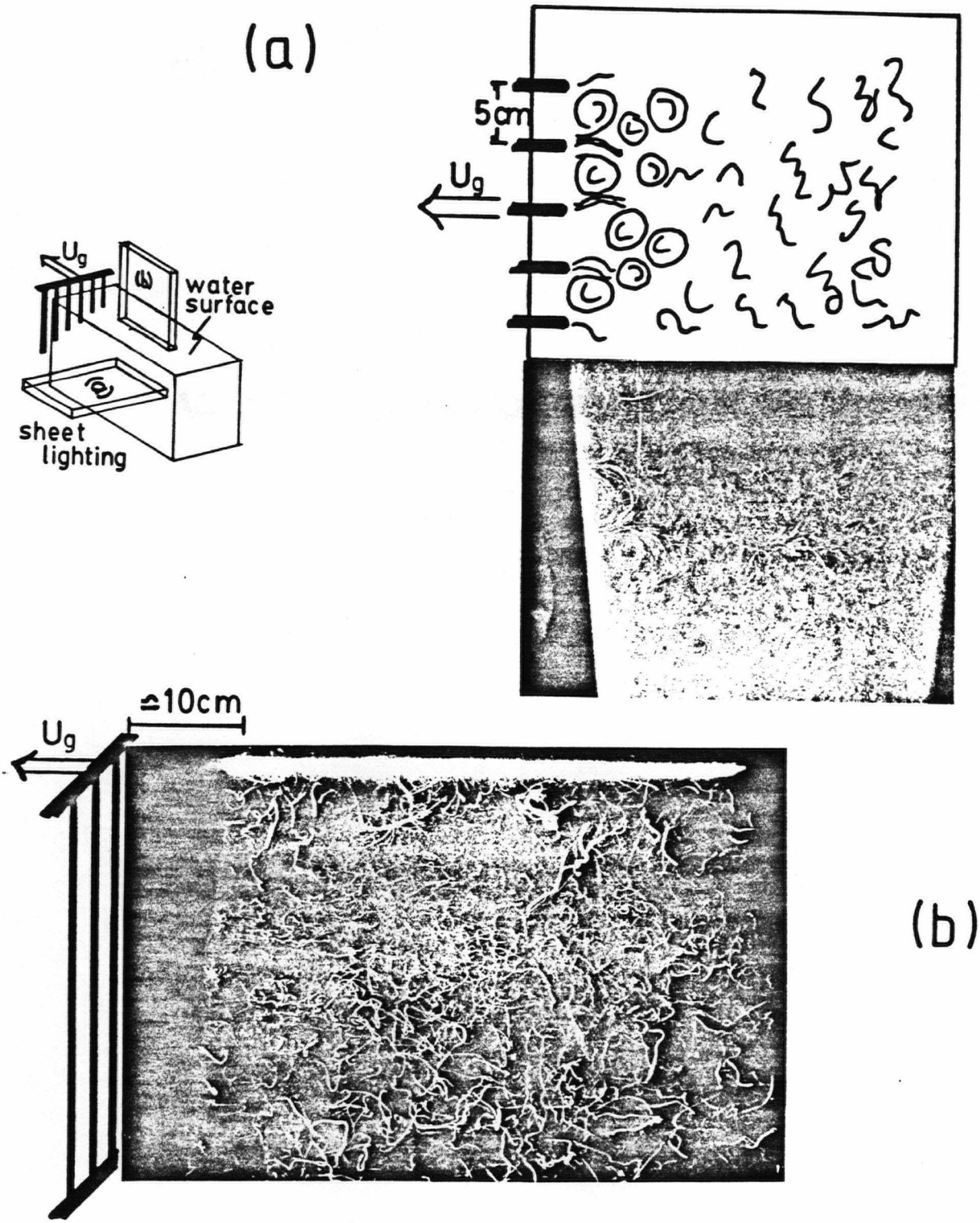

Figure 5-2 Bulk motion of turbulent grid-flow. Sheet lighting: (a) parallel to and 3cm beneath the surface, (interpretation shown alongside photo) (b) parallel to side walls.

the length scales indicates that a similar size distribution may be found. The bulk flow structures are three-dimensional in nature, have a more complex internal flow structure, and will interact with their environment in the additional manner of energy pumping through vortex stretching. It is reasonable to expect that the more complex subsurface flow will evolve through some of the processes found in the surface flow.

As a final point it should be noted that implicit to the entire flow visualization analysis has been the assumption that the motion of the tracer particles accurately represents the motion of the underlying fluid. The difference between the tracer and fluid motion was calculated following Zalutskii [56] and found to be less than 1% for the $\sim 0.4mm$ aluminum filings used. The difference in radius of curvature was similarly determined to be less than 1% for the flow conditions generated. These calculations apply to the interior of the fluid. We expect even closer coupling between the filings and the surface motion due to the action of surface tension and surface viscosity.

5.2 Structure Evolution

Figure 5-3 shows a classification scheme of the eddy decay dynamics observed in time-exposed photographs and video sequences of the surface flow on grid-generated turbulence. Five distinct types of evolution processes were distinguished. These were the initial vortex production, eddy tearing, eddy pairing, viscous decay and the omega decay. The initial vortex production is described in section 5.3. Eddy tearing is a very rare occurrence in this grid-flow and was only observed once amongst the many structure evolutions followed. That instance occurred a few mesh widths from the grid in the initial

production region where the shear stresses are highest. A simple model for this process has been proposed [1] and a rate coefficient determined. This process will be significant for flows with high velocity gradients over areas large compared with the structure size but is not a significant factor in the dynamics of grid-generated turbulence.

Eddy pairing is a frequently observed collisional process which is the dominant mechanism by which structure size is increased in the equilibrium region of the flow. Figure 5-4 shows a sequence of flow photos depicting the amalgamation of a number of structures. Eddy pairing is a well known phenomenon in which like-signed vortices combine to form a single larger structure. This author first observed structure pairing as the growth of a separated peak in the size spectra. Figure 5-5 depicts this evolution.

In grid-generated flow, structures of like rotation sense are occasionally brought together through the action of the surrounding flow. A stagnation zone of high pressure will appear in the high stress contact patch, see Fig.5-5. Gradually more and more of the flow from each structure is redirected around both structures. When all the flow has been redirected the original structures have ceased to exist, leaving in their place a single eddy with somewhat less energy than that of the two parent structures combined. Similar local dynamics are responsible for the omega decay discussed in section 5.5.

The ultimate fate of all the fluid motion is viscous decay to a quiescent state. The flow becomes viscous dominated at small scales and in the final period. Section 5.4 discusses the viscous decay of the structures in the near grid region.

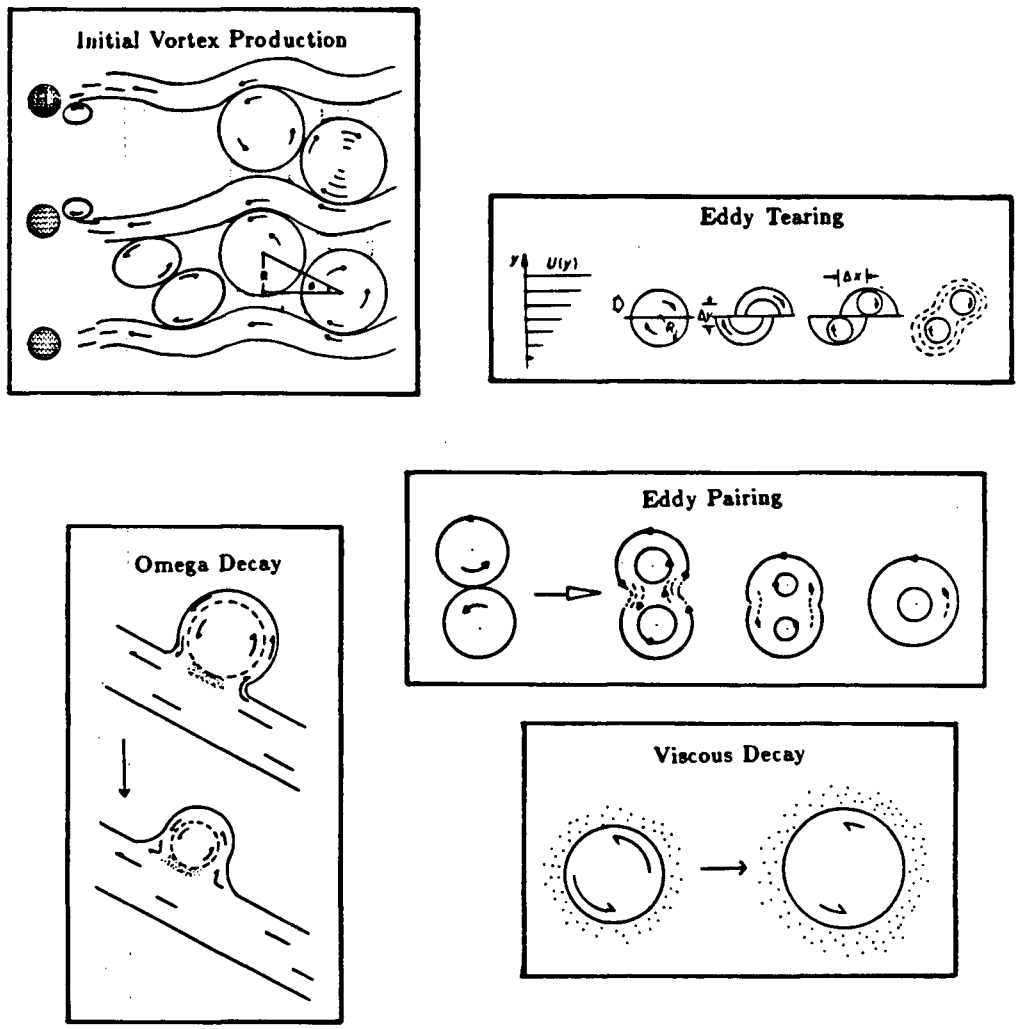

Figure 5-3 Structure evolution types.

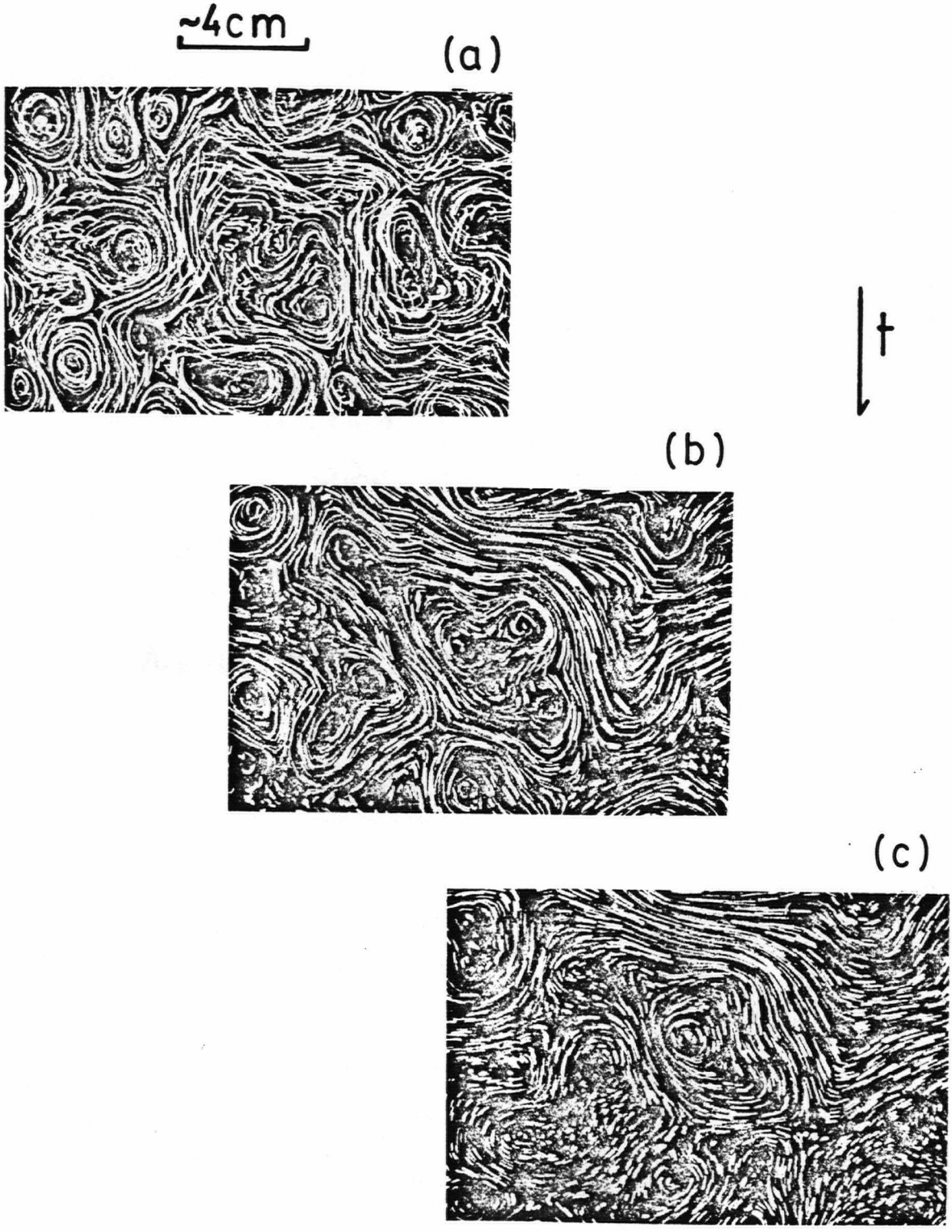

Figure 5-4 Eddy amalgamation. (seen in center of photo series) (a) $t = 3$ sec, (b) $t = 6$ sec, and (c) $t = 9$ sec.

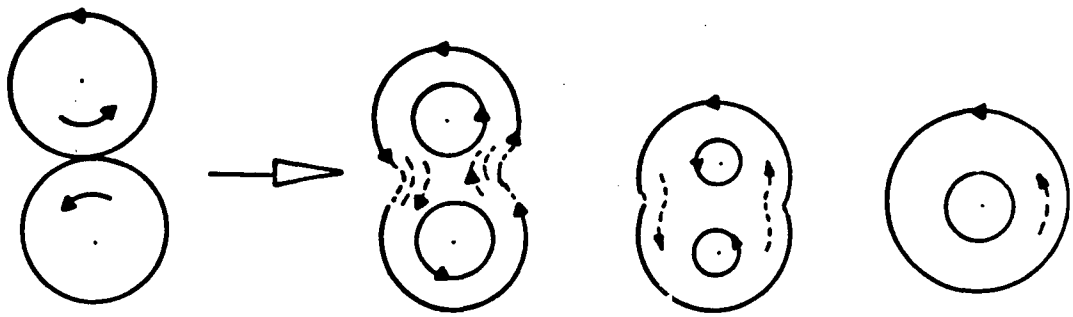

Figure 5-5 Eddy pairing.

5.3 Initial Vortex Production

The flow field becomes amenable to the photographic analysis method at about $X = 30cm$ ($X' \approx 6$) when the structures are fully formed and relatively stationary in the tank frame of reference. In order to study the initial vortex production the flow was recorded on a 30 frame per second (fps) video cassette recorder. A qualitative analysis of the video sequence was then performed in order to obtain a description of the production dynamics. The computer-automated coherent structure identification system described in the third chapter of this thesis was then used to extract quantitative information. The same flow conditions were used as for the structure statistics studies, namely: a 4:1 cylinder spacing to diameter ratio grid moving with a Reynolds number based on bar separation of 20,000.

At this grid speed of $U_g = 20cm/sec$ the inital vortex production did not resemble isolated von Kármán vortex streets of individual rods as might be expected; the major

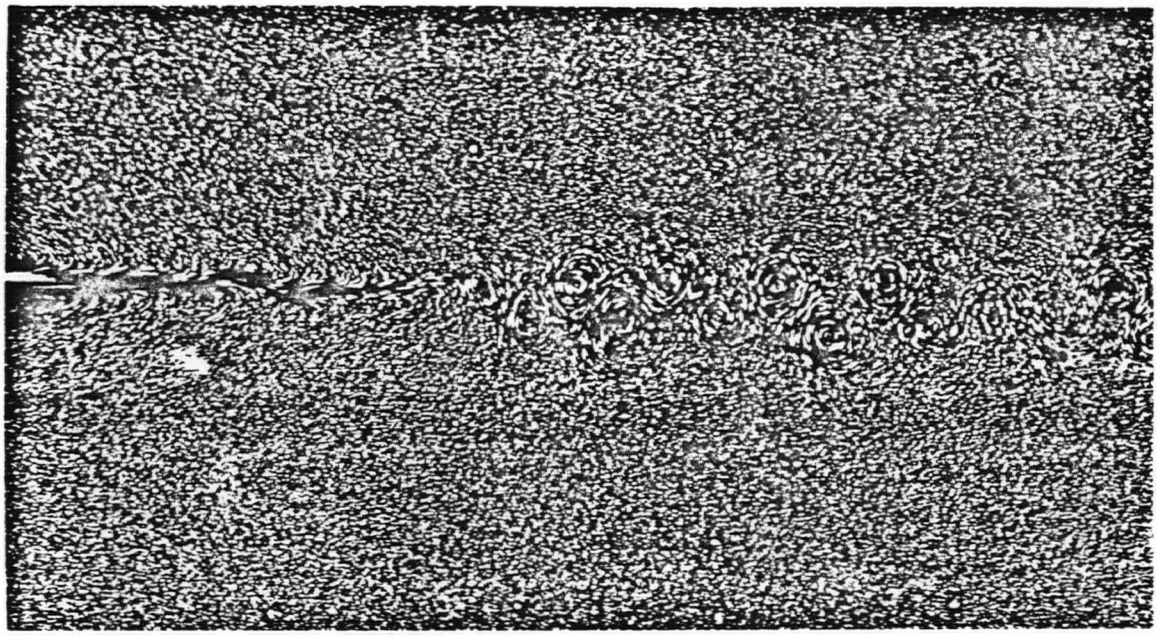

Figure 5-6 von Kármán vortex street. Flow photo from F. Ahlborn $\approx$ 1905.

difference being the much more rapid growth in size of the vortices. The alternate shedding of vortices from cylinders, see Fig.5-6, over a wide range of Reynolds numbers has been known for many decades and was first examined by von Kármán in 1911 [2].

Figure 5-7 depicts the formation dynamics determined by observing 13 sets of video sequences of the flow between adjacent bars. Figure 5-8(a) shows a superposition of 20 frames of raw digitized data taken with the grid bars leaving the left hand side of the first frame. Figure 5-8(b) shows the same "time exposure" but with the shed vortices traced in by hand. This figure closely resembles the idealized flow of Fig.5-7. The picture of the

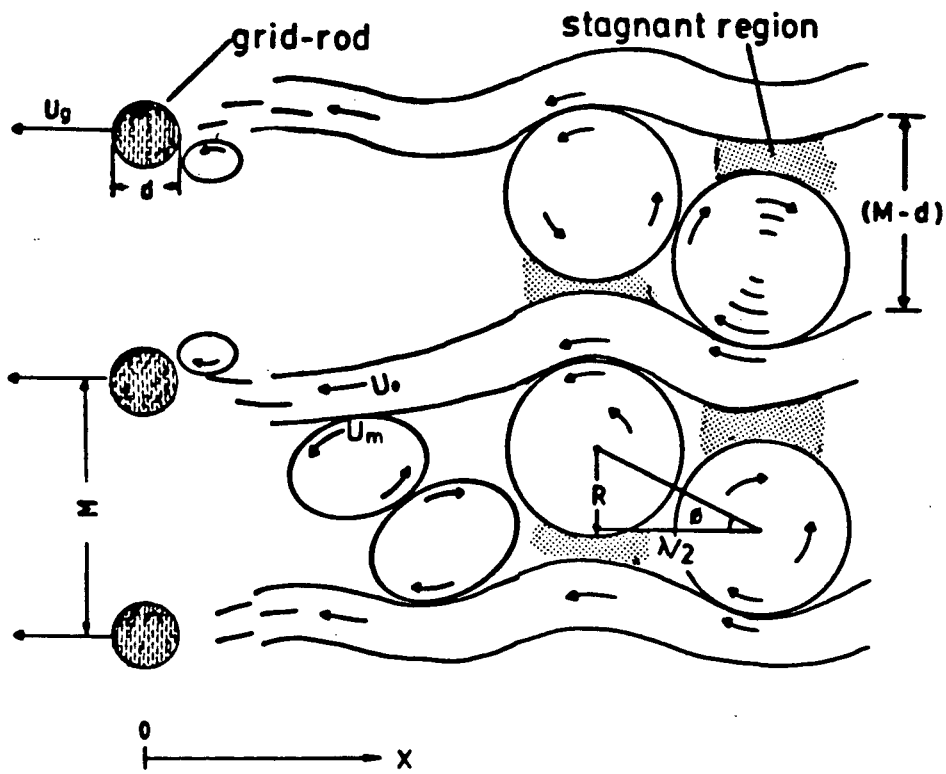

Figure 5-7 Initial vortex formation.

formation dynamics is as follows: The vortices have their origin in the vortex shedding region at individual cylinders and their production rate is found to be equal to that of an isolated cylinder of diameter d. The shedding frequency f is determined by the non-dimensional Strouhal number

$$S = \frac{fd}{U_g}. \qquad (5-1)$$

The Strouhal number is well known [16] to be equal to 0.2 for circular cylinders over a wide range of Reynolds numbers, including the present value of Re=2,500 based on cylinder diameter. A curious additional feature is that the formation dynamics appear to be π

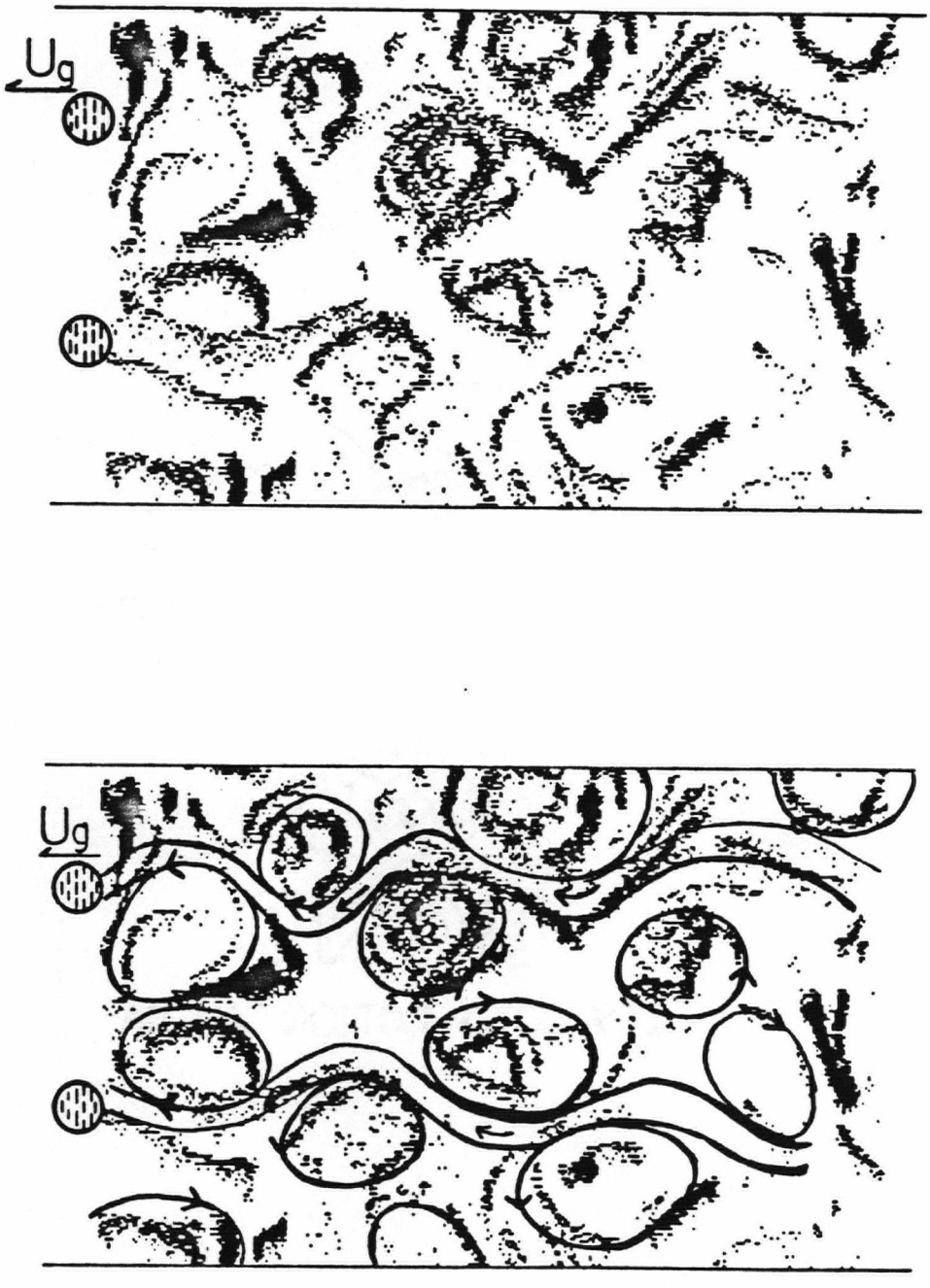

Figure 5-8 Near grid video "time" exposure. (a) Raw digitized data, (b) Identification superimposed

radians out of phase immediately behind adjacent bars. The vortices rapidly (within~ 1-2 M) grow to fill in the region between the momentum defect "shadows" of the grid bars and simultaneously shift to the tandem arrangement shown in the downstream end of Fig.5-7.

From these observations a simple kinematic model was advanced in a recent publication [6]. It was observed that in the resulting wavy configuration the vortices (or eddies) are nested in a manner which reduces the overall strain in the fluid. The resulting flow pattern exhibits phase locking between adjacent vortex streets. Alternate eddies rotate in opposite directions so that points of common tangents experience little shear stress. Also, their diameter is slightly smaller than the free space between the rods: $R \leq (M - d)/2 = 1.9cm$, where M is the mesh width and d is the bar diameter. The eddies are slightly offset to the side where their edge velocity is parallel to the flow in the momentum defect region, leaving a stagnant region to separate flows of opposing direction (the shaded areas of Fig.5-7). The resulting initial eddy size at $X' \approx 2M$ is in reasonable agreement with the observed population peak of $1.6cm$ radius. The initial concentration would be

$$C_o = (\pi R^2/M2R) = 0.59, \qquad (5-2)$$

which is consistent with the measured values shown in Fig. 4-3a.

Assuming these structures rotate in a strain free manner with edge velocity equal to that of the adjacent moment defect region ($U_o \approx 5cm/sec$ from observation), the initial internal energy of the surface eddies will be approximately

$$\tilde{E}_1 = (\pi/4)\rho R_1^2 U_o^2 \approx 70(erg/cm) \qquad (5-3)$$

and the energy density becomes $e_o \approx 6erg/g$ as indicated in Fig.4-12. The above scenario was the most predominant evolution observed. On occasion however, the vortices were observed to suddenly reorganized into a different geometry. A likely reason is that the flow field cannot simultaneously satisfy the constraints of the structure production rate, grid speed and preferred structure size. The relationship between these effects was studied using the computer-automated analysis system described in chapter three.

The system was used to study the properties of the structures when they were first identifiable. Typically 3 or 4 complete structures were found within the viewing area of $11.3 \times 8.5cm$ $(2.3 \times 1.7M)$. For each run, about 3-4 seconds of the video recording was digitized and analyzed. This corresponds to a distance of $X' = 12 - 16$ mesh widths.

Part of the power of the automated system is that it extracts instantaneous information about the velocity field from the polynomial fits to the tracer paths. The system thus allows for the study of rapidly evolving flows which enables us to examine the production regime, something that we cannot do with the photographic flow visualization. Typically, the system was able to recognize structures starting from 6 video frames $(t = 6/30sec)$ after the grid passed out of the field of view. This corresponds to 0.8M from the moving grid. The image dimension in the direction of the moving grid is $11.4cm$ $(2.3M)$.

From contour plots of the recognized structures we can calculate the initial structure production rate. Referring back to Fig.5-7, the number of structures with a given rotation sense, produced per unit time by an individual rod is equal to the vortex shedding frequency

$$f = U_g/\lambda \qquad (5-4)$$

This frequency was determined from a number of contour plots of recognized structures. Cast into its non-dimensional form using eqn.(5-1) the experimental result was

$$S = 0.20 \pm 0.01, \qquad (5-5)$$

which agrees well with the Strouhal number for isolated circular cylinders under the same flow conditions. A prediction of the angle between edge adjacent eddy centers in the fully formed wavy region may be obtained. Again, referring to Fig.5-7 we observe the geometric relation between the angle ϕ, eddy radius R and longitudinal separation λ,

$$\frac{\lambda}{2} = 2Rcos\phi. \qquad (5-6)$$

As the structures are stationary in the tank frame of reference λ can be used to determine the shedding frequency (the rate at which like signed vortices are produced) using eqn.(5-4) to get

$$f = \frac{U_g}{\lambda} = \frac{U_g}{4Rcos\phi}. \qquad (5-7)$$

If we assume that the resultant structures grow to completely fill the region between the momentum defect shadows we have

$$R = (M-d)/2 \qquad (5-8)$$

which may be used in eqn.(5-7) to get

$$f = \frac{U_g}{2(M-d)cos\phi}. \qquad (5-9)$$

If we now assume that the initial eddy creation is determined by the dynamics of the individual cylinder vortex shedding we have $S = 0.2$ and using eqn.(5-1) for the Strouhal number we find

$$S = \frac{fd}{U_g} = \frac{d}{2(M-d)cos\phi} \qquad (5-10)$$

Calling $\eta = M/d$, the cylinder spacing to diameter ratio, and rewriting the above equation to form a prediction for ϕ we have

$$\phi = Arccos\left(\frac{1}{2S(\eta-1)}\right) = 34^o \qquad (5-11)$$

upon inserting the values $\eta = 4$ and $S = 0.2$. This equation describes a relationship between the mesh ratio η, the Strouhal number S, and the angle preferred by adjacent eddies. The angle ϕ was measured from the plots of identified structures in the thesis of Lau [38] and reported to be

$$\phi = 33 \pm 4^o \qquad (5-12)$$

for well formed structures. The result is in good agreement with the proposed model. Further experimental testing of eqn.(5-11) and the proposed model by varying η would be worthwhile. It should be mentioned that eqn.(5-11) implies a compression of the vortex street in order to accomodate all new vortices produced between two bars. For a finite span grid competition for space must occasionally destroy the orderliness of this locally preferred pattern.

In the same experimental series the eddy diameters D were also measured. By choosing well recognized structures at the initial times ($t \leq 12/30sec$ *or* $X' \leq 1.6M$),

it was found that the average initial diameter (calculated from the area by circular approximation) of the structure was

$$D = 0.8 \pm 0.1M \qquad (5-13)$$

Using the assumption that the structures grow to fill the space between the "shadows" of the cylinders, eqn.(5-8), to determine D we have

$$D = 2R = (M - d) = (1 - \frac{1}{\eta})M = 0.75M, \qquad (5-14)$$

in good agreement with the measured result above.

As a final study of the initial vortex production the initial boundary speed of the structures was determined. This was done by comparing the mean velocity of the recognized structure with that of an idealized rigidly rotating one. The mean speed in the ideal structure is $\frac{2}{3}U_m$ where U_m is its boundary speed. Therefore, the boundary speed of the structure can be estimated as

$$U_m = \frac{3}{2}U' \qquad (5-15)$$

where U' denotes the measured average speed within the structure. Similar considerations on root mean squared speed also provides an estimate of U_m. Moreover, the speed can be calculated from either the grid of tangential speed or from the grid of velocity components. These four different estimates of U_m turned out to be in agreement with each other and it was found that

$$\overline{U}_m = (0.28 \pm 0.08)U_g, \qquad (5-16)$$

a value of $\overline{U}_m = 5.6 \pm 1.6 cm/sec$ for our $20 cm/sec$ grid speed. This value is in good agreement with the observed momentum defect velocity of $U_o \approx 5 cm/sec$, thus supporting the no slip assumption used to obtain eqn.(5-3). As a final point it should be noted that a consistent difference was found between the mean square and square mean angular velocity averagings. This was interpreted as evidence of departure from the ideal rigidly rotating eddies. More will be said about these results in the next section.

5.4 Spontaneous Decay

The simplest decay archetype that can be characterized is the viscous decay of an isolated rotating structure. In the introductory paper "A model for turbulence based on rate equations" [1] a simple model was presented for the spontaneous decay rate. The derivation is reproduced here.

A cylindrical eddy of length ℓ, radius R and angular velocity ω contains at a given time the total energy

$$E = \frac{1}{2} I \omega^2 \qquad (5-17)$$

where $I = \frac{1}{2} m R^2 = \frac{1}{2} \pi \rho \ell R^4$ is its moment of inertia. If R remains approximately constant the energy will be lost at the rate $\frac{dE}{dt} = \pi \rho \ell R^4 \omega \dot{\omega}$, where $\dot{\omega}$ is a negative quantity.

A typical time τ_o for the energy loss is used to define the energy decay rate $A = 1/\tau_o$. The energy loss from the assumed rigid body structure is due to the frictional drag acting on its surface

$$F_{fr} = (area) \rho \nu \frac{\partial u}{\partial r} \approx 2\pi \ell R \rho \nu \frac{u(R)}{\delta} \qquad (5-18)$$

giving a dissipation power $F_{fr}\dot{u}(R)$. Here $\frac{u(R)}{\delta}$ is the difference between the eddy peripheral velocity and the stagnant surroundings divided by the width δ over which this velocity change occurs. The width δ of the boundary layer in which this dissipation occurs steadily increases. The boundary layer growth rate is similar to the Rayleigh problem of an infinite flat plate starting suddenly from rest. There $\delta = 4\sqrt{\nu t}$, so that the dissipation power can be written as

$$F_{fr}\dot{U}(R) = 2\pi\rho\nu R^2\omega^2/(4\sqrt{\nu t}). \qquad (5-19)$$

This power dissipation must be equal to the power loss of the rotating structure. This leads to

$$\frac{d\omega}{dt}\sqrt{t/\omega} = \nu^{\frac{1}{2}}R. \qquad (5-20)$$

This relation can be integrated to yield the instantaneous angular velocity

$$\omega = \omega_o exp(-2\sqrt{\nu t}/R) \qquad (5-21)$$

and the eddy energy becomes

$$E = const\ \dot{\omega}^2 = E_o exp(-4\sqrt{\nu t}/R). \qquad (5-22)$$

A significant amount of the eddy energy will be dissipated during the e-folding time τ_o defined by eqn.(5-22), namely

$$\tau_o = R^2/16\nu. \qquad (5-23)$$

The energy decay rate is hence

$$A = 1/\tau_o = 16\nu/R^2. \qquad (5-24)$$

This result shows that smaller structures have a higher frictional decay rate. The interaction with the fluid (the spontaneous decay) therefore dominates the low end of the eddy size distribution, while large structures suffer relatively little energy loss due to frictional decay.

The above crude model motivated a more extensive study of the viscous decay of two-dimensional axisymmetric flow structures [57]. The computer model was an attempt to obtain rate coefficients from more physical velocity profiles than a rigid body. The Navier-Stokes equations in cylindrical coordinates were used as a starting point. For $\vec{v} = \hat{\theta} v_\theta(r,t)$ only ($\hat{\theta}$ being the unit polar vector) and $(\nabla p)_\theta = 0$ by symmetry, the Navier-Stokes equations reduce to

$$\frac{\partial v_\theta}{\partial t} = \frac{\nu}{r}\frac{\partial}{\partial r}(r\frac{\partial v_\theta}{\partial r}) = \nu\left[\frac{\partial^2 v_\theta}{\partial r^2} + \frac{1}{r}\frac{\partial v_\theta}{\partial r}\right] \qquad (5-25)$$

since $(v \cdot \nabla)\vec{v} = 0$ for $v = v_\theta(r,t)$. Equation (5-25) is the simple diffusion equation for fluid momentum. A discrete version of this equation was used to compute the evolution of a given velocity profile $v_\theta(r)$.

At the end of the specified evolution time, plots were made of the eddy kinetic energy, boundary layer thickness, boundary layer to core energy ratio, and the rate coefficient, all as functions of time. The total eddy kinetic energy per unit mass was found by summing up the contributions from the discrete radii. The evolution of this energy was then used to determine the rate coefficient

$$A(E) = -\frac{1}{E}\frac{dE}{dt}. \qquad (5-26)$$

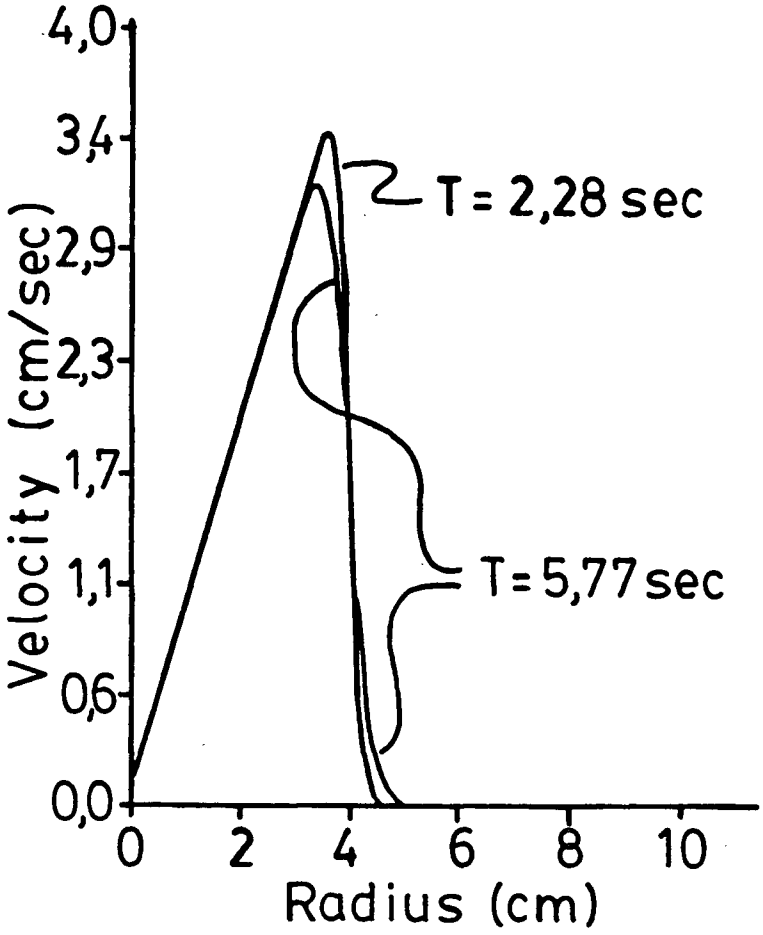

Figure 5-9 Evolution of velocity profile. Computer modelled profiles at two different times.

Figure 5-9 shows the evolution of the velocity profile between two times.

The rate coefficient curves show that A depends on time. However, if one allows the originally unrealistic velocity profile to evolve to a more physically meaningful state, a relatively constant decay rate is found. Figure 5-10 shows how this A value varies with $1/R_o^2$. The range bars for the A values reflect the weak time dependence over the 10 sec evolution interval in which the stable value was determined. An estimated line through the bars yielded $A \sim \beta/R_o^2$ ($\beta \approx 4.2(5) \times 10^{-2} cm^2/sec$). Dimensionally one must have $A \propto \nu/R_o^2$ implying that $A \simeq 4\nu/R_o^2$ as ν was taken as $1.0 \times 10^{-2} cm^2/sec$ in

the computer modelling. The difference between the constant above and the value of 16 in eqn.(5-24) being the arbitrary choice of the e-folding time to characterize the decay rate.

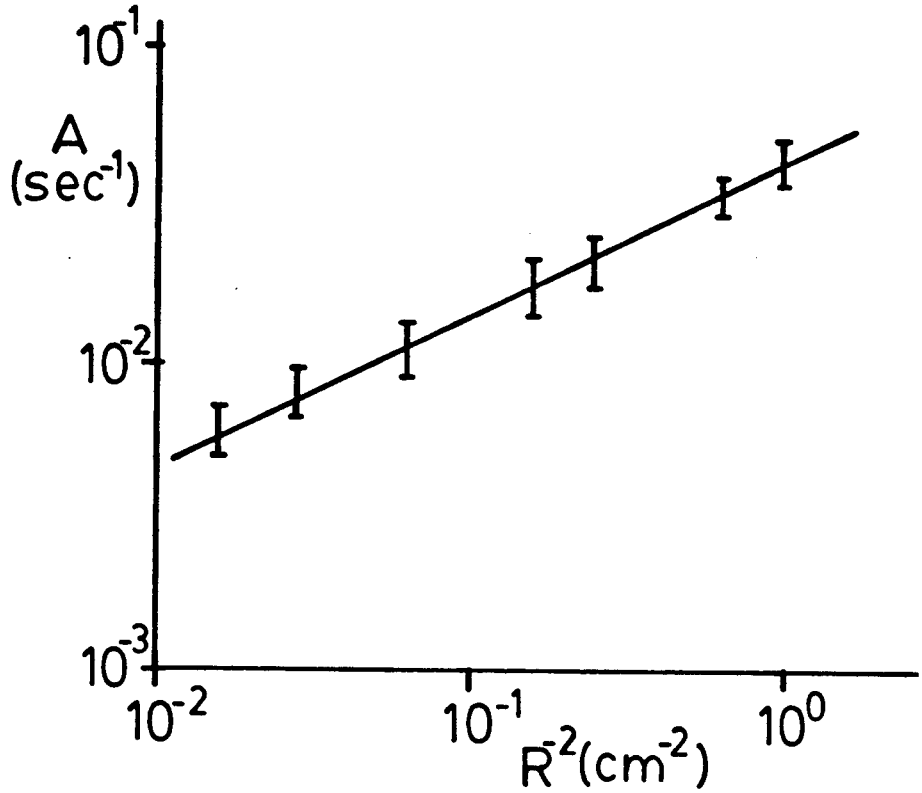

Figure 5-10 Variation of rate coefficient A with structure size. Computer modelled.

The video-computer analysis system was used to study, experimentally, the decay of stable surface structures in the initial period of the grid flow. Due to the low resolution of the present hardware the analysis system is inaccurate in determining the location of the structure outline, and hence the radius. The structure recognition plots were

thus overlayed on the streak data to judge whether the boundary region has sufficient information density for accurate size determination. A visual check was also made to ensure a steady viscous decay was the dominant influence on the structure. Thus, only well defined structures which underwent a steady decay, free from interference from other structures, were chosen for this analysis.

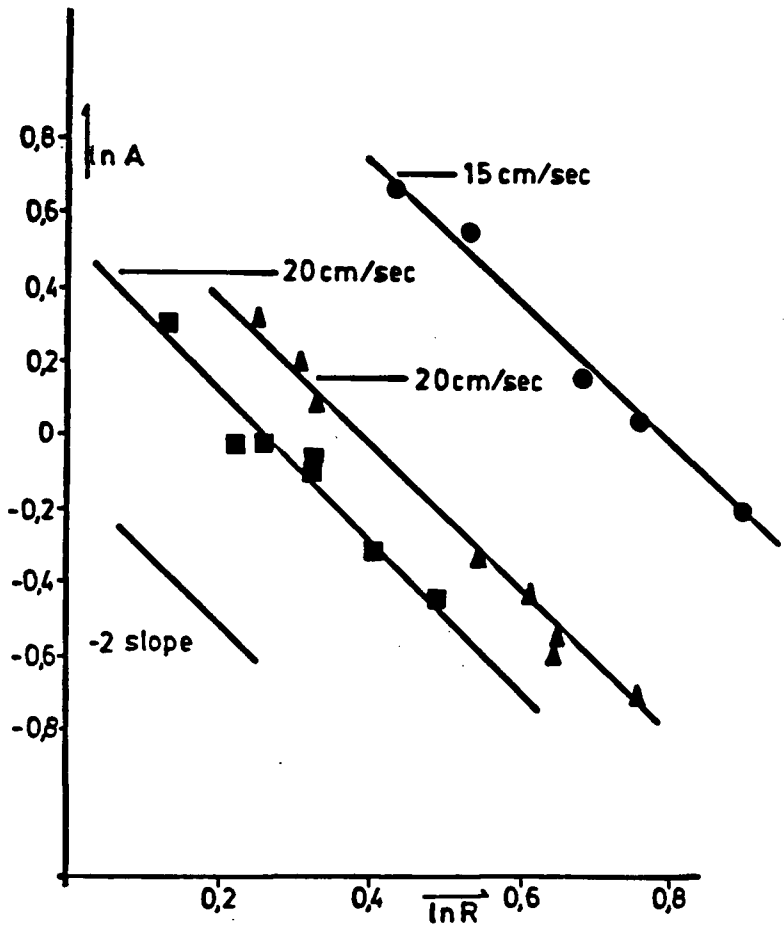

Figure 5-11 Proportionality constant determination for $A = \beta/R^2$.

Figure 5-11 shows a log-log plot of the decay rate against the eddy size R. The plot shows a good power law relationship with an exponent of -2 as predicted by eqn.(5-24).

However, the proportionality constant changes between different runs. For the left-most curve the value for ν, assuming $\beta = 16\nu$ from eqn.(5-24), was $0.10 \pm 0.05 cm^2/sec$. This is an order of magnitude higher than the established bulk viscosity of water of $0.01 cm^2/sec$. It was also found that the calculated viscosity values increased during the course of the day long experimentation. This was interpreted as the effect of increasing surface contamination. The order of magnitude difference has already been discussed in section 5.1 on surface fluid mechanics. With this ν value and the $R = 1.4cm$ structure size of section 4.4 a rate coefficient for the spontaneous decay may be obtained from eqn.(5-24), $A = -1.6 sec^{-1}$. This value is of the same order of magnitude as the value $A + B = -0.7 sec^{-1}, \sigma = 0.55 sec^{-1}$ obtained from the structure statistics analysis of chapter four. A decay value obtained from a more thorough study of the statistics evolution would allow for a more conclusive comparison.

Before going on to discuss other decay types some observations on the eddy's internal velocity profile are in order. In the course of testing the self consistency of the analysis system it was noted that kinetic energies determined by a rigid body fit to the angular velocity defined as

$$\omega' = \frac{1}{N} \sum_{structure} v_\theta / |R - R_{CM}| \qquad (5-27)$$

were consistently larger than what was directly determined for the recognized structures from the interpolated velocity grid. The rotational energy of the structure is calculated as

$$E_r = \frac{1}{2} I \omega'^2 \qquad (5-28)$$

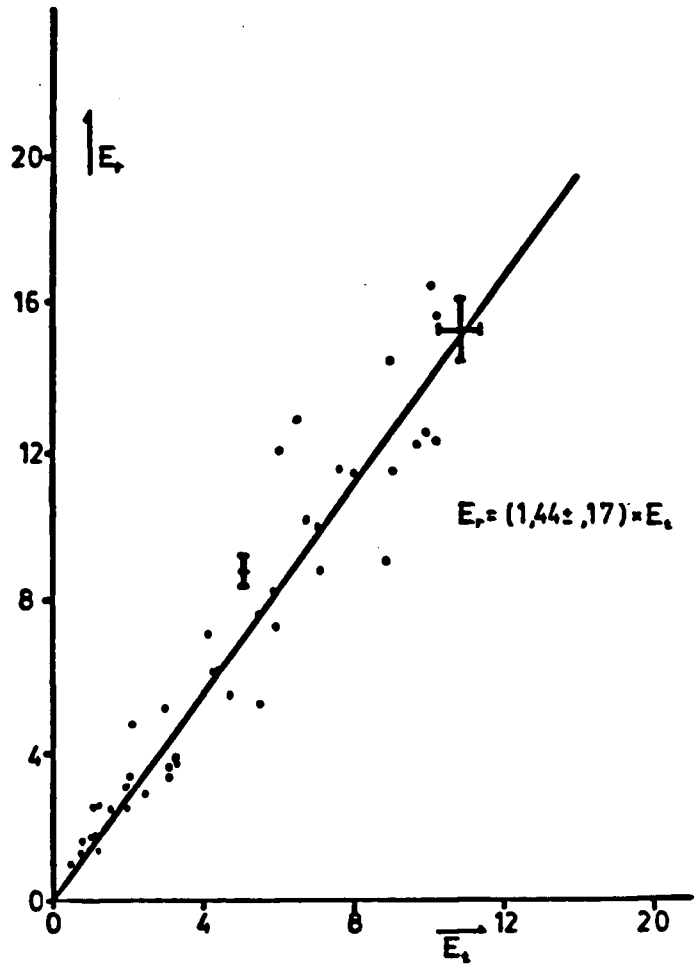

Figure 5-12 Relation between rotational energy and total energy. Non-unity proportionality indicates systematic deviation from $\omega = const$ profile.

Figure 5-12 shows a plot of this energy against the kinetic energy calculated directly from the velocity grid (E_t) for all the recognized structures. A consistent deviation between the average squared data in the form of E_r and the square averaged data of E_t,

$$E_r = (1.44 \pm .17) \times E_t \qquad (5-29)$$

was found. This indicates the actual profiles were a consistent deviation, or members of a family of deviants, from the assumed rigid body profile.

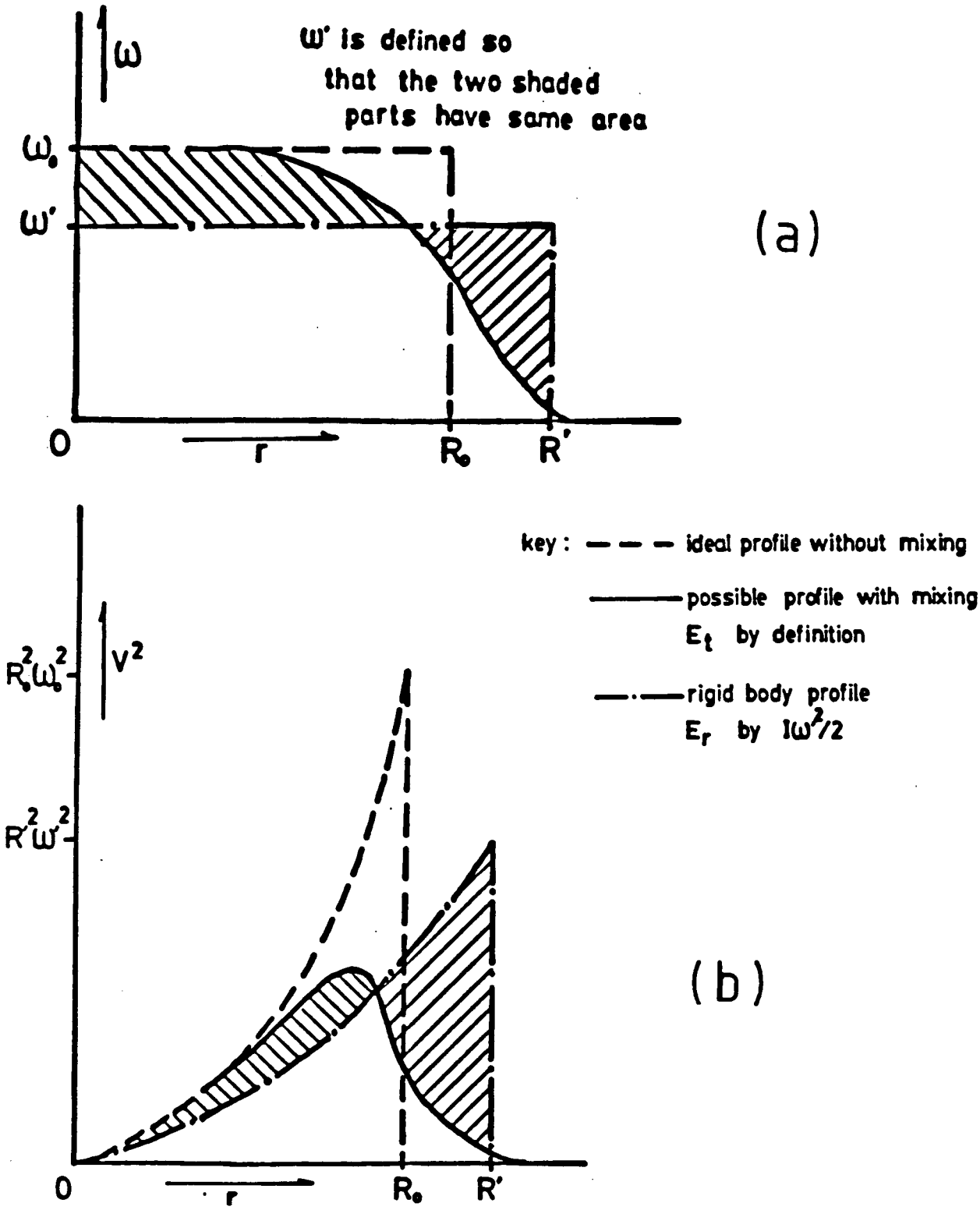

Figure 5-13 Internal flow structure. (a) Angular velocity profiles. (b) Corresponding velocity profiles.

Considering eqn.(5-29) we realize that for the deviation from a rigid body profile to produce a larger square average than average square the angular velocity profile must be skewed with lower ω at larger radius as shown in Fig.5-13a. This is consistent with both our understanding of what viscosity will do to the profile and direct observation of angular velocity plots. Unfortunately, at the present time, the data density available from our analysis hardware is too low to merit a quantitative study of an individual structure's internal velocity profile.

5.5 The Omega Decay

The omega decay was first observed in the time exposed flow photos such as Figs.4-1. These short lived structures comprise about one in twenty of the flow structures in the equilibrium and decay flow regions. Figure 5-14 shows the omega decay dynamics. The process is similar to that of eddy pairing described in section 5.2 except one of the structures is infinitely large. In the present analysis the river motion is considered to be part of the background flow environment. The omega decay is thus a type of structure-fluid interaction and so would be characterized by a B coefficient.

In the course of a study of staggered cylinder flow dynamics a method was found to produce, predictably, a flow situation which resulted in the omega decay. Its structure is similar to that shown in Fig.5-7 of the initial vortex production. In this instance however the structures are pulled into the oppositely moving momentum defect "river" by the elastic nature of the fluid being pulled by the cylinder and dragged through the surrounding fluid. Figures 5-15 show surface and subsurface time exposed flow photos of

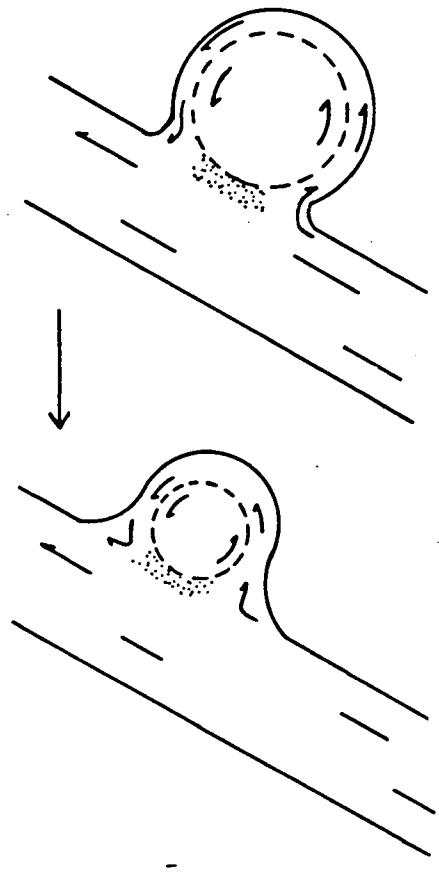

Figure 5-14 The omega decay dynamics.

this flow for an object speed of 20cm/sec. An omega decay structure can be seen very near ($\sim 1M$) to the two cylinders' starting position in Fig.5-15a. The photo does not show the phenomenon as clearly as can be observed by stepping through the video frames. In the time exposure the rapid structure evolution and non-negligible drift velocity tend to smear out the flow features.

Figure 5-15b is taken with a 3.5cm wide sheet of light parallel to the water surface at a depth of 14cm. The pattern is similar to the surface photo in structure and velocity.

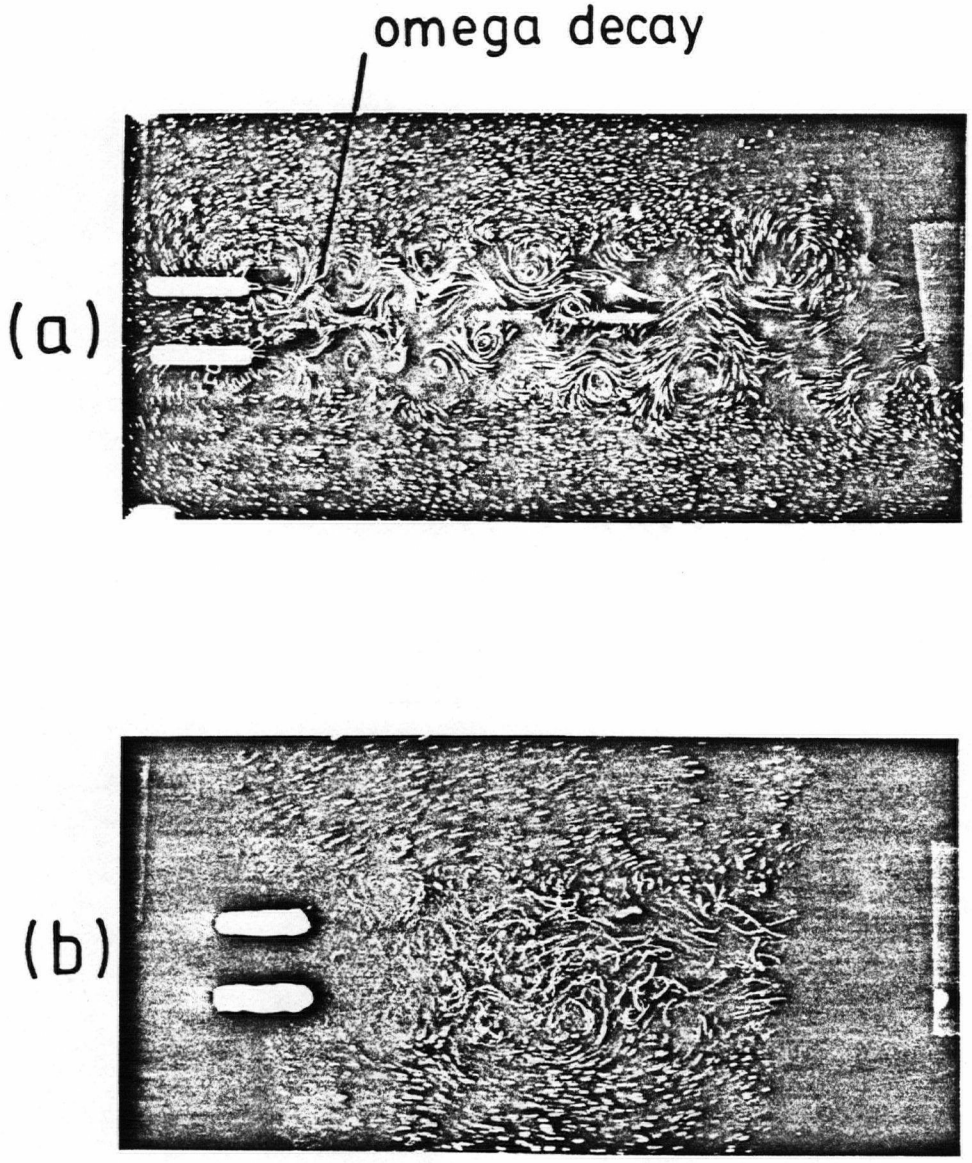

Figure 5-15 Time-exposed flow photo of two-cylinder flow. (a) surface flow showing omega decay (b) sheet-lighting (20cm depth) parallel to surface showing predominantly 2-D flow.

However, evidence of three dimensional motion is visible in the form of irregular tracer paths.

An attempt was made to use the computer-automated analysis system to study the omega decay in this flow. That attempt was unsuccessful due to the resolution limits and lack of compensation for structure drift in the present analysis system. A more powerful analysis system needs to be developed in order to study the omega decay.

5.6 Statistics from Dynamics

An initial vortex production model has been presented which agrees with the experimentally determined structure population. Also, a simple model has been proposed for the spontaneous decay rate A. It was also found to agree with experimental observation. The remaining structure dynamics of eddy pairing and the omega decay have been examined but as yet no model has been developed for these processes. The real test of the rate equation approach would be to use rate coefficients to predict the size, angular speed and energy distributions measured in the last chapter. This would proceed by using the rate equation, (2-35), on the initial distribution determined by the vortex production of section 5.3. Such a comparison would be a powerful test of the rate equation approach to describing the evolution of the ensemble of coherent flow structures in turbulent fluid flow. The development of such a powerful predictive tool for turbulent flows should be the primary objective of any research arising from this thesis work.

CHAPTER 6
CONCLUSION

" It was on a dreary night of November that I beheld the accomplishment of my toils."
in *Frankenstein* by Mary Shelly (1818)

This thesis has examined the validity and viability of a model for turbulence based on rate equations by studying the statistics and dynamics of coherent structures on grid-generated turbulence. The experimental study focussed on the surface motion of grid-flow produced in a towing tank. For the structure statistics investigation surface flow patterns were recorded as time-exposed photographs of tracer paths following the motion of the fluid. The flow patterns were manually analyzed to determine the size and velocity structure of the surface eddies. Structure dynamics were investigated using a computer-automated structure identification and flow field analysis package. This system analyzed video recordings of the tracer motion. Results from hot-film anemometry and subsurface flow visualization were used to compare the surface and subsurface flows.

The flow photos revealed a profusion of coherent surface structures that either rotate (surface eddies), translate (river flow), or are relatively stagnant. The size and angular velocities of the surface eddies were determined and used to calculate the eddy energy distribution. Kinetic energy distributions of the river motion were also determined. When

fitting empirical formulas to these distributions, equations similar to a Boltzmann energy distribution for a system of particles in thermal equilibrium were found. This result has two consequences: first, it implies that "collisional" interactions must dominate, and second, it is possible to characterize an energy distribution by a temperature parameter. Eddy and river "temperatures" were determined and it was found that θ_e and θ_r are about the same in the equilibrium region. These temperatures slowly decay and the distributions remain Boltzmann-like throughout the equilibrium region. As well, interaction and decay rates of the surface eddies were extracted from the evolution of the size spectrum $N(R, X)$. The surface flow is predominantly two dimensional and no source or sinks of fluid were observed to penetrate the material surface. This is in sharp contrast to the subsurface motion which rapidly becomes three dimensional.

Study of video sequences of the near-grid flow led to a model for the initial vortex production. The model assumes that the structures are produced at the Strouhal frequency of the individual cylinders but are constrained in size and spatial orientation by the mesh-width. The model predicts values for structure size, initial population density and angle between adjacent structure centers, all in good agreement with observation. Further experimental study of this model using different grid speeds and mesh-width to bar-diameter ratios would be both worthwhile and possible using the existing analysis system.

In the rate equation model the change of the eddy distribution is attributed to three distinct interactions that are characterized by rate coefficients A, B and C. Structure interaction with the surrounding fluid is termed viscous or spontaneous decay and is quantified by the rate coefficient A. Interaction with the fluid flow is quantified by rate

coefficient B. Structures may gain energy from the flow environment as in the initial vortex production region of the grid-flow or lose energy to the river-flow as in the omega decay. They may also be torn apart in sufficiently high strain-fields. The process of vortex stretching is not found in our two-dimensional surface flow. Finally, structures may interact with other structures as seen in the eddy pairing process (C coefficient).

Study of video recordings of the surface motion showed the dominant evolution processes to be viscous dissipation, eddy pairing and the omega decay. Relatively few eddy splitting events were found. Analysis of the viscous decay of steadily evolving structures was presented. These results were compared with computer and analytic models of isolated vortex evolution. Agreement on the dependence of the decay rate A on structure size ($A \propto 1/R^2$) was found although there was some ambiguity about the value of the proportionality constant.

The omega decay, a sudden relaminarization of a rotating structure, was found to be a frequent occurrence in the production and equilibrium regions of the flow. This type of evolution was found to occur when an eddy contacted a river motion with direction opposite to that of the eddy contact point. Study of the omega decay rate would be a good first application of the present analysis system once fit with more powerful image acquisition hardware because of practical limitations of the existing analysis system. There exists the possibility of eddy production by an inverse omega decay process. A search for this river evolution may prove rewarding.

Many eddy pairings were observed in the flow photos and video sequences. Quantification of the encounter statistics and pairing dynamics of this decay process is the

last major step needed before the rate equation can be used for a meaningful prediction of the structure population. The success in the statistical analysis and description and in the isolation of the significant structure dynamics show the great promise of the rate equation model for the statistics of the large scale structures in a turbulent fluid flow.

This thesis has presented a number of my original contributions to the understanding of turbulent fluid dynamics. The discovery of surface flow structures on grid-generated turbulence has already been reported in my M. Sc. thesis [59]. The statistical analysis of the size, angular speed and energy distributions of the *eddies* and *rivers* (closed and open flow structures) described in chapter four has been presented elsewhere [5]. The size and angular speed distributions were used to predict an integral length scale which was compared with one obtained from Fourier analysis of hot-film anemometry signals measured in the bulk of the flow [30]. The results of this comparison were used in chapter five of this thesis in a study of the relationship between the surface and subsurface flow. The rate equation model, originally proposed by Dr. B. Ahlborn [1], led to the discussion of the energy distributions in terms of a temperature. My contributions to this approach are contained in a recent publication [6] as well as in chapter four of this thesis. The need to automate the recognition and analysis of a coherent structure led to the M. Sc. work of A. Lau [38] which was used in the structure dynamics study of chapter five. Although some earlier work on structure dynamics was published [4], the initial vortex production model, comparison of the spontaneous decay experiment and theory, as well as the isolation of the structure decay types on the surface flow of grid-generated turbulence are original to this thesis.

It is hoped that the results and approach presented in this thesis will stimulate further research. In order to complete the demonstration of the rate equation approach, models need to be developed to quantify the omega decay (B rate) and eddy pairing (C rate) processes. Once this has been accomplished, the initial vortex production model provides an initial structure distribution which should evolve according to the rate equation. The observed statistics can then be compared with those predicted. As indicated in Fig.2-5, the ultimate test of the model is to use moments of the predicted structure statistics to determine such macroscopic flow properties as drag, mixing rates, and gust levels. In fact, after further verification of the initial vortex production model presented in this thesis it should be straightforward to predict the form drag acting on parallel bar grids.

While an attempt has been made to understand the coupling between the surface and subsurface motions it would be desirable to repeat the statistics and dynamics study for a system which is more closely two-dimensional. Structure identification and analysis could then proceed using an automated analysis system such as the one described in section 3.3.2. Extension of the model to three-dimensional flows would require the inclusion of vortex stretching into the B coefficient in addition to including the added dimension into the interaction statistics. Whomever embarks on such an ambitious task faces many years of challenging and interesting work.

References

[1] B. Ahlborn, F. Ahlborn and S. Loewen, "A model for turbulence based on rate equations", Applied Physics **18**, pp. 2127-41 (1985)

[2] Th. von Kármán , "Über den mechanismus des widerstandes, den ein bewegter körper in einer flüssigkeit erzeugt", *Nachr. Ges. Wiss. Göttigen, Math. Phys. Klasse* pp. 509-517 (1911) and pp. 547-556 (1912); see also Coll. Works *I*, pp. 324-338

[3] G. L. Brown and A. Roshko, "On density effects and large structures in turbulent mixing layers", *J. Fluid Mech.* **64**, pp. 775-816 (1974)

[4] B. Ahlborn, A. Filuk and S. Loewen, "Eddy formation and break-up in a turbulent flow", in *Proc. Fifth Eng. Mech. Conf.*, U. of Wyoming (1984), Ed by A. P. Boresi and K. P. Chong, Am. Soc. Civ. Eng., New York

[5] S. Loewen and B. Ahlborn, "Empirical energy distribution functions of decaying grid turbulence", pp. 196-99, in *Seventh Symposium on Turbulence and Diffusion*, pub. by the American Meteorological Society, Boston, Mass. (1985)

[6] S. Loewen, B. Ahlborn, and A. B. Filuk, "Statistics of surface flow structures on decaying grid turbulence", Physics of Fluids **29** (8), pp. 2388-97 (1986)

[7] A. Lau, S. Loewen, B. Ahlborn, and V. Bareau, "Automated recognition of internal structures in 2D fluid flow", Bul. Am. Phys. Soc. **30**, pp. 1729 (1985)

[8] A. Lau, S. Loewen and B. Ahlborn, "Automated two-dimensional flow visualization and coherent structure recognition", submitted to Experiments in Fluids (August 1986)

[9] M. Broze, "Safety: The open coast or all your eggs in one kayak", pp. 27, *Sea Kayaker* **3** No.1 1986

[10] B. E. Launder and D. B. Spalding, *Mathematical Models of Turbulence*, Academic Press (1972)

[11] O. Reynolds, "On the dynamical theory of incompressible viscous fluids and the determination of the criterion", Philosophical Transactions of the Royal Society of London, Series A, **186**, pp. 123 (1895)

[12] J. Boussinesq, "Essai sur la théorie des eaux courantes.", Mém. prés. Aca. Sci. *XXIII*, 46, Paris (1877)

[13] J. Boussinesq, "Theorie de l'écoulement tourbillonant et tumultueux des liquides dans les lits rectilignes à grande section (tuyaux de conduite et canaux découverts), quand cet écoulement s'est régularisé en un régime uniforme, c'est-à-dire, moyennement

pareil à travers toutes les sections normales du lit." Comptes Rendus de l'Académie des Sciences *CXXII*, pp. 1290-95 (1896)

[14] L. Prandtl, "Über die ausgebildete turbulenz", ZAMM 5, pp. 136-39 (1925). Also, S. Goldstein "Modern Developments in Fluid Dynamics", **1** p205, Oxford University Press, New York (1938)

[15] H. Tennekes and J. L. Lumley, *A First Course in Turbulence* , MIT Press (1972)

[16] H. Schlichting, *Boundary Layer Theory*, McGraw-Hill, New York (1979)

[17] W. C. Reynolds, "Computation of turbulent flows", Ann. Rev. Fluid Mech., **8** pp. 183-208 (1976)

[18] M. T. Landahl and E. Mollo-Christensen, *Turbulence and random processes in fluid mechanics* , Cambridge University Press (1986)

[19] J. O. Hinze, *Turbulence*, McGraw-Hill (1975)

[20] A. N. Kolmogorov, "The local structure of turbulence in incompressible viscous fluid for very large Reynolds numbers", Dokl. Akad. Nauk. SSSR 30, pp. 299-303, (1941). see also G. K. Batchelor, "Kolmogorov's theory of locally isotropic turbulence", Proc. Camb. Phil. Soc., **43**, pp. 533-59, (1947)

[21] H. L. Grant, R. W. Stewart and A. Moillet, "Turbulence spectra from a tidal channel", *J. Fluid Mech.* **12**, pp. 241-63 (1962)

[22] R. W. Stewart, "Turbulence and waves in a stratified atmosphere", *Radio Sci.*, **4**, pp. 1289 (1969)

[23] R. H. Kraichnan, "Inertial ranges in two-dimensional turbulence", *Phys. Fluids*, **10** (7) pp. 1417-23 (1967)

[24] J. H. Ferzinger, "Simulation as an aid to phenomenological modelling", in *Macroscopic Modelling of Turbulent Flows*, edited by U. Frisch et al, Proceedings, Sophia-Antipolis, France 1984, pp. 263-76, Springer-Verlag (1985)

[25] A. Leonard, "Energy cascades in large eddy simulations of turbulent fluid flow", *Advances in Geophysics* **18A**, pp. 237-48 (1973)

[26] B. Aupoix, "Eddy viscosity subgrid scale models for homogeneous turbulence", in *Macroscopic Modelling of Turbulent Flows*, ed. U. Frisch et al, Proceedings, Sophia-Antipolis, France 1984, pp. 45-64, Springer-Verlag (1985)

[27] S. Orszag, "Analytic theories of turbulence", *J. Fluid Mech.* **41**, pp. 363-86 (1970)

[28] P. Perrier, "Large and small structures in the computation of transition to fully developed turbulent flows", in *Macroscopic Modelling of Turbulent Flows*, ed. U. Frisch et al, Proceedings, Sophia-Antipolis, France 1984, pp. 32-44, Springer-Verlag (1985)

[29] Brian J. Cantwell, "Organized motion in turbulent flow", *Ann. Rev. Fluid Mech.* **13**, pp. 457-515 (1981)

[30] S. Loewen, "Statistics of Coherent Structures in Turbulent Fluid Flow", M. Sc. thesis, The University of British Columbia, Vancouver, Canada (1983) (unpublished)

[31] W. Merzkirch, *Flow Visualization*, Academic Press (1974)

[32] W. Merzkirch, *Flow Visualization* II, Proc. Second Int. Symp. Flow Vis., 1980 Bochum, West Germany, McGraw-Hill (1980)

[33] T. Asanuma, *Flow Visualization*, Proc. Int. Symp. Flow Vis., 1977 Tokyo, Japan, McGraw-Hill (1979)

[34] M. Van Dyke, *An Album of Fluid Motion*, The Parabolic Press, Stanford (1982)

[35] W. Lauterborn and A. Vogel, "Modern optical techniques in fluid mechanics", *Ann. Rev. Fluid Mech.* **16** , pp. 223-44 (1984)

[36] M. A. Hernan and J. Jimenez, "Computer analysis of high-speed film in the plane turbulent mixing layer", J. Fluid Mech., **119** pp. 323, June (1982)

[37] F. Ahlborn, "Über den Mechanismus des hydrodynamischen Widerstandes", Abhandlungen aus dem Gebiet der Naturwissenschaften", Naturwiss. Verein, Hamburg Bd XVII, L. Friedrichsen & Co. (1902)

[38] A. Lau, "Automated Two Dimensional Flow Visualization and Coherent Structure Recognition", M. Sc. thesis, The University of British Columbia, Vancouver Canada (1986) (unpublished)

[39] T. Utami and T. Ueno, "Visualization and picture processing of turbulent flow", Experiments in Fluids **2**, pp. 25-32 (1984)

[40] M. Mory and E. J. Hopfinger, "Structure functions in a rotationally dominated trubulent flow", Physics of Fluids, **29** pp. 2140-47 (1986)

[41] Y.-H. E. Sheu, T. P. K. Chang, G. B. Tatterson and D. S. Dickey, "A three-dimensional measurement technique for turbulent flows", *Chem. Eng. Commun.*, **17**, pp. 67-83 (1982)

[42] J. L. Lumley, "Coherent structures in turbulence", in *Transitions and Turbulence*, Academic Press, pp. 215-42 (1981)

[43] James C. McWilliams, "The emergence of isolated coherent structures in turbulent fluid flow", J. Fluid Mech. **146**, pp. 21-43 (1984)

[44] A. K. M. F. Hussain, "Coherent structures - reality and myth", Phys. Fluids, **26** (10) pp. 2816-50 (1983)

[45] G. I. Taylor, "Statistical theory of turbulence", Proceedings of the Royal Society of London, Series A, **151**, pp. 421 (1935)

[46] R. A. Antonia, "Conditional sampling in turbulence measurement", *Ann. Rev. Fluid Mech.* **13** , pp. 131-56 (1981)

[47] G. Comte-Bellot and S. Corrsin, "The use of a contraction to improve the isotropy of grid-generated turbulence", J. Fluid Mech. **25**, pp. 657 (1966)

[48] Dean W. Criddle, "The viscosity and elasticity of interfaces", in *Rheology Volume 3*, edited by F. R. Eirich, pp. 429-42, Academic Press (1960)

[49] J. C. R. Hunt and J. M. R. Graham, "Free stream turbulence near plane boundaries", J. Fluid Mech., **84** (2), pp. 209-35 (1978)

[50] E. C. Itsweire and K. N. Helland, "Turbulent mixing and energy transfer in stably stratified turbulence", pp. 172-175 in *Seventh Symposium on Turbulence and Diffusion*, pub. by the American Meteorological Society, Boston, Mass. (1985)

[51] J. T. Lin and Y. H. Pao, "Wakes in stratified fluids", *Annual Review of Fluid Mechanics,* **11**, pp. 317 (1979)

[52] J. Sommeria, "Two-dimensional behaviour of MHD fully developed turbulence ($R_m \gg 1$)", *J. Mecanique Theor. App. l.* Supp. l, **169**, ed. by R. Moreau (1983)

[53] R. W. Stewart, "Turbulence and waves in a stratified atmosphere", *Radio Sci.*, **4**, pp. 1289 (1969)

[54] G. Veronis, "The analogy between rotating and stratified fluids", *Annual Review of Fluid Mechanics*, **2**, pp. 37-66 (1970)

[55] Blair Brumley, "Turbulence measurements near the free surface in stirred grid experiments", in *Gas Transfer at Water Surfaces*, pp. 83-92, edited by W. Brutsaert and G. H.Jirka, D. Reidel Pub. Co. (1984)

[56] E. V. Zalutskii, "Some estimates of the accuracy of defining flow turbulence characteristics by the flow visualization method", *Fluid Mechanics-Soviet Research*, **2**, No.1-February (1973)

[57] A. B. Filuk, "Computer modelling for spontaneous vorton transition rates", *UBC Plasma Physics Group Lab Report#95* (1985) (unpublished)

[58] A. Roshko, "Structure of turbulent shear flows: A new look", AIAA Journal, **14** No.10, pp. 1349-57 (1976)

[59] S. Loewen and B. Ahlborn, "Statistical analysis of coherent structures in turbulent grid-flow", Plasma Group Lab Report # 103, U.B.C. Physics Department, Vancouver, Canada (1984) (unpublished)

[60] I. A. Hannoun, H. J. S. Fernando and E. J. List, "The nature of turbulence near a density interface", Bul. Am. Phys. Soc. **30**, pp. 1735 (1985)

[61] A. Hasegawa, "Self organization processes in continuous media", Adv. Phys. **34**, 1 (1985)

[62] E. Hopfinger, M. Griffiths and M. Mory, "The structure of turbulence in homogeneous and stratified rotating fluids", *J. Mecanique Theor. App. l.* Supp. l, **21**, ed. by R. Moreau (1983)

[63] Th. von Kármán , and H. Rubach, "Über den mechanismus des flüssigkeits- und luftwiderstandes", *Phys. Z.* **13**, pp. 49-59 (1912); see also Coll. Works *I* pp. 339-358

[64] *Macroscopic Modelling of Turbulent Flows*, ed. U. Frisch et al, Proceedings, Sophia-Antipolis, France 1984, Springer-Verlag (1985)